論文 / 著書情報
Article / Book Information

題目(和文)	
Title(English)	STUDY OF CO2 PERMEATION AND SEPARATION THROUGH IONIC LIQUID MEMBRANE
著者(和文)	JindaratsameePinyarat
Author(English)	Pinyarat Jindaratsamee
出典(和文)	学位:博士(工学), 学位授与機関:東京工業大学, 報告番号:甲第9283号, 授与年月日:2013年9月25日, 学位の種別:課程博士, 審査員:下山 裕介,伊東 章,Wiwut Tanthapanichakoon,関口 秀俊,谷口 泉,松本 秀行
Citation(English)	Degree:Doctor (Engineering), Conferring organization: Tokyo Institute of Technology, Report number:甲第9283号, Conferred date:2013/9/25, Degree Type:Course doctor, Examiner:,,,,,
学位種別(和文)	博士論文
Type(English)	Doctoral Thesis

STUDY OF CO_2 PERMEATION AND SEPARATION THROUGH IONIC LIQUID MEMBRANE

DEPARTMENT OF CHEMICAL ENGINEERING

PINYARAT JINDARATSAMEE

STUDY OF CO_2 PERMEATION AND SEPARATION THROUGH IONIC LIQUID MEMBRANE

PINYARAT JINDARATSAMEE

IN THE PARTIAL FULFILLMENT OF THE REQUIREMENT FOR
THE DEGREE OF DOCTOR OF ENGINEERING (CHEMICAL ENGINEERING)
THE GRADUATE SCHOOL OF SCIENCE AND ENGINEERING
TOKYO INSTITUTE OF TECHNOLOGY
SEPTEMBER 2013

Acknowledgements

This doctoral thesis was successful due to direct and indirect assistance from many kind people around me. Firstly, I would like to express the deepest appreciation and gratitude to my advisor Associate Professor Yusuke Shimoyama for his motivation, enthusiasm, immense knowledge and excellent ideas. Without his persistent help this thesis would not have been possible.

I would also like to express my sincere thanks to my committee members, Professor Akira Ito, my second advisor, Professor Wiwut Tanthapanichakoon, Professor Hidetoshi Sekiguchi, Associate Professor Izumi Taniguchi and Associate Professor Hideyuki Matsumoto from department of chemical engineering for valuable guidance and comments.

I would also like to acknowledge Associate Professor Hitoshi Kosuge, my first advisor, who gave me the great opportunity to study here as well as his encouragement.

Thanks also go to the members of Shimoyama laboratory especially the former members of CO_2 sequestration group, Mr. Hironobu Morizaki and Mr. Shogo Komuro, for assist me to set up the experimental apparatus and perform some experiments.

Last but not least, I wish to thank my parents, grandmother and friends for their supports throughout five years in Tokyo Institute of Technology. I would not have been able to complete the thesis without continuous love and encouragement.

Nomenclature

A	Membrane area
C	Solubility coefficient
D	Diffusion coefficient
f_{CO2}^{ref}	Fugacity of CO_2 in liquid at the standard state
F	Permeation rate
F_{p}	Sweep air flow rate
G	Sweep gas flow rate at permeate side
H	Higher membrane area value
L	Lower membrane area value
m_{IL}	Mass of ionic liquid
M	Molecular mass
M_{IL}	Molar mass of ionic liquid
$M_{\mathrm{IL+w}}$	Molar mass of mixture between ionic liquid and water
M_{w}	Molar mass of water
n_{IL}	Mole of ionic liquid component
n_w	Mole of water component
$p_{\mathrm{CO_2}}$	Partial pressure of CO_2
p_{f}	Pressure at feed side
p_{p}	Pressure at permeate side
Q_{CO2}	Permeability of CO_2
Q_{H2O}	Permeability of water
Q_{IL}	Permeability of gas through ionic liquid membrane
Q_{IL+w}	Permeability of gas through ionic liquid membrane with presence of water
R	Rate of the enhancement of the compound
V_{CO2}	Molar volume of CO_2 at normal boiling point
S	Selectivity
T	Operating temperature
T_{b}	Boiling point

T_m	Melting point
x	CO_2 mole fraction at feed side
x_{CO2}	Mole fraction of CO_2
X	Volume fraction
y	CO_2 mole fraction at permeate side
y_p	CO_2 mole fraction in outlet sweep air

Greek Letters

α	Difference parameter of enhancement ratio between experiment and theoretical data
γ_{CO2}	Activity coefficient of CO_2
δ	Membrane thickness
Δp	Partial pressure difference
η_{IL}	Viscosity of ionic liquid
ρ_{IL}	Density of ionic liquid

Contents

List of Tables

List of Figures

Chapter 1

Introduction

1.1 Background and motivation

Carbon dioxide (CO_2) is an acid gas which is generated from land, ocean, respiration, combustions of fossil fuels or coals and biomass burning. CO_2 is classified as a greenhouse gas that causes the global warming phenomena. Increasing emission of CO_2 to the atmosphere is classified as a severe problem in the world. During 1750-2005 A.D., a report shows the remarkable CO_2 concentration in the atmosphere rises from 280 to 379 ppm which is the highest statistic in the last 650,000 years [1]. The CO_2 concentration of each emission sources are listed as follow: 7 to 14% power plant, 24% cement plant, 27% steel plant and 30 to 50% chemical plant. Therefore, it is very important issue to find out methods for CO_2 sequestration.

1.2 Technologies for CO_2 sequestration

Due to the increment of CO_2 emission to atmosphere, a number of researchers have attempted to capture CO_2 by many techniques. The current techniques for CO_2 sequestration contain adsorption [2-4], absorption [5, 6], cryogenic [7, 8] and membrane separation technology [4]. The detail of each method is provided as follows:

1.2.1 Adsorption

The separation of CO_2 by adsorption process can be conducted by several techniques: vacuum swing adsorption (VSA), pressure swing adsorption (PSA) and temperature swing adsorption (TSA). At first, the desired gas, CO_2, is adsorbed on to the surface of adsorbents. To desorb the gas (or regenerate the adsorbents), the process then swing to vacuum, decrease the pressure or increase the temperature, respectively. The conventional adsorbents for CO_2 capture consist of zeolite [2], activated carbon [3, 9] and molecular sieve [4, 10]. The characteristics of effective adsorbent should have low regeneration energy and cost, high selectivity and adsorption capacity for CO_2. The principle of adsorption process is illustrated in Fig. 1.1.

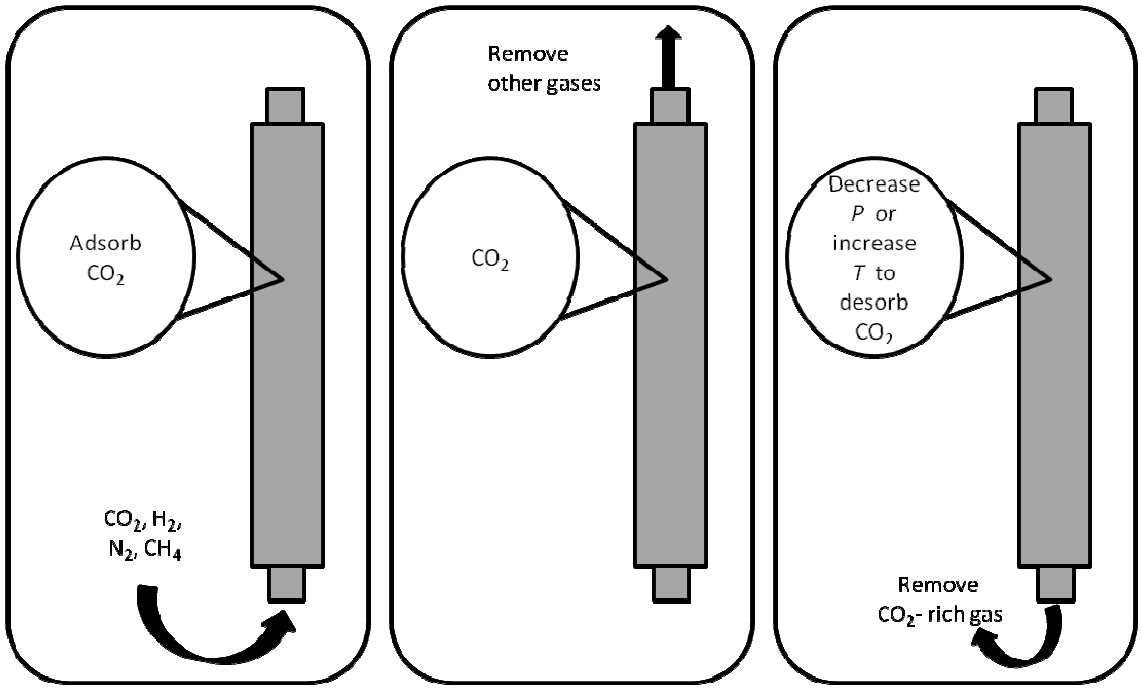

Fig. 1.1 The principle of CO_2 adsorption process

1.2.2 Absorption

Absorption process has been widely applied for CO_2 separation in oil and gas industries, chemical processing industries, and power plant. CO_2 is removed from the fuel gas stream by absorbing to the solvent, typically amine solution. The solvent is fed into the top tray of the absorber, while sour gas is fed into the bottom tray. The function of packing inside the absorber is to increase the contacting surface area between CO_2 and amine. The sweet gas is released at the top of absorber. Rich amine is delivered to the top tray of the regenerator. Reboiler, at the regenerator tower, supplies the heat to remove CO_2 from rich amine. CO_2 is purged at the top of the regenerator. Lean amine is recycled and routed to the top tray of the absorber. To understand some effects of the variables on the process and energy requirements, the researchers used Aspen Plus as a simulation tool to study [11]. It is the quite advantage to understand the whole absorption process for the practical point of view without performing the experiments. The principle of CO_2 absorption process is shown in Fig. 1.2.

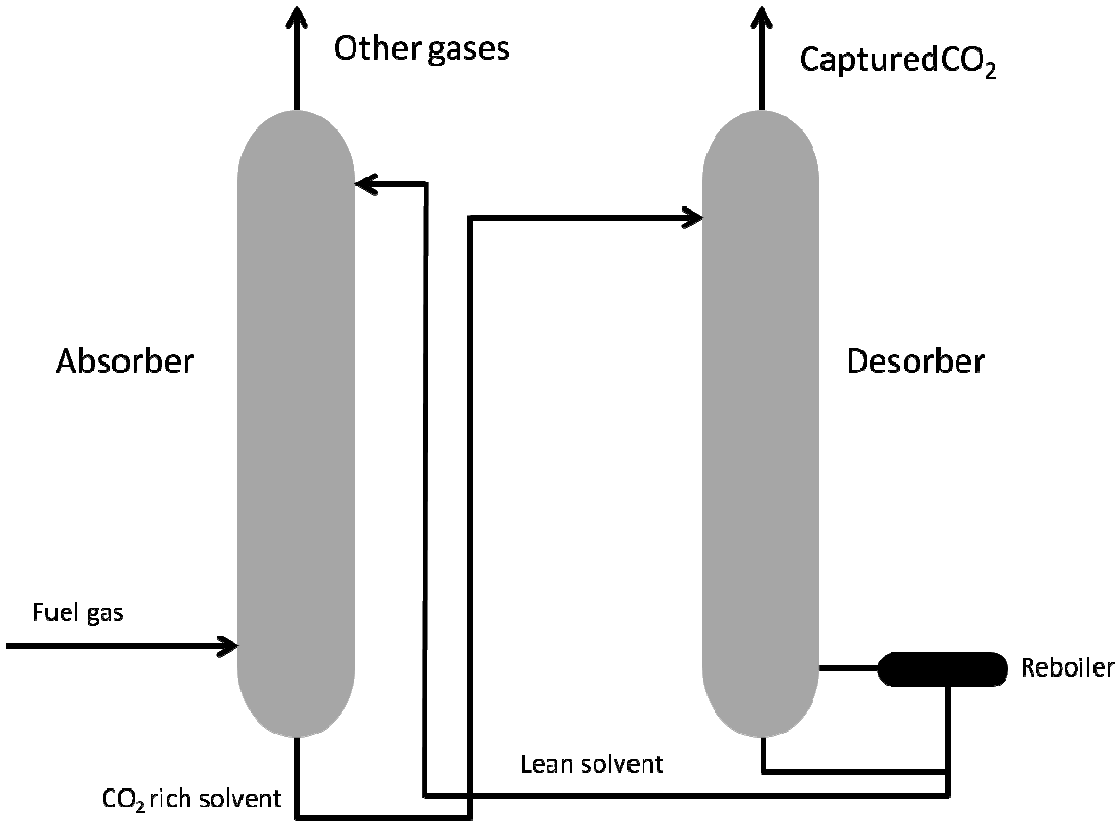

Fig. 1.2 The principle of CO_2 absorption process

1.2.3 Cryogenic

This method is generally used for separation of the acid gases, such as CO_2, from the gas stream, which contain high amount of methane such as natural gas [12] and coal-fired plants [13]. If the amount of CO_2 is relatively high, it may cause the high corrosion of the distillation column and cause the sales gas to be out of the specification. CO_2 is separated from the fuel gas by cooling the stream to sub-zero temperatures then only CO_2 is condensed. The principle of cryogenic method using cold from LNG is shown in Fig. 1.3. Moreover, the solid formation from CO_2 can occur during the operation, this process also prevents the plugging trays inside the column by adding the solids-preventing agents (C_2-C_5 alkanes or non-polar liquids which dissolve with methane) [14]. Fig. 1.4 shows the cryogenic process for CO_2 capture.

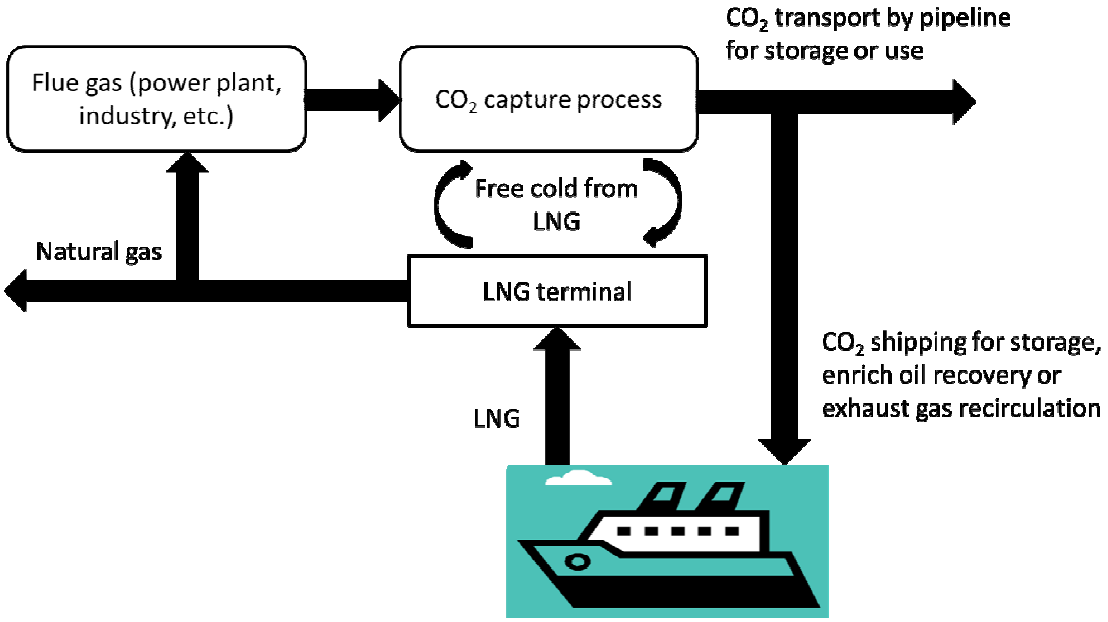

Fig. 1.3 The principle of the CO_2 capture using cold from LNG

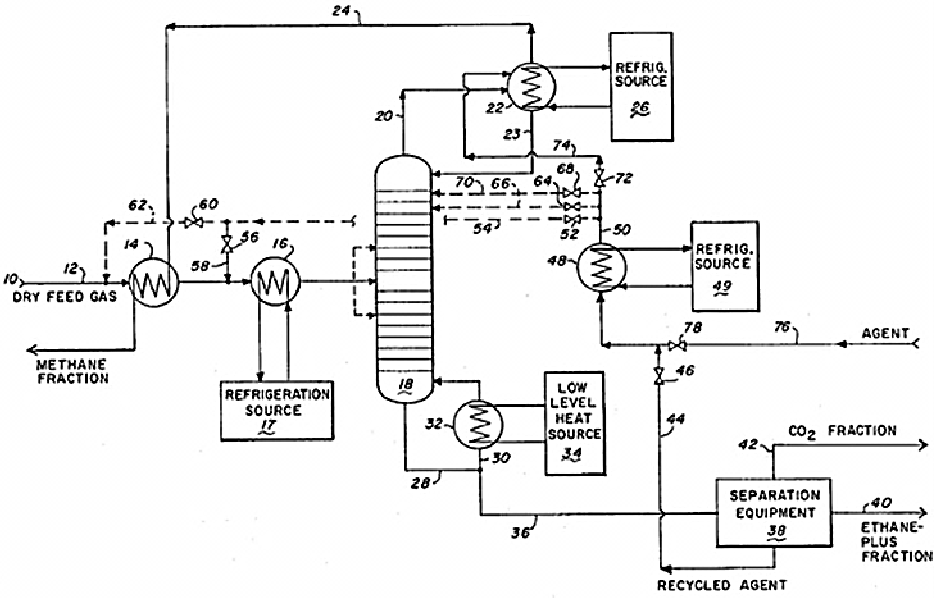

Fig. 1.4 Cryogenic process for CO_2 capture [14]

1.2.4 Membrane separation

Membrane can be expressed as a thin film, glassy polymeric, microporous inorganic (e.g. zeolite), nonporous, ceramic, liquid or metal materials [15, 16]. Membrane is used to separate the desired fluid by the differences of the molecular size,

solubilities and diffusivities. The general membrane process is shown in Fig. 1.5. The feed mixture is separated into two streams: retentate (the feed that cannot pass through the membrane) and permeate (the feed that can pass through the membrane). The sweep, e.g. gas or liquid, is used to sweep the permeate.

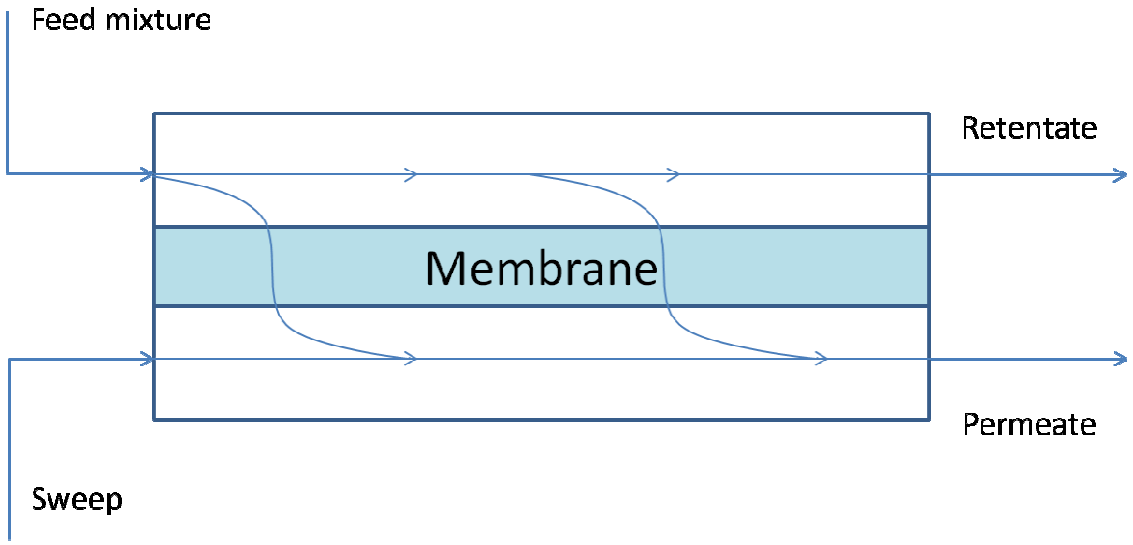

Fig. 1.5 The general membrane process

Due to compact equipment, low energy consumption, simple operation and low cost of equipment [17, 18], membrane separation technologies have been introduced for gas separation over one and half decades [17]. Gas separation technology using membrane has widely applied to many industries such as purification of H_2 in steam reforming process from natural gas, separation of CO_2 in the chemical or power plants, enrich O_2 in air. Based on material, the types of membranes can be roughly classified into 2 basic categories: solid (well known as polymers) and liquid.

1.2.4.1 Solid membrane (polymeric membrane)

Currently, the solid polymeric membrane has been used for CO_2 sequestration in many industries due to the prompt technology, no additional reagents, moderate conditions (temperature and pressure) and long-lasting. The list of polymers used in membranes and their properties is shown in Table 1.1.

Table 1.1 Polymers used in membranes and their properties

Polymer	Type	Representative repeat unit	*Tg* (°C)
Polyarylate	Rubber	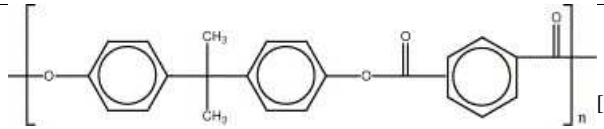 [17]	260 [19]
Polycarbonate	Glassy	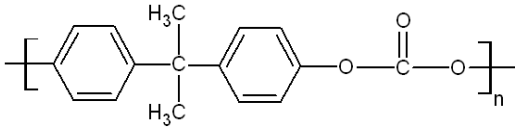	150 [16]
Polyimide	Glassy	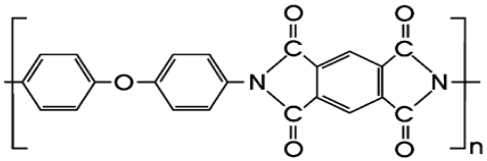 [20]	310-365 [16]
Polyisoprene	Rubber	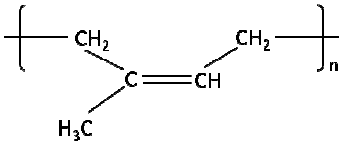	-70 [16]
Polysulfone	Glassy	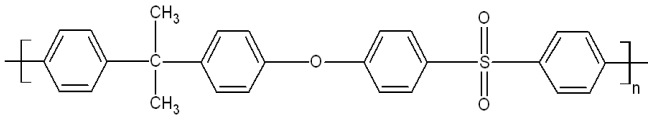	190 [16]
Polystyrene	Glassy	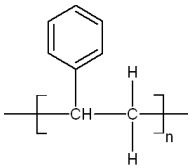	74-110 [16]

Table 1.2 expresses the permeability of CO_2 (Q_{CO2}) through solid and liquid membranes. From Table 1.2, the solid membranes present the low permeability of CO_2 than that of liquid membranes. However, the dominant advantage of polymeric membranes is the long durations of the membrane life, around 3-5 years [21].

Table 1.2 Comparisonsof CO_2 permeability between solid and liquid membranes

Membranes	Feed pressure (atm)	Temperature (K)	Q_{CO2} (Barrer*)
Polyimides (mtBuCat-DMOB) [17]	1	303.15	7
Polycarbonate (PC) [17]	1	308.15	6
Poly(ethylene oxide) (PEO) [17]	4.40	308.15	13
Polysulfones (PSF) [17]	1	308.15	6
Poly(dimethyl siloxane)(PDMS) [22]	0.53	298.15	2850
Matrimid®5218 [23]	34.05	308.15	10
6FDA—1,5-NDA [23]	9.87	308.15	23
6FDA-durene/mPDA(50:50) [23]	9.87	308.15	85
Amine liquid (DGA 50wt%/TEG 50wt%) [24]	1	293.15–298.15	20
Amine liquid (PZ) [25]	0.001	298.15	24750
Amine liquid (MEA 50wt%/TEG 50wt%) [26]	1	298.15	20902
Ionic liquid [emim][BF_4] [27]	1.21	303.15	189
Ionic liquid [bmim][BF_4] [27]	1.21	303.15	200
Ionic liquid [bmim][dca] [27]	1.21	303.15	199
Ionic liquid [bmim][OTf] [27]	1.21	303.15	205
Ionic liquid [emim][Tf_2N] [28]	1.1	303.15	1702
Ionic liquid [bmim][Tf_2N] [27]	1.21	303.15	349
Ionic liquid [hmim][Tf_2N] [28]	1.1	303.15	1136
Ionic liquid [bmim][PF_6] [27]	1.21	303.15	121
Ionic liquid [bmim][$B(CN)_4$] [29]	2	308.15	1778

Note - *barrer = $10^{-10}$$cm^3$(STP)cm cm^{-2} s^{-1} $cmHg^{-1}$

1.2.4.2 Liquid membrane

In general, permeation of gases through a dense or non-porous membrane can be described by solution-diffusivity mechanism which firstly proposed by Graham [30]. Those gases are separated by their difference of solubility and diffusivity. A liquid membrane can be treated as a dense membrane. This mechanism can be used to derive

suitable transport equation for membrane separation of dialysis, reverse osmosis, pervaporation and gas separation [31]. Basically, the transportation of gas through a non-porous membrane is described into five steps [32]:

1.) Gas diffuses through the boundary layer at the feed side.
2.) Gas dissolves into the membrane phase.
3.) Gas diffuses down like a nonlinear concentration gradient. This step is the slowest and can be judged as the rate-determining step.
4.) Gas desorps from the membrane phase at the permeate side.
5.) Gas diffuses out from the boundary layer of the permeate side.

The partial pressure difference between the feed and the permeate side act as a driving force. The solution-diffusion mechanism is shown in Fig. 1.6.

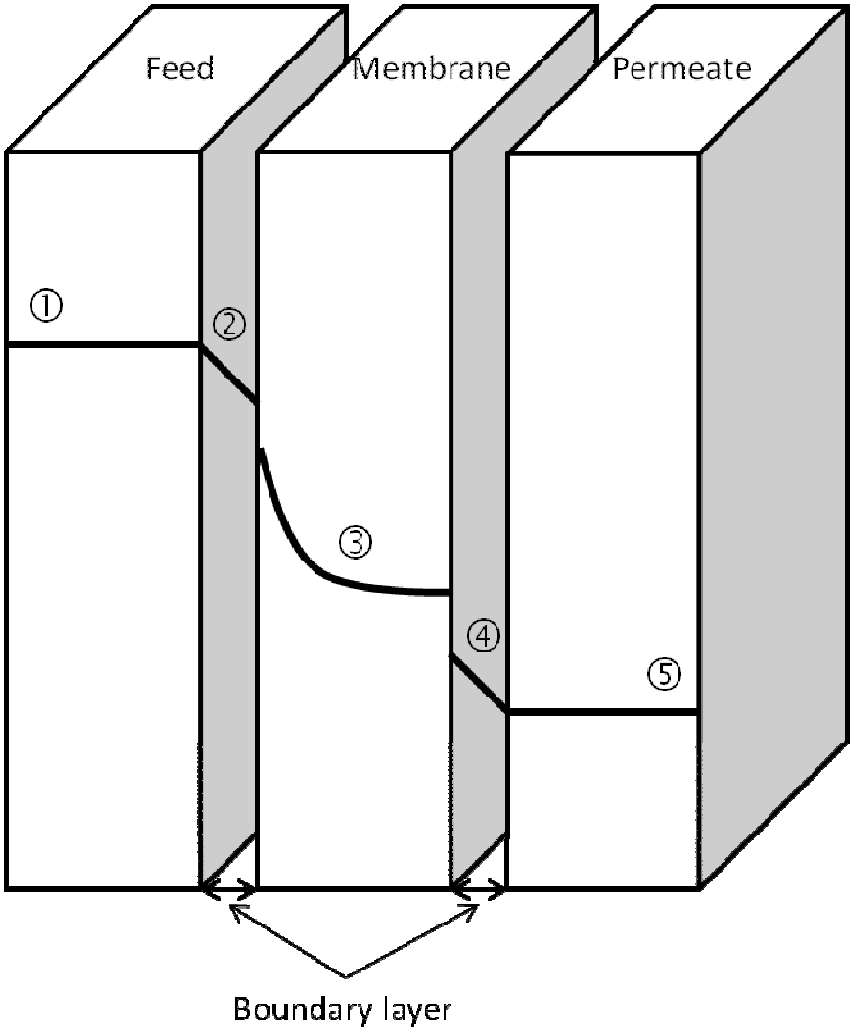

Fig. 1.6 Schematic of gas permeation across membranes based on solution-diffusion mechanism

Permeability of gas is controlled by both the solubility of the gas in the membrane material and the diffusivity of gas through the membrane material. The relationship between permeability, solubility, and diffusivity can be described by following equation:

$$Q = CD \tag{1.1}$$

where Q, C and D mean permeability coefficient in $cm^3(STP)cm\ cm^{-2}\ s^{-1}\ cmHg^{-1}$, solubility coefficient in $cm^3(STP)cm^{-3}\ cmHg^{-1}$ and diffusion coefficient in $cm^2\ s^{-1}$, respectively.

Normally, the types of liquid membrane can be divided into two main types: with and without supports. In the case of the liquid membranes that require the supports, three types are found: immobilized liquid membranes (ILM), supported liquid membranes (SLM), and contained liquid membranes (CLM). For the liquid membranes without supports can be separated into two sub-varieties: bulk liquid membrane (BLM) and emulsion liquid membrane (ELM). The explanations of the principle of each liquid membrane are given below. All types of liquid membrane configurations are shown in Fig. 1.7.

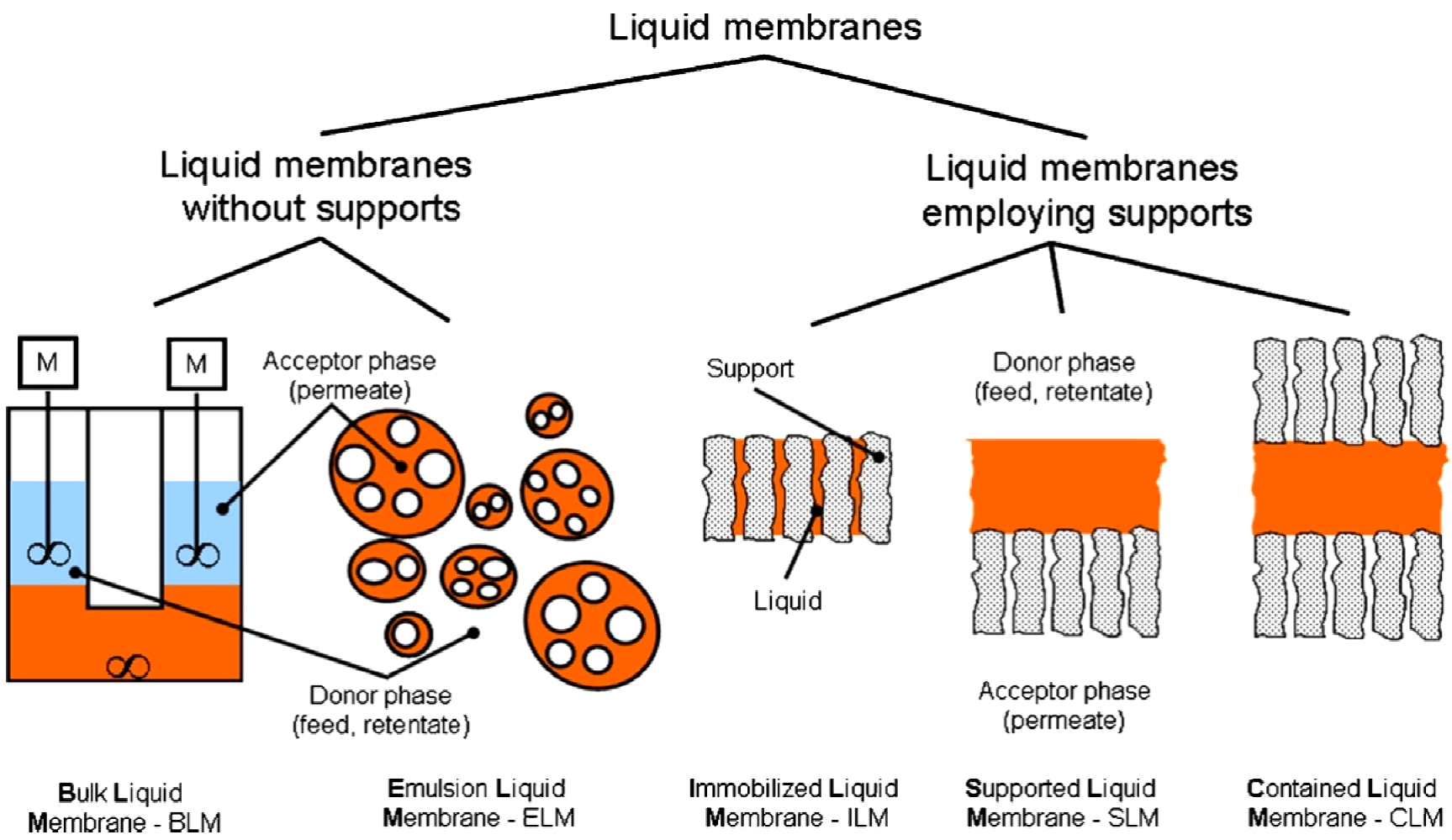

Fig. 1.7 Liquid membrane configurations [33]

(a) Immobilized liquid membranes (ILM)

Immobilized liquid membrane (ILM) consists of support and liquid, which is selective to a specific target. Normally, the liquid is supported in small pores and is kept there by capillary forces. There are many kinds of porous polymer such as polyvinylidene fluoride, cellulose acetate, microporous polypropylene, polyvinyl chloride and so on [12]. ILMs can be used in industrial scale to separate or recovery gas. In addition, this method is play an important role to assist environment such as volatile organic compound (VOC) separation for gas stream, capture acid gas e.g. CO_2 SO_2 and H_2S, and recovery and enrichment of biohydrogen [34, 35].

Advantages:

- High permeability
- High selectivity

Disadvantages:

- Loss of solvent and loss or deactivation of carrier due to solubility, osmotic flow of water across membrane and a pressure differential across the membrane
- Limitation of stability and life time

(b) Supported liquid membrane (SLM)

Supported liquid membrane (SLM) composes of an organic solution adsorbed onto a microporous supported membrane. SLMs are used for separation two solutions: 1.) contained the permeating ions (feed solution) and 2.) free of these ions (stripping solution). The ions transportation through the membrane takes place when a chemical potential gradient is established between the two solutions. This type of LM is the useful method for the separation of costly compound or solvent extraction. Moreover, SLM is widely used in pollutant separation from gaseous or liquid solvent that the mainly metal ions are not required [36]

Advantages:

- High fluxes and especially selective separations
- Small quantities of potentially expensive carriers are required
- Low capital, operating, and energy costs

Disadvantages:

- Lack of long term membrane stability
- Carrier loss to the feed or the receiving phases

(c) Contained liquid membrane (CLM)

There are two configurations of contained liquid membrane (CLM): 1.) CLM which requires two glass cell compartments for separating extraction and stripping phase and 2.) hollow fiber contained liquid membrane (HFCLM) configuration, but the principle of both CLM and HFCLM is similar. CLM comprises of the liquid solution, which sandwiched between two microporous membranes. The extraction and stripping phase are separated by CLM. Any liquid solution lost to the gas streams during the operation, it is automatically replaced from a liquid membrane reservoir. The employment of this system is to separate metal ions from aqueous solution such as recovery copper, zinc and uranium from water and extraction strontium ion from sea water [37, 38]. This method can also use for organic extraction from aqueous solutions such as phenols or citric acid [38]. Moreover, it can be applied for gas separation: CO_2/N_2, CH_4/CO_2, $SO_2/CO_2/N_2$ and others.

Advantages:

- Membrane stability is longer than ILM
- Liquid solution replenishment is automatic and easy
- Low ratio of organic/aqueous phase
- Higher surface area per unit contactor volume

Disadvantages:

- Very hydrophobic membrane solvents are required to maintain integrity
- This system must be cleaned between uses or there will be aqueous and contaminant buildup
- Easy for pore fouling
- High capital costs

(d) Bulk liquid membrane (BLM)

Bulk liquid membrane (BLM) consists of three phases: donor, receiving and membrane phase. The donor and receiving phases are separated by immiscible membrane phase. This system is required a device, which is constructed in U-type or H-type hinging on the density of the solvent [39]. These devices are used to confine bulk volumes of organic liquids between donor and receiving phase. This technique is helpful for treatment of contaminated the aqueous streams from metal ions: mercury, cobalt, cadmium, chromium etc [39-42].

Advantages:

- Lower sample manipulation and lower time needed for sample pre-treatment
- The simplest design for performing liquid membrane processes

Disadvantage:

- Require large amount of carrier relative to the effective area

(e) Emulsion liquid membrane (ELM)

The principle of ELM is described in this section. ELM consists of three phases (i.e. water/oil/water). The oil phase behaves like a membrane between the external (donor) and the internal (receiving) phase. Feed solution is at the external phase whereas the extracted solution is in the internal phase. The ELM is great technique for recovery and removal of many types of heavy metals such as uranium, copper, zinc, nickel, and cadmium [43, 44]. Furthermore, it can use in biotechnology and pharmaceutical separations. This technique can apply for industrial wastewaters treatment containing a broad range of toxic contaminants such as phenol, chlorophenol, and nitrophenol [44].

Advantages:

- Low energy consumption when compared to other separation processes
- High efficiency due to large surface area available for mass transfer
- High selectivity when carrier agents are used in the membrane phase that binds with target compounds

Disadvantages:

- The swelling of the system can occur because water transports from the external to the internal phase resulting in a decrease in the degree of concentration of the solute achieved inside the membrane
- The emulsion requires the stable and it is easy to break down

The CO_2 permeations through liquid membrane have been investigated since 1967 by Enns et al [45]. The membrane was manufactured by carbonic anhydrase soaked in a Millipore filter. Otto et al [46] studies the facilitated transport of CO_2 using bicarbonate solution liquid membrane in order to improve the heterogeneous of the medium. Amine solutions became the attractive solutions for CO_2 removal from natural gas stream because of high solubility of CO_2, inexpensive chemicals, easy for waste disposal and a lot of number trust in chemical industries. Hence, a number of researchers [24-26, 47-49] have delved into the application of amine solution for liquid membrane. Amine solutions can be applied with several types of membrane modules such as flat and hollow fiber. Moreover, pure, aqueous and mixed amine liquid membranes have been applied for CO_2 separation as well. Gorji et al [25] have determined CO_2/H_2 separation by facilitated transport membranes immobilized with aqueous single and mixed amine solutions: monoethanolamine (MEA), diethanolamine (DEA), monoprotonated ethylenediamine ($EDAH^+$) and piperazine (PZ). Among these amine aqueous solutions, PZ showed the highest CO_2 permeation rate. In addition, the viscosity of mixed amine solution also affects the CO_2 permeability. Ito et al [24] studied the permeation of wet CO_2/CH_4 mixed gas through diglycolamine (DGA) ortriethylene glycol (TEG) hydrophobic microporous flat sheet membrane. The results suggested that DGA solution impregnated with hydrophilictreated polytetrafluoroethylene (PTFE) microporous membrane was successful for CO_2 separation. CO_2 permeability was 30–100 Barrer and the CO_2/CH_4 separation factor of 40–100. Gong et al. [47] have investigated the CO_2 removal using methyldiethanolamine/monoethanolamine (MDEA/MEA) aqueous solutions through a hollow fiber membrane module. It was found that the absorption flux and fractional removal enhanced with increasing amount of MEA in the MDEA/MEA aqueous solution. Paul et al [48, 49] studied CO_2 separation by single and blended aqueous

alkanolamine solvents: monoethanolamine (MEA), diethanolamine (DEA), N-methyldiethanolamine (MDEA) and 2-amino-2-methyl-1-propanol (AMP) in hollow fiber and flat sheet membrane. Their results strongly indicated that the performance of flat sheet membrane contactor is better than that of hollow fiber membrane contactor for consideration only the absorption flux of CO_2 in the amines.

Amine liquid membranes achieve the goal to capture CO_2 from mixed gas. However, oxidative degradation, toxicity and volatile organic compound are still the big disadvantages of amine solution. To improve the CO_2 sequestration, the required material should be green chemical, non-volatility and strong affinity with CO_2. One of the candidates is ionic liquid. The general description and basic properties of ionic liquids are interpreted in next section.

Up to this section, the general description of the principle of CO_2 separation of classical method has already mentioned. The summary of advantages and disadvantages of CO_2 separation technology are shown in Table 1.3.

Table 1.3 Advantages and disadvantages of CO_2 sequestration methods

Methods	Advantages	Disadvantages
Adsorption	• Ripe technology • Flexibility • Fully automated operation of the process	• Low capacity of sorbents • High contaminants • High energy consumption • Large footprint
Absorption	• Ripe technology • Cheap, easily available, and tunable of solvent (amine)	• High energy consumption • High capital and operational costs • Large footprint • Evaporation of amine into gas stream • Required large amount of solvent
Cryogenic	• Ripe technology • CO_2, N_2 and H_2O can be separated in different parts of the process • No loss of CO_2 latent heat of fusion	• Complicated operation • High cost of heat exchanger • Take long time to reach the required condition • High energy consumption
Membrane -Solid -Liquid	• Simple operation • Compact • Long membrane life • Simple operation • Compact • High permeability of CO_2	• Low permeability of CO_2 • Short durability due to evaporation of liquid

(f) Ionic liquid membrane

Ionic liquid is a kind of molten salt at room temperature which contains bulky and asymmetric organic cation and inorganic or organic anion. Ionic liquid was discovered since 1914 by Welton [50]. In 1970s, Wilkes innovated nuclear warheads batteries and the space probes using some molten salts but the big problem was that the heat from such molten salts was able to destroy the equipment [51]. Therefore, ionic liquid was introduced to use as an electrolytes in batteries because it still maintains the liquid state at room temperature and high thermal conductivity. In addition, ionic liquids were employed for many applications as shown in Fig. 1.8 [50].

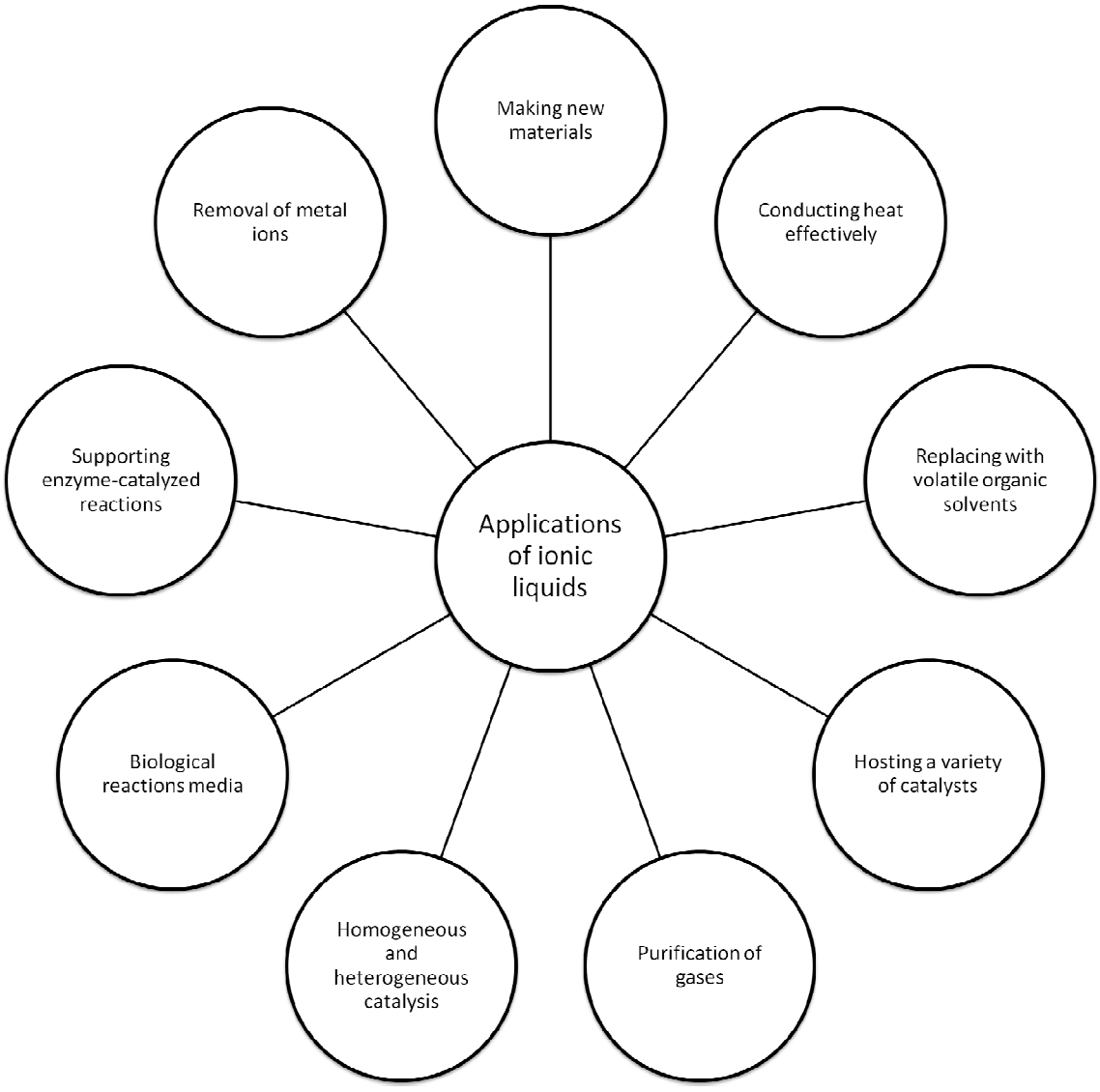

Fig. 1.8 Applications of ionic liquids

Ionic liquids have promoted to apply in the CO_2 separation process, due to the great solubility of CO_2 into the ionic liquids [52], green chemistry and neoteric solvents [53], high thermal stability, very low vapor pressure [54], non-flamable, renewable and reusable [55]. Therefore, ionic liquid was classified as a new alternative chemical for CO_2 sequestration. Some examples of chemical structures of ionic liquids are shown in Fig. 1.9. Table 1.4 shows physical properties of these ionic liquids.

(a)

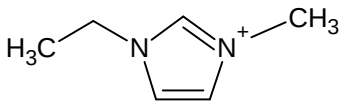

[emim]

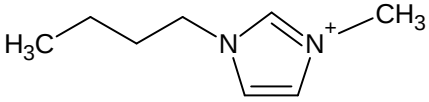

[bmim]

(b)

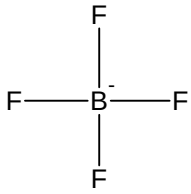

[BF_4]

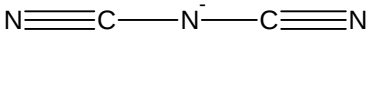

[dca]

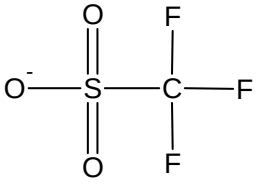

[OTf]

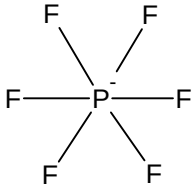

[PF_6]

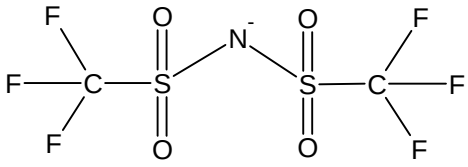

[Tf_2N]

Fig. 1.9 Chemical structures of (a) cation and (b) anions of ionic liquids in this study

Table 1.4 Physical properties of ionic liquids in this study at 303.15 K

Short name	IUPAC name	M (g mol^{-1})	T_m (K)	ρ (g cm^{-3})	η (cP)
[emim][BF_4]	1-ethtyl-3-methylimidazolium tetrafluoroborate	197.97	279.15 [56]	1.28* [57]	37* [57]
[bmim][BF_4]	1-butyl-3-methylimidazolium tetrafluoroborate	226.02	191.15 [56]	1.2 [57]	75 [57]
[bmim][PF_6]	1-butyl-3-methylimidazolium hexafluorophosphate	284.18	283.15 [57]	1.37 [57]	182 [57]
[bmim][Tf_2N]	1-butyl-3-methylimidazolium bis(trifluoromethylsulfonyl)imide	419.36	270.15 [57]	1.43 [57]	40 [57]
[bmim][OTf]	1-butyl-3-methylimidazolium trifluoromethanesulfonate	288.29	289.15 [56]	1.29 [58]	63 [59]
[bmim][dca]	1-butyl-3-methylimidazoliumdicyanamide	205.26	267.15 [60]	1.06 [61]	24 [61]

* At 293.15 K

The use of ionic liquid with supported membrane has started since 2002 by Branco et al [62]. They applied ionic liquid to hydrophilic polyvinylidine fluoride (PVDF) membrane in order to recover the liquid organic compounds.

In the same year, the attempt to study on gas separation using ionic liquid assisted with the supported membrane was investigated by Scovazzo et al [62, 63]. Gas separations of CO_2 from air, mixed gas including N_2 and CH_4 using supported ionic liquid membrane were reported [63, 64]. The first generation of anion species of ionic liquid for using as liquid membranes consist of $[Tf_2N]^-$, $[PF_6]^-$, $[Cl]^-$, $[OTf]^-$. Neves et al [52] examined gas permeation both pure and mixed gas of CO_2/N_2 and CO_2/CH_4 using ionic liquids and the flat type of hydrophobic and hydrophilic PVDF membranes. The stability of the hydrophobic membrane is higher than that of the hydrophilic. The ionic liquid membrane duration was successful over 100 days [65]. Kim et al [66] inspected the mechanism of the gas permeation by varying the pressure. They found that the permeability of gas by the facilitated transport was at 0.30 atm or less, whereas solution-diffusion theory took place at over 0.30 atm.

There are several methods to improve the efficiency of CO_2 separation through ionic liquid membranes such as the change of the membrane preparation and the addition of water in the separation system. Chen et al [29] studied a new membrane preparation by blending of PVDF powders with room temperature ionic liquid (RTIL), $[emim][B(CN)_4]$. The ratios of PVDF–RTIL were varied. The results imply that their membrane preparation method was more success than the use of miscible ionic liquid based blends. The ratio of PVDF–RTIL (1 : 2) gave the highest CO_2 single gas permeability and selectivity. Li et al [1] reported that a new material for CO_2/N_2

separation process is the use of poly(RTIL)–RTIL composites. Two types of composites i.e. poly([vbim][dca])–[emim][dca] (1 : 2) and poly([vbim][dca])–[emim][$B(CN)_4$] (1 : 2) shows the best CO_2/N_2 mixed gas separation performance. The attempt to develop the CO_2 separation efficiency has not only the adjustment of ionic liquid species, membrane materials and liquid membrane preparation technique, but also the reconsideration of water in the system. Other researchers [67] have examined the additional water in amino acid ionic liquid membrane. The results pointed out that the great CO_2 permeability from CO_2/N_2 pairs gas was obtained from tetrabutylphosphonium proline membrane. Hence, the presence of water has a vital influence on the permeability of CO_2.

From overall point of view, to deeply understand the whole process of CO_2 separation using ionic liquid membrane, the important operating conditions which considerably affect CO_2 permeability should be clearly investigated by mean of both actual experimental and simulation. Thus, this dissertation would like to report both experimental and simulated results in order to extend the knowledge of such separation process with focusing on ionic liquid membrane. Furthermore, these results would be useful not only for research and academic area but also for pilot plant construction as a preliminary direction guide as well.

1.3 Objectives of this research

1.) Preliminary study of CO_2 recovery from air using amine/glycol solution as a liquid membrane.

2.) Study the effect of temperature and anion species on CO_2 permeabilities and selectivities through ionic liquid membrane and discuss based on solution-diffusion theory.

3.) Investigate the operating conditions: pressure, CO_2 concentration, total flow rate at feed stream that affect CO_2 permeabilities and selectivities, using facilitated transport to explain the phenomena.

4.) Determine the impact of the presence of water in ionic liquid membranes on CO_2 permeabilities through ionic liquid membrane and interpret in term of permeation mechanism.

5.) Designs the membrane area, estimate the reduction of membrane size and predict the CO_2 concentration at permeate side in order to apply for the CO_2 separation process.

1.4 Contents of dissertation

Chapter 2 talks about the preliminary study of CO_2 permeability mechanism through liquid membrane using amine mixed with glycol solution with the flat type of membrane module. CO_2 is removed from air with the starting concentration of 400 ppm. Amine used in this study is diglycolamine (DGA). The glycols consist of ethylene glycol (EG), triethyleneglycol (TEG), polyethylene glycol 200 (PEG200) and polyethylene glycol 400 (PEG400). The membrane durability, amine concentration and molecular structures of the amine components are investigated in terms of the CO_2 concentration ratio.

Effects of temperatures and anion species of ionic liquid on CO_2 permeabilities and selectivity are investigated. Six species of ionic liquid: 1-ethtyl-3-methylimidazolium tetrafluoroborate ([emim][BF_4]), 1-butyl-3-methylimidazolium tetrafluoroborate ([bmim][BF_4]), 1-butyl-3-methylimidazolium bis(trifluoromethylsulfonyl)imide ([bmim][Tf_2N]), 1-butyl-3-methylimidazolium hexafluorophosphate ([bmim][PF_6]), 1-butyl-3-methylimidazolium trifluoromethanesulfonate ([bmim][OTf]) and 1-butyl-3-methylimidazolium dicyanamide ([bmim][dca]) are used in this study. The microporous polyvinylidene fluoride (PVDF) and polytetrafluoroethylene (PTFE) membranes are tested for the appropriate gel structure with the ionic liquids. The CO_2 permeabilities are discussed by solution-diffusion theory. All of these are presented in Chapter 3.

Chapter 4 focuses on total pressure difference, CO_2 concentration and total feed flow rate of the mixed gas CO_2/N_2 resulting in CO_2 permeability and selectivity. Our main material for this section is two species of ionic liquids: [bmim][PF_6] and [bmim][Tf_2N], which give the lowest and highest CO_2 permeabilities, respectively. Temperature was kept constant at 313.15 K for all experiments. Total pressure difference is changed from 0.05 to 0.21 atm. CO_2 volume fraction is varied from 0.3 to 0.5. Feed flow rates of the mixed gas are 100 and 300 ml min^{-1}. CO_2 permeation is explained by facilitated transport.

CO_2 permeabilities through ionic liquid membrane with the presence of water vapor are examined in Chapter 5. This Chapter still uses [bmim][PF_6]and [bmim][Tf_2N] as the liquid membranes. The experimental results of the CO_2 permeabilities obtained from dry feed stream in Chapter 3 are compared with the results in this Chapter. The effects of water vapor at feed and permeate side on CO_2 permeabilities are discussed in

term of the permeation mechanism based on the solution-diffusion theory. The water permeabilities are also examined.

In order to reduce the investment cost of CO_2 removal process using ionic liquid membrane in the real industries, the computational simulation is always necessary to be performed before starting construction of removal process unit. In simulation step, there are also, however, still need some input data from actual experiment. It is well known that such input data play a key effect on CO_2 permeabilities demonstrated in Chapters 3 to 5. Typically, these input data are experimentally obtained by varying certain parameters, for example, temperature, pressure, CO_2 concentration, anion species of ionic liquid, and total flow rate at feed side. Consequently, the required membrane area, the percent reduction of membrane size as well as target amount of CO_2 at permeate side shown in Chapter 6, are predicted by the mean of computational simulation using the as-mentioned input data. By this mean, an insight-understanding in CO_2 separation process would be developed with a one-step progress for a practical implementation for real industries in the near future.

Overall results of each Chapter are summarized in Chapter 7. The recommendation points for future study are discussed.

The overall content of dissertation is illustrated in Fig. 1.10

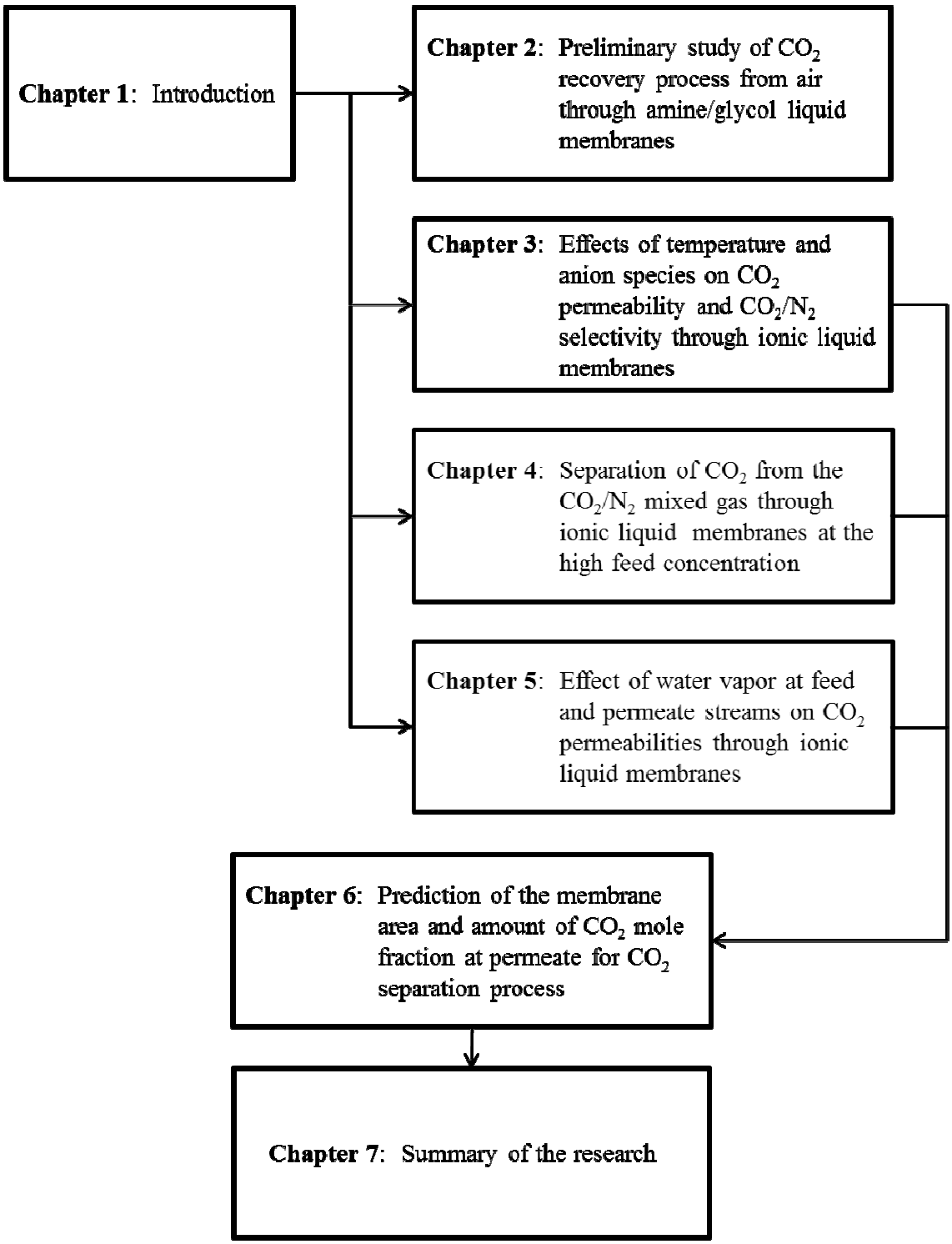

Fig. 1.10 Content of dissertation

Chapter 2

Preliminary study of CO_2 recovery process from air through amine/glycol liquid membranes

2.1 Statement of problem and objectives

To preliminary study the CO_2 separation process through liquid membranes, the use of amine/glycol as the liquid impregnated with microporous membrane is quite attractive. Since amine is a well-known chemical for capture CO_2 emissions from power plants and factories. Novel separation processes are expected to be developed in addition to the conventional absorption process using aqueous amines. A membrane process is counted on a new separation process for CO_2 capture from flue gases, especially a liquid membrane with amines because of its high selectivity for the CO_2 gas. Another application field of CO_2 membrane separation exists, that is removing CO_2 from the air and utilizing it. Because the CO_2 concentration in atmospheric air is 400 ppm or 0.04%, CO_2 separation based on a facilitated transport mechanism has an advantage for this application. If an energy-effective membrane process is developed for CO_2 removal from air, the captured CO_2 will be used for the forced culture of vegetables or strawberries in greenhouses.

In this study, the amine liquid membranes with various glycol compounds were used for the CO_2 separation from atmospheric air [26]. CO_2-enriched air was made by a membrane process using a flat membrane module with an amine-liquid membrane. The liquid membrane durability, amine concentration and molecular structures of the amine components on the CO_2 permeabilities were investigated.

2.2 Experimental

2.2.1 Liquid membrane and membrane preparation

The composition of the liquid membrane was a liquid amine dissolved in liquid glycol. The amine component was mainly diglycolamine (DGA), and the glycols were ethylene glycol (EG), triethyleneglycol (TEG), polyethylene glycol 200 (PEG200) and polyethylene glycol 400 (PEG400). All chemicals were purchased from Wako Pure Chemical Industries, Ltd., Japan. A liquid membrane was made by soaking a thin microporous membrane in the amine/glycol mixture. This liquid-supporting membrane was a polytetrafluoroethylene (PTFE) microporous sheet with a nominal thickness of 2 μm and a porosity of 80%, which was made hydrophilic by treatment with polyvinyl alcohol as a surfactant [68]. The amine/glycol mixture easily penetrated into the microporous sheet. The thickness of the liquid membrane could be estimated from the liquid amount held in the sheet. For example, when 1.4 g of the liquid was applied, the liquid membrane thickness was 19 μm.

The liquid membrane was placed on a hydrophobic microporous membrane with a 0.2 μm pore size and 95 μm thickness (Durapel membrane, Millipore). The amine/glycol liquid with a high surface tension was supported on the surface of the hydrophobic membrane under a transmembrane pressure condition because of the repellency of the membrane material to the liquid. This construction allows the liquid membrane to undergo vacuum-mode permeation [69]. The top surface of the liquid layer was then covered by a PTFE microporous membrane with a 0.5 μm pore size and 35 μm thickness. This sheet also repels the membrane liquid. The top of the cover

membrane faced the room air flow. This 3-layered construction of the liquid membrane will make the liquid membrane thin with a uniform thickness.

The body of a flat membrane module was made of a polypropylene (PP) porous plate and an aluminum frame. The porous plate was used to minimize the pressure loss of the permeate side flow. The liquid membrane was placed on top of the plate and kept in a horizontal position. The membrane area was 650 cm^2 (25.5 cm × 25.5 cm). The details of the membrane module were described in our previous report for the dehumidification of air [70]. The chemical structure of microporous membrane, amine and glycol solutions are shown in Fig. 2.1.

(a)

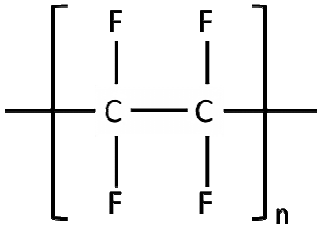

PTFE

(b)

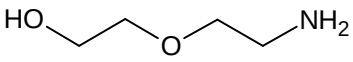

DGA

(c)

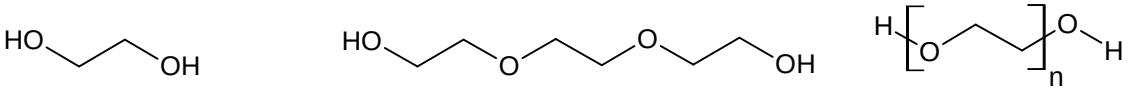

EG TEG PEG

Fig. 2.1 Chemical structures of, (a) PTFE, (b) DGA, (c) glycols

A schematic diagram of the experimental apparatus for the CO_2 recovery from air is shown in Fig. 2.2. One permeate-side port of the membrane module was connected to a diaphragm vacuum pump (DP-12, ULVAC Corp., Japan). The sweep air flowed through the permeate side from an intake port at the flow rate of F_p. The permeate side of the liquid membrane was evacuated using a diaphragm vacuum pump at the pressure, p_p. The permeate side pressures were 5.3-15.8 cmHg, which depended on the sweep air flow rate, F_p. The permeate-side pressure (p_p) slightly changed from the inlet to the outlet, for example, 17.3 cmHg at inlet and 13.5 cmHg at the outlet due to the pressure loss through the permeate-side path. The average value was used for p_p in this study. The air flow rate at the permeate side, F_p, was treated as a constant, because of the small permeation rate of the air and CO_2.

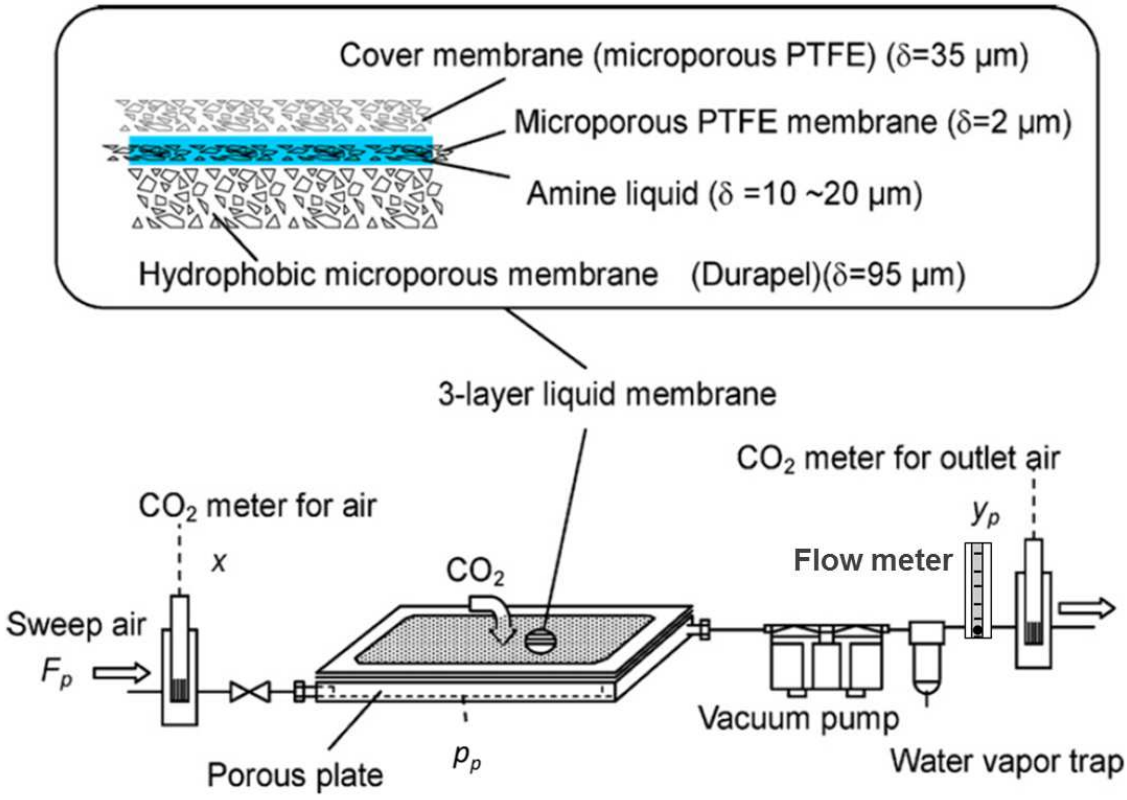

Fig. 2.2 The membrane construction and the CO_2 recovery apparatus.

Because the present hydrophilic liquid membrane could allow water vapor in the air to simultaneously permeate, a water vapor trap was used to remove it from the outlet air before measuring the CO_2 concentration, y_p. The CO_2 concentrations in the air and the outlet sweep air were monitored by CO_2 transmitters (GMT220, Vaisala Oyj, Finland). The experimental conditions were room temperature, 297.15 to 299.15 K, 40 to 60 %RH humidity and atmospheric pressure, p_f. The humidity in the air was proven to have a negligible effect on the CO_2-permeability of the DGA liquid [24] under ambient conditions. All the permeation tests for different mixed liquids were conducted over 24 h, and the CO_2 concentration results were averaged over this period. The absorption equilibrium was also measured between the amine liquid and CO_2 at a 400 ppm concentration. The absorption amount of CO_2 was measured using a magnetic suspension balance (FMS-LP, RUBOTHERM, Germany). The viscosities of the liquid mixtures were measured by a vibro viscometer (SV-10, A&D Company, Ltd.).

2.2.2 CO_2 recovery process from air

Fig. 2.3 is a schematic explanation of the present CO_2 recovery process from air. The concentration of CO_2 in air, x, was about a 0.0004 mole fraction. When the sweep air flow was F_p = 1 L min^{-1} = 682 × 10^{-6} mol s^{-1}, the permeate-side pressure, p_p, was 15 cmHg. Under this typical condition, the permeation rate of CO_2 was 0.55 × 10^{-6} mol s^{-1}. On the other hand, the air permeation rate through the liquid membrane was 0.34 × 10^{-6} mol s^{-1}. At the outlet of the vacuum pump, the total CO_2 flow rate was 0.82 × 10^{-6} mol s^{-1} in the outlet air and y_p = 0.0012. This means that the CO_2 concentration ratio (y_p/x) is 3. The maximum attainable concentration ratio will reach the pressure ratio of p_f/p_p = 5.

This process had a 60 %efficiency for CO_2 recovery compared to a process with an infinite membrane area.

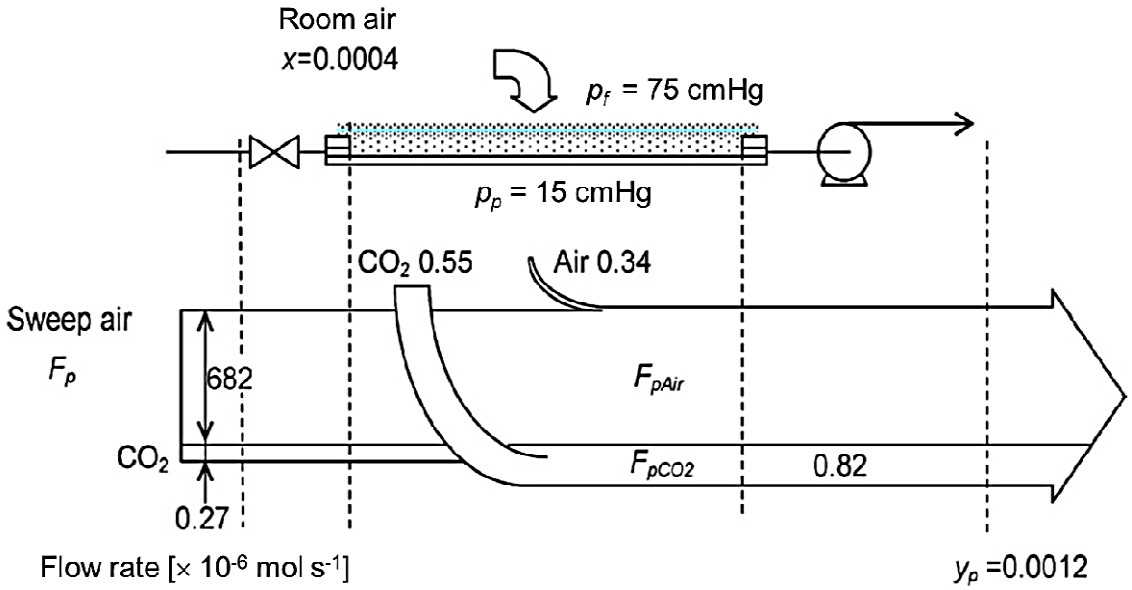

Fig. 2.3 Flow of air and CO_2 through the membrane module (F_p= 1 L min^{-1} = 682 × 10^{-6} mol s^{-1})

2.2.3 Determination of CO_2 permeability

In our membrane module, the thickness of the liquid membrane, δ, could be calculated from the amount of applied liquid. Using the membrane thickness, area and partial pressures across the membrane, the gas permeability was defined and estimated as a characteristic of the membrane liquid. A model calculation was used for estimation of the permeability of CO_2 through the amine liquid membrane, Q_{CO2} , as follows:

The CO_2 flow rate on the permeate side, F_{pCO2}, is described by the permeability, Q_{CO2}, and the partial pressure difference.

$$\frac{dF_{pCO2}}{dA} = \frac{Q_{CO2}}{\delta}\left(xp_f - yp_p\right) \tag{2.1}$$

$$y = \frac{F_{pCO2}}{F_{pAir} + F_{pCO2}} \tag{2.2}$$

where F_{pAir} is the flow rate of the sweep air on the permeate side. A is the membrane area in cm^2, and Q_{CO2} is the permeability of CO_2 in cm^3(STP)cm cm^{-2} s^{-1} $cmHg^{-1}$ x and y are the feed and permeate-side CO_2 mole fractions, respectively. p_f and p_p are the pressure on the feed (atmospheric pressure) and permeate sides in cmHg, respectively. Integration of Eq. (2.1) from A = 0 (inlet) to $A = A_0$ (outlet) results in the CO_2 concentration in the outlet air, y_p. Q_{CO2} for a liquid membrane can be estimated as a fitted value to an experimental result of y_p. Once the permeability of a liquid membrane is assigned, the model will predict the separation performance of the process under other operating conditions.

2.3 Results and discussion

2.3.1 CO_2 concentration in the sweep air

The experimental results for a liquid membrane of DGA 50%/TEG (19 μm thickness) are shown in Fig. 2.4a. When the average CO_2 concentration in the ambient air was 0.00042 in mole fraction, the CO_2 concentration in the outlet air, y_p, was 0.00123 at F_p = 1 L min^{-1}. The CO_2 concentration, y_p, increased with the decreasing sweep air flow rate, F_p, because the CO_2 permeation rate was not significantly changed by the air flow rate.

The solid line stands for the permeability of $Q_{CO2} = 1.8 \times 10^{-6}$ cm^3(STP)cm cm^{-2} s^{-1} $cmHg^{-1}$. This permeability value for the liquid membrane is greater than that of the polymer membranes, for example, a silicone rubber membrane (Q_{CO2} = 1.5 × 10^{-7}

cm^3(STP)cm cm^{-2} s^{-1} $cmHg^{-1}$). On the other hand, based on another air permeation measurement, the permeability of air through the liquid membrane was determined to be 4.33×10^{-10} cm^3(STP)cm cm^{-2} s^{-1} $cmHg^{-1}$. The separation factor of CO_2 over air was 4100 for the DGA 50%/TEG liquid membrane.

The dashed line in Fig. 2.4a is the calculation for an infinite membrane area ($A = \infty$). Our membrane module with A_0 = 650 cm^2 attained over a 60% performance for a maximum CO_2 recovery due to the high CO_2 permeability through the amine liquid membrane.

Fig. 2.4b presents the enhancement of pressure at permeate side with the increase in sweep air flow rate.

Fig. 2.4c shows the CO_2 recovery rate of the process, $F_p(y_p - x)$. The present membrane process showed a 0.08 g-CO_2 h^{-1} recovery from air. For comparison, the electric power of the vacuum pump, 30 W, corresponds to 12 g-CO_2 h^{-1} emission. The absolute efficiency of the CO_2 recovery from air was still low using the present membrane process.

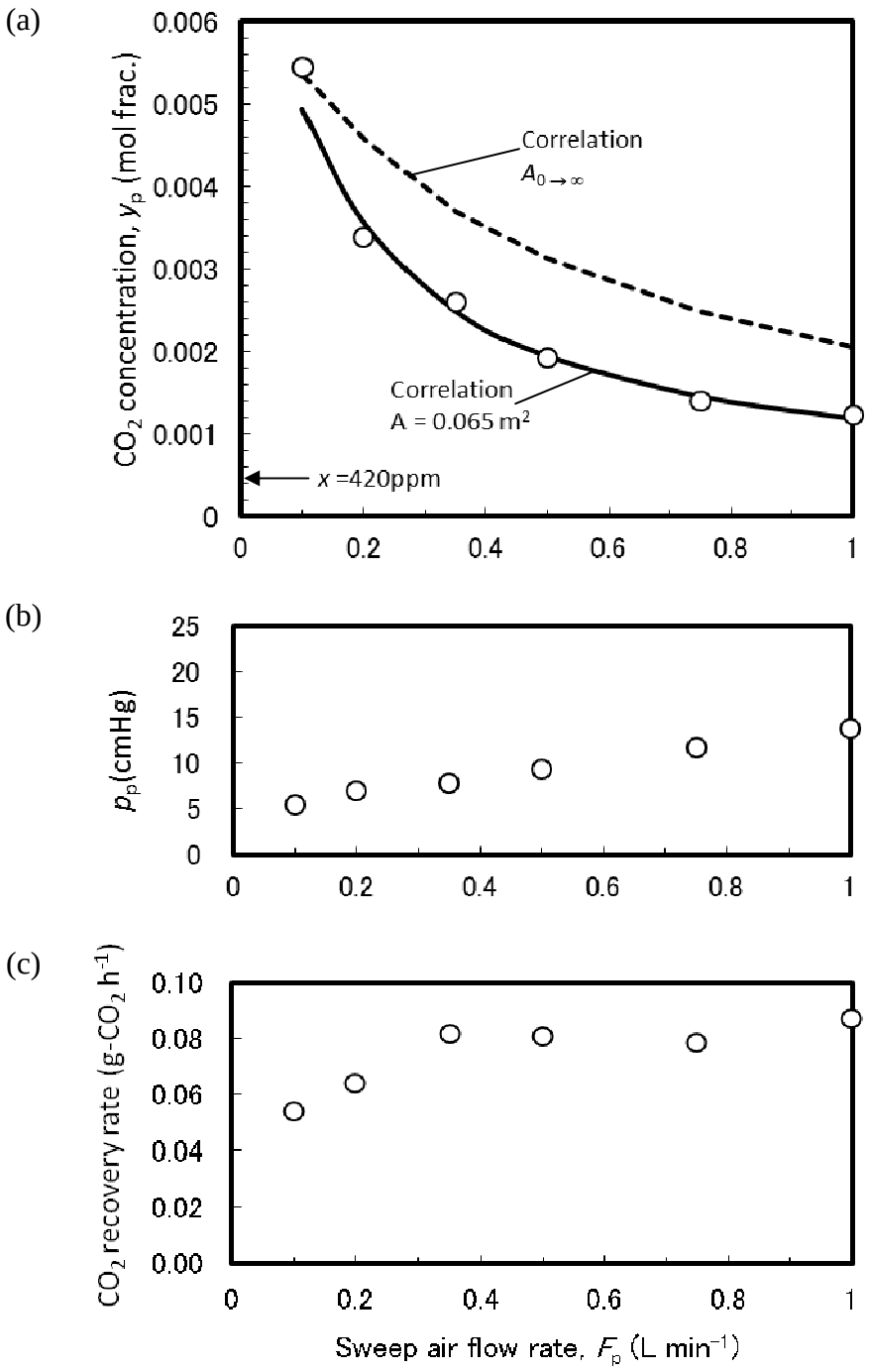

Fig. 2.4 CO_2 concentration in the outlet air and the model calculation for Q_{CO2} = 1.8 × 10^{-6} cm^3(STP)cm cm^{-2} s^{-1} $cmHg^{-1}$ for DGA 50%/TEG liquid membrane (T = 297.15 to 299.15 K).

Fig. 2.5 shows other experimental results where the sweep air was replaced with pure N_2 gas of zero CO_2 concentration. Compared to the data in Fig. 2.4a, the CO_2 concentration, y_p, was reduced by 0.0004 over the whole range, which contained CO_2 in the inlet sweep air. The correlated result with the same permeability as Fig. 2.4a also agrees with the experimental results.

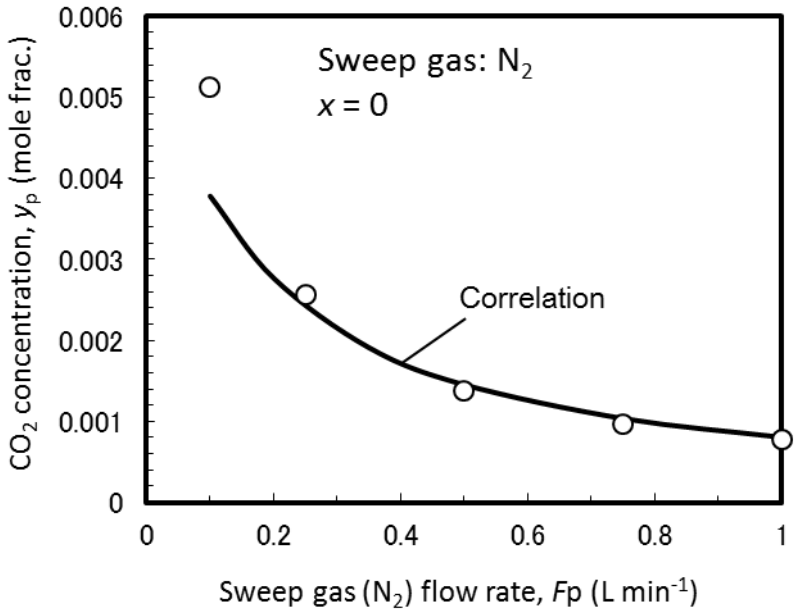

Fig. 2.5 CO_2 concentration in the outlet flow with nitrogen as sweep gas at the permeate side for DGA 50%/TEG liquid membrane (δ = 19 μm, T = 297.15 to 299.15 K).

Because a liquid membrane inherently has a limited lifetime, the durability of the amine/glycol liquid membranes was examined with different components. Three kinds of liquids were used for a long run time, which were DGA/EG (50:50 wt%), DGA/PEG400 (82:18 wt%) and MEA/PEG400 (50:50 wt%) mixtures. The results are shown in Fig. 2.6 for the CO_2 concentration ratio (y_p/x) versus operating time. The

liquid membranes with PEG400 as the solvent showed no air leak for over 10 days because it is a non-volatile solvent with a boiling point (T_b) of 523.15 K. However, the CO_2 separation performance of MEA/PEG400 decreased within 24 h, which was due to the vaporization of the volatile MEA liquid with T_b = 444.15 K. When the volatile EG (T_b = 470.15 K) was used for the solvent, the liquid membrane was only durable for 24 h. The liquid mixture of both relatively non-volatile components, DGA (T_b = 493.15 K)/PEG400, showed a durability of over 10 days and retained its CO_2 separation performance. A slightly decreasing CO_2 concentration ratio may be attributed to the partial vaporization or degradation of the DGA.

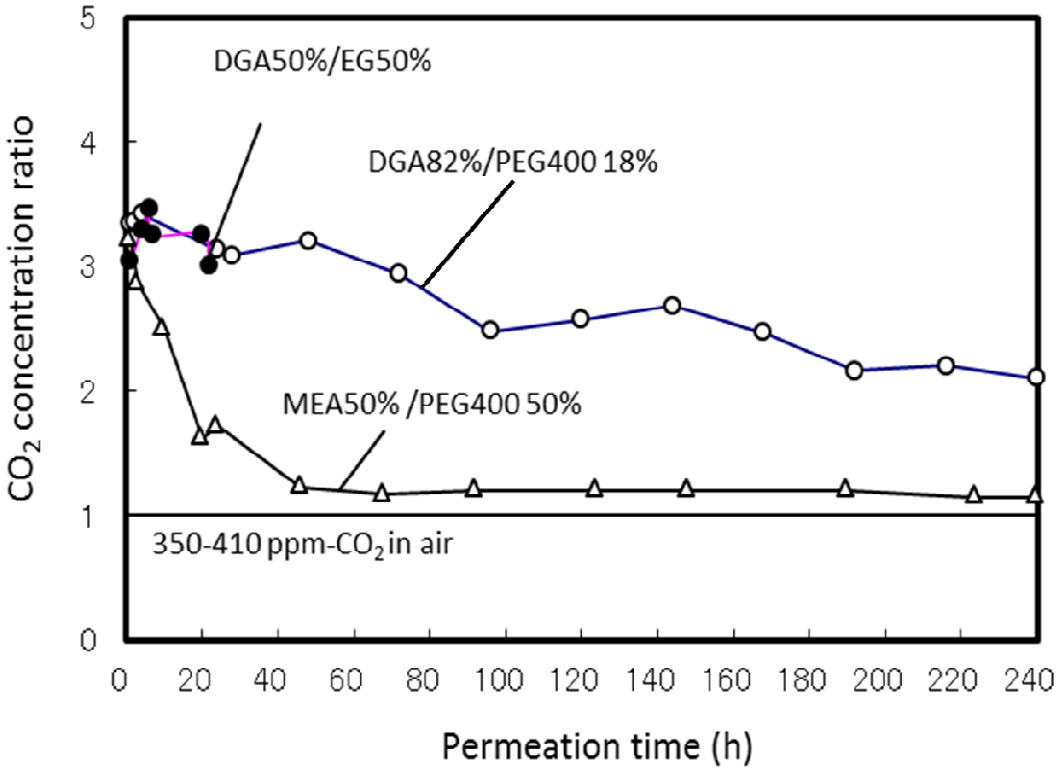

Fig. 2.6 Durability of the liquid membranes (δ = 19 μm, p_l = 15 cmHg, F_p = 1 L min^{-1}, T = 297.15 to 299.15 K).

2.3.2 Effect of amine components

The ability for CO_2 capture by an amine liquid varies with its chemical structure [71]. Alkanolamines other than DGA were used in the liquid membrane with a 50% TEG solution. Fig. 2.7 shows the CO_2 concentration ratio in the module outlet air and the resulting permeability for liquid membranes with different amine species. The primary amines, monoethanolamine and 3-amino-1-propanol, provided a high CO_2 permeability comparable to that of DGA. The secondary and tertiary amines had a lower CO_2 permeability. In the additional tests, an amino acid (glycine) solution also shows a rather high permeability for CO_2, the result of which is similar to that reported by Matsumiya et al [72].

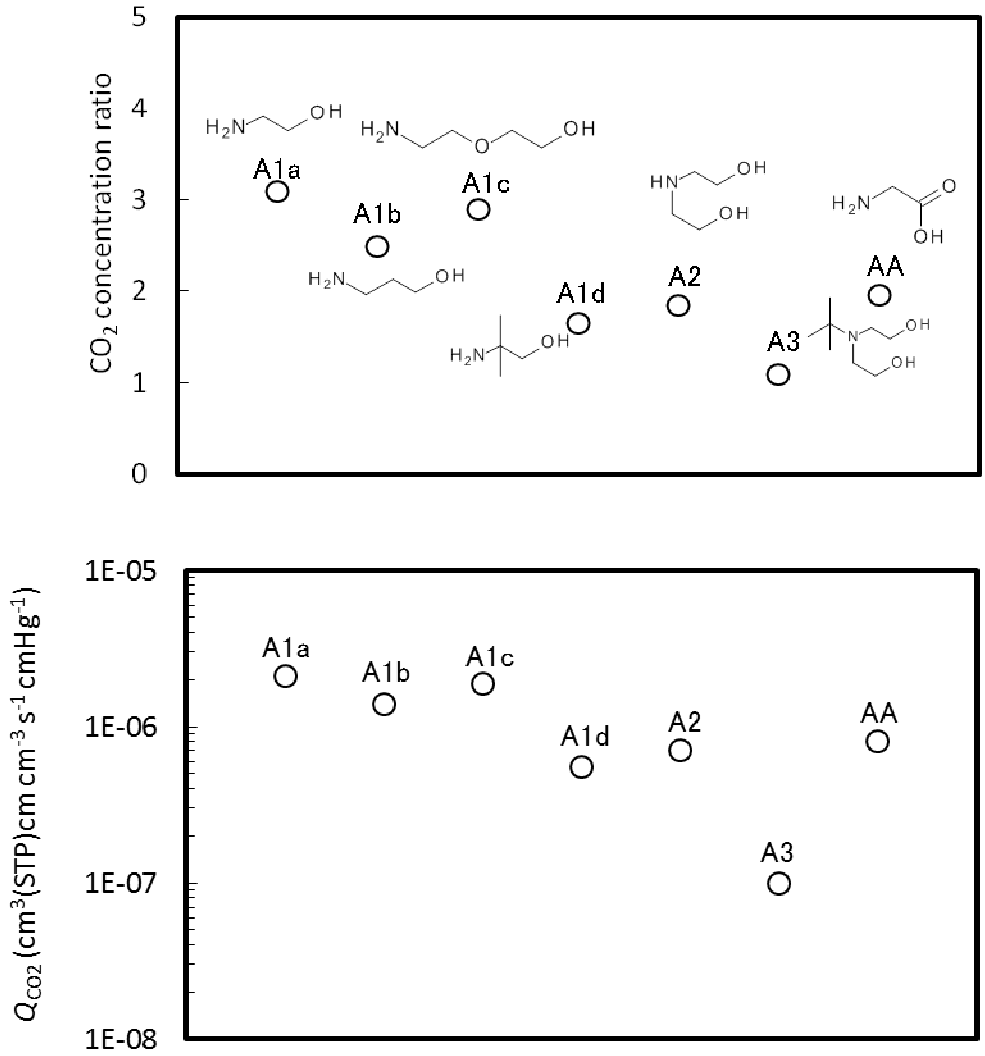

Fig. 2.7 Permeability of CO_2 through amine liquid membranes of 50 wt% solution in TEG (δ = 18-20 μm, F_p = 1 L min^{-1}, x = 0.0004, T = 296.15 to 299.15 K), (A1a) monoethanolamine, (A1b) 3-amino-1-propanol, (A1c) diglycolamine, (A1d) 2-amino-2-methyl-1-propanol, (A2) diethanolamine, (A3) N-t-butyldiethanolamine, (AA) glycine (glycine 50%/potassium hydroxide 50%).

An extensive study of various aqueous alkanolamines had been reported on the CO_2 absorption/desorption properties [71]. Their experimental results show that the CO_2

loading capacity and absorption rate of the alkanolamines were in the order of primary alkanolamines > secondary alkanolamines > tertiary alkanolamines. Our permeability results showed a similar trend, which means that the CO_2 loading capacity and absorption rate determine the permeability of amine liquid membranes.

2.3.3 Correlation consideration for CO_2 permeability

A basic equation for the permeability through a non-porous membrane is the solution-diffusion mechanism:

$$Q = CD \tag{2.3}$$

where Q is the permeability coefficient in cm^3(STP)cm cm^{-2} s^{-1} $cmHg^{-1}$, C is the solubility coefficient in cm^3(STP) cm^{-3} $cmHg^{-1}$, and D is the diffusion coefficient in cm^2s^{-1}. The solubility coefficient and the diffusivity depend on the solubility of the gas and the viscosity of the membrane material, respectively. The special feature of the liquid membrane is that these properties are measurable and could be changed by the composition.

For the first consideration, the effect of the liquid viscosity was examined. By selecting a glycol component between EG through PEG400, the viscosity of liquid membranes with 50% DGA increased from 30 to 61 mPa s. The permeation results using these liquid membranes are shown in Fig. 2.8. In general, the diffusion coefficient of a molecule will be inversely proportional to the liquid viscosity. The experimental results, however, showed that the liquid viscosity had a small effect on the CO_2 permeability.

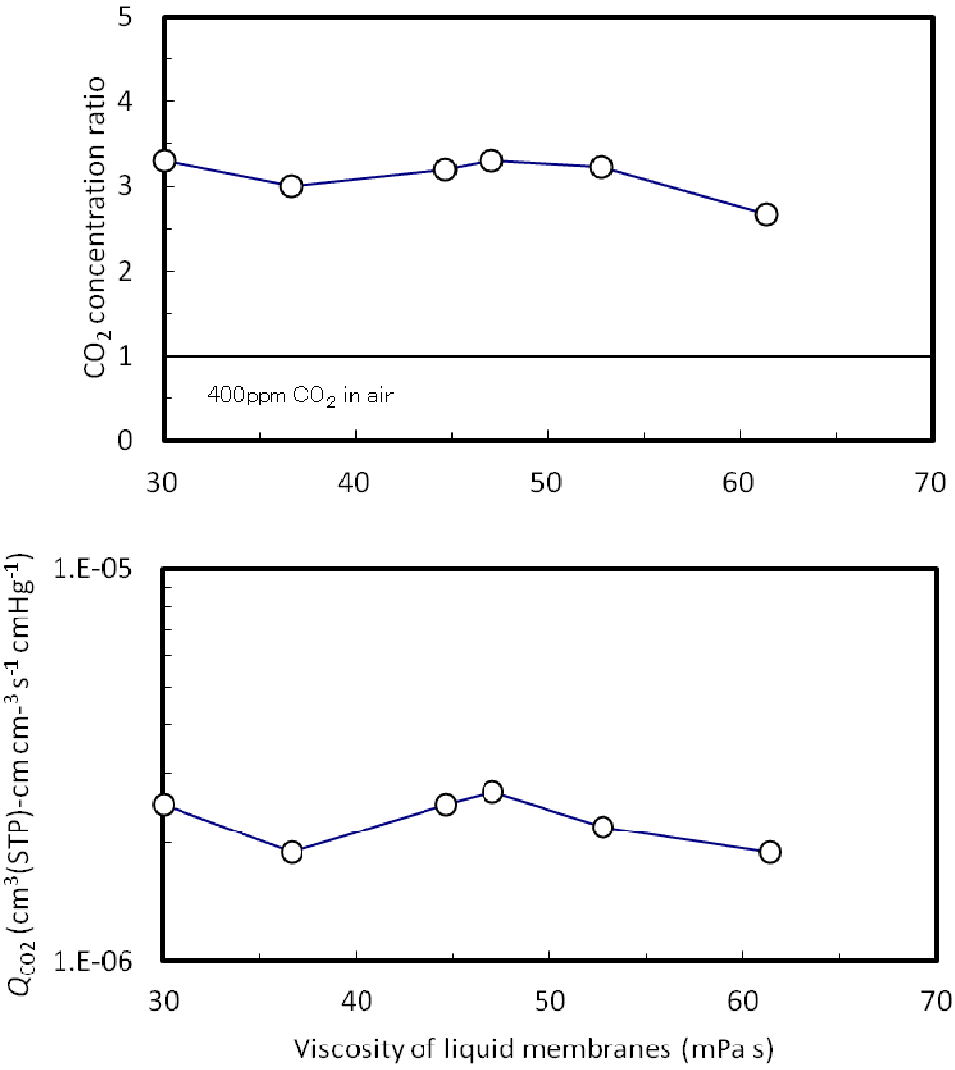

Fig. 2.8 Effect of viscosity of the liquid at 298.15 K on the permeability of CO_2 through DGA liquid membranes of 50 wt% solution in glycols.

For the second consideration, the effect of the solubility of CO_2 was examined. Membrane liquids of different DGA contents, 7 to 88 wt%, in glycols were prepared, while the viscosity of these liquids were fitted to a nearly constant 36 to 38 mPa s using the appropriate glycol solvents or mixtures. In Fig. 2.9c, the CO_2 sorption of the liquids

is shown, which was at equilibrium at 0.0004 CO_2 in 76 cmHg N_2. The CO_2 sorption amount was nearly proportional to the DGA mass fraction in the liquid. The average solubility in the amine-mol base was 0.2 mol-CO_2/mol-amine. This solubility is rather high for a low CO_2 partial pressure of 400 ppm or 0.003 cmHg. Fig. 2.9a and b depicts the CO_2 concentration ratio and the calculated permeability for each DGA/glycol liquid membrane. The permeability increases with the amine concentration in the liquid. This indicates that the CO_2 permeation rate depends on the molar density of the amine molecule in the liquid.

Finally, the permeability was compared by the solution-diffusion theory, Eq. (2.3). The diffusion coefficient, *D*, could be readily estimated by the Wilke-Chang equation [10]. The association factor in this study was unity. The calculated diffusion coefficient of the DGA molecule in a glycol liquid with a viscosity of 36 mPa s was $D = 8.06 \times 10^{-7}$ cm^2 s^{-1}. The solubility coefficient for a 50 wt%-DGA liquid was $C = 670$ cm^3(STP) cm^{-3} $cmHg^{-1}$. These values determine the permeability in the solution-diffusion model of $Q = CD = 5.4 \times 10^{-4}$ cm^3(STP)cm cm^{-2} s^{-1} $cmHg^{-1}$. The permeability based on the model is shown in Fig. 2.9b by the dashed line. Compared to the experimental results (solid line), the correlation well predicts the dependence on the amine concentration but fails to predict the absolute permeability value. The permeability data for CO_2 was 1/100 of that by the correlation. Because the solubility coefficient was directly measured, the difference between the correlation and the data is attributed to the uncertain diffusion coefficient. In the amine–liquid membrane, the dissolved CO_2 molecule will associate with an amine molecule as a carrier [73]. The association of CO_2 and the amine molecule will increase the molecular weight of the diffusion species and the viscosity of the liquid. These effects, which are phenomena

specific to facilitated transport, will cause a decreasing diffusion coefficient of the permeate.

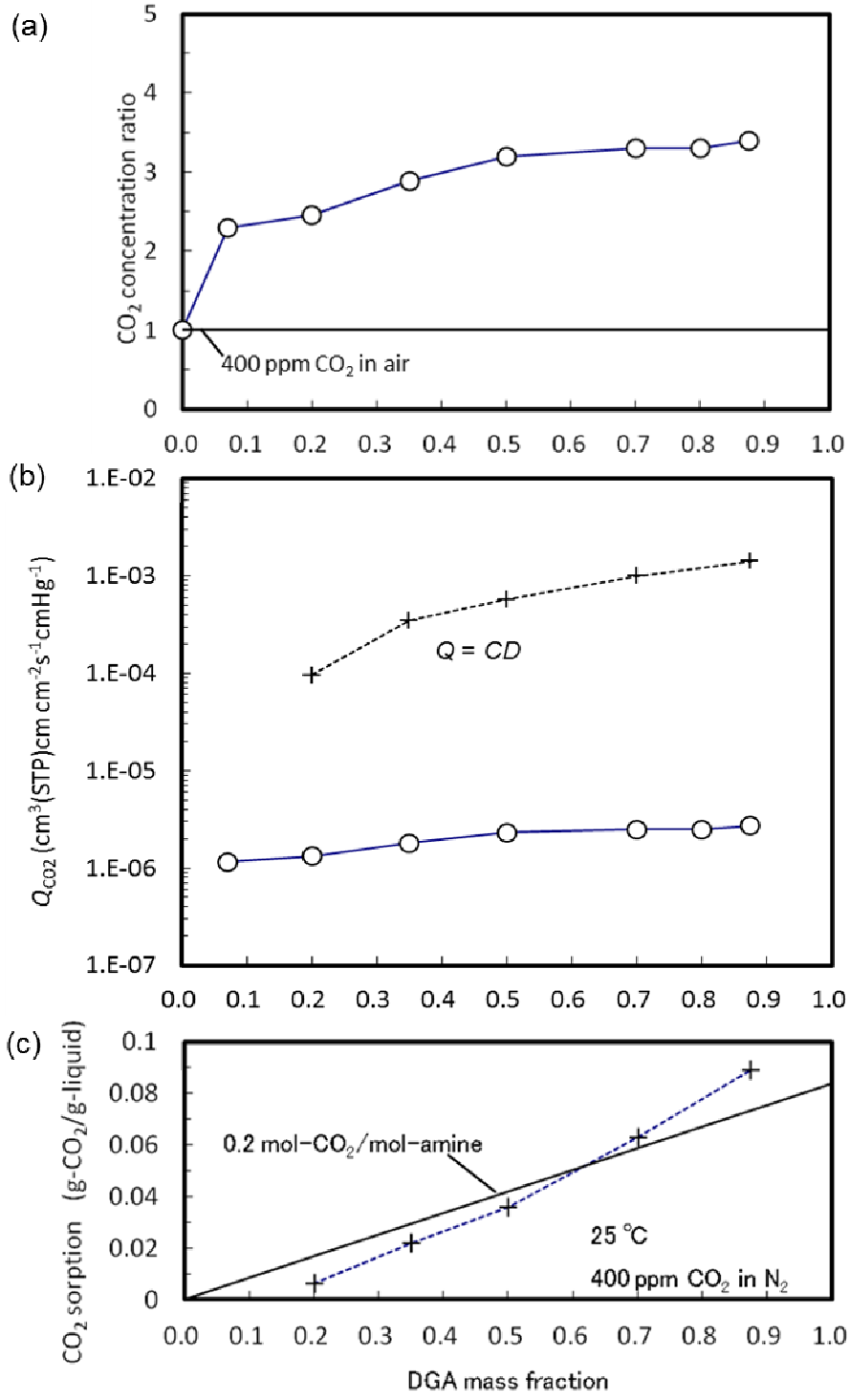

Fig. 2.9 Effect of amine concentration on CO_2 permeability (liquid viscosity = 36 to 38 mPa s, δ = 19 μm, p_l = 15 cmHg, F_p = 1 L min^{-1}, T = 296.15 to 299.15 K)

For a further discussion on the facilitated transport, a more exact correlation must be considered by including the reaction kinetics between CO_2 and an amine [25, 73]. For example, the permeability of CO_2 through an aqueous MEA liquid membrane was reported by Gorji and Kaghazchi [25]. They successfully predicted the permeability using a diffusion-reaction analysis based on the reaction rates between CO_2 and the amine. Their experimental and predicted permeability significantly depends on the CO_2 partial pressure. An extrapolation of their CO_2 permeability through the aqueous MEA liquid membrane to our low atmosphere level, x = 0.0004, was made. The estimated permeability was compared to that of the MEA/TEG 50% liquid membrane in this study in Table 2.1. In spite of differences in amine concentration and membrane thickness in these liquid membranes, the CO_2 permeabilities are similar. This diffusion-reaction analysis [25] gives a much better prediction than the simple solution-diffusion model. The CO_2 recovery process from air by the amine liquid membrane should be theoretically treated based on the diffusion-reaction analysis.

Table 2.1 Permeabilities of CO_2 through supported liquid membranes with monoethanolamine (MEA) at 298.15 K and 0.03 cmHg-CO_2 partial pressure.

Liquid membrane	MEA/Water	MEA/TEG (this work)
Membrane thickness (μm)	125	20
Liquid viscosity (mPa s)	1.2	39
MEA concentration (mol L^{-1})	1	8.7
Permeability of CO_2 (cm^3(STP)cm cm^{-2} s^{-1} $cmHg^{-1}$)	$8.9 \times 10^{-6*}$	2.1×10^{-6}

*Extrapolated from the theoretical value in 0.5–13.4 cmHg-CO_2 partial pressure.

2.4 Conclusions

An amine/glycol mixed liquid membrane was used for the recovery of CO_2 from atmospheric air. A supported liquid membrane of a diglycolamine/triethylene glycol mixture with a 19 μm thickness was sandwiched by hydrophobic microporous membranes. Using a flat membrane module of the liquid membrane, CO_2 in the air was recovered by vacuum-mode permeation of the sweep air.CO_2 in the air preferentially permeated through the liquid membrane and was concentrated into the sweep air. The durability and separation performance of a liquid membrane depended on the selection of the amine and the glycol component. The effects of amine concentration and different amine species were significant on the CO_2 permeability of the amine–liquid membrane. The simple solution-diffusion theory for the permeability predicted the amine-concentration dependence but the predicted value was much greater than the data.

Chapter 3

Effects of temperature and anion species on CO_2 permeability and CO_2/N_2 selectivity through ionic liquid membranes

3.1 Statement of problem and objectives

According to the previous experiment using an amine/glycol as a liquid membrane, the experimental results show that the amine-based liquid membranes were successful to capture CO_2 from air. However, the results of the durability test demonstrated that the amine liquid membranes were effective the longest performance about 10 days because of the vaporization of liquid into air. Ionic liquids, novel chemicals for CO_2 separation process, have been used as a liquid membrane in this study. The ionic liquids have been promoted to be the superb alternatives for CO_2 separation process since the unique physical properties of ionic liquids, such as a low vapor pressures and miscibility with polar or non-polar solvents. These excellent properties especially, the very low vapor is expected to prevent the problem of the solvent evaporation from the supported liquid membrane. For CO_2 separation process, it is important to understand the fundamental properties of ionic liquid and supported membrane and the major parameters that influence on CO_2 permeability and selectivity.

In this work, two types of porous membranes were tested for suitability of liquid membrane preparation [27]. The effects of temperature and anion species on CO_2 permeability through ionic liquid membranes were also investigated. The permeability was measured by a sweep gas method at T = (303.15 to 343.15) K. Six species of ionic liquids with imidazolium cation were used for the permeability measurements. A solution-diffusion theory is applied for the discussion of the contributions of solubility and diffusion coefficients of CO_2 with the temperature dependence on the permeability through ionic liquid membranes. The selectivity between CO_2/N_2 mixed gas with CO_2 0.1 volume fraction through the ionic liquid membranes was also determined. The effects of temperature and anion species on the values of selectivity were investigated.

3.2 Experimental

3.2.1 Materials

Ionic liquids, 1-ethtyl-3-methylimidazolium tetrafluoroborate ([emim][BF_4], 95% purity) and 1-butyl-3-methylimidazolium bis(trifluoromethylsulfonyl)imide ([bmim][Tf_2N], 96% purity) were purchased from Kanto Chemical Co., Inc. The other types of ionic liquid, 1-butyl-3-methylimidazolium tetrafluoroborate ([bmim][BF_4], 98% purity), 1-butyl-3-methylimidazolium hexafluorophosphate ([bmim][PF_6], 98% purity), 1-butyl-3-methylimidazolium trifluoromethanesulfonate ([bmim][OTf], 99% purity) and 1-butyl-3-methylimidazolium dicyanamide ([bmim][dca], 97% purity) were purchased from Wako Pure Chemical Industries, Ltd. The porous polymer membrane, hydrophobic polyvinylidene fluoride (PVDF) and polytetrafluoroethylene (PTFE) membranes with the pore size 0.2 μm. also was supplied from Wako Pure Chemical Industries, Ltd and ADVANTEC Toyo Roshi Kaisha, Ltd., respectively. The gases used in the experiments were carbon dioxide (CO_2, 99.95% purity), nitrogen (N_2, 99.95% purity) and helium (He, 99.9995% purity) gases were provided from Kayama Oxygen Co. Ltd.

3.2.2 Ionic liquid membrane preparation

A microporous hydrophobic PVDF membrane with diameter of 5 cm and membrane area 19.6 cm^2 was placed in a Petri dish. The PVDF membrane was impregnated with 1 ml of ionic liquid for 30 min. Fig. 3.1 shows PVDF membrane (a) unprocessed and (b) after impregnation with ionic liquid.

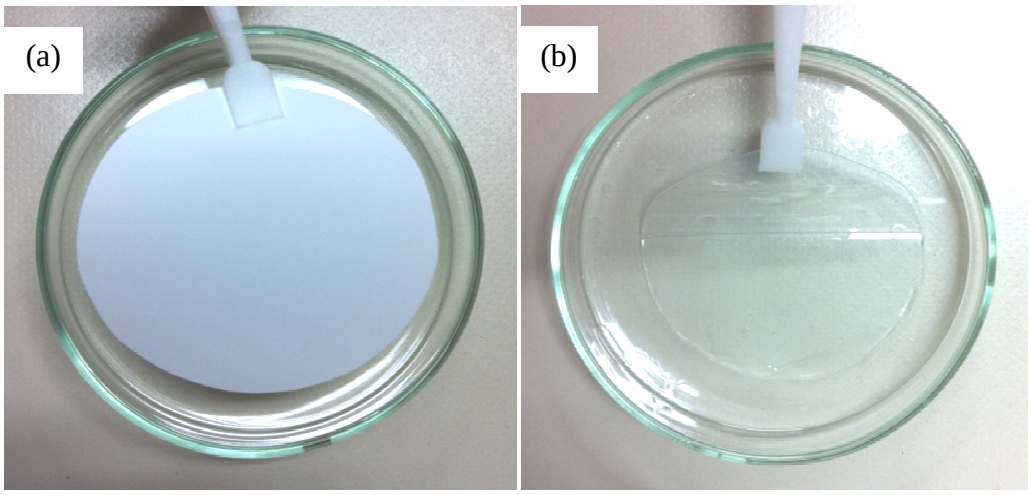

Fig. 3.1 PVDF membrane (a) unprocessed and (b) after impregnation with [bmim][PF_6]

After the impregnation, the liquid membrane became transparent like a gel due to the ionic liquid infiltrated into membrane pores. After the membrane was completely transparent, the excess ionic liquid was carefully removed from the surface of the membrane using soft tissue. To determine the thickness of the liquid membrane, the membrane was weighed before and after impregnation with ionic liquid. The calculation of membrane thickness is proposed as following equations:

$$\delta = \frac{m_{IL}}{A\rho_{IL}} \tag{3.1}$$

where δ, m, A, and ρ are membrane thickness in cm, mass in g, membrane area in cm^2 and density in g ml^{-1}, respectively. The subscript IL means ionic liquid. The density data of ionic liquid focused in this work are listed in Table 1.4 in Chapter 1. The amount of ionic liquids and their thickness are listed in Table 3.1.

Table 3.1 The used data for calculation and membrane thickness

Ionic liquid	m_{IL} (g)	δ (μm)
[emim][BF_4]	0.4060	162
[bmim][BF_4]	0.4059	171
[bmim][PF_6]	0.4087	152
[bmim][Tf_2N]	0.4860	173
[bmim][OTf]	0.4160	163
[bmim][dca]	0.3343	161

3.2.3 Measurement of CO_2 permeability

The schematic diagram of the experimental apparatus for CO_2 permeability is shown in Fig. 3.2. Carbon dioxide from a cylinder was supplied to the feed side of membrane module at a flow rate 70 $cm^3\ min^{-1}$. The ionic liquid membrane prepared above was previously set in the membrane module and was placed in the water bath for the temperature control. The feed side compartment of the membrane module was connected to a pressure gauge. The pressure at the feed side was 92 cmHg for the all measurements. Nitrogen gas was supplied at the permeate side of the membrane module as a sweep gas. The flow rate of N_2 was 100 $cm^3\ min^{-1}$. The permeate side was at atmospheric pressure. The mixed gas of CO_2 and N_2 at the permeate side was injected directly into gas chromatograph (GC) equipped with thermal conductivity detector. The compositions of the permeated mixed gas were analyzed by GC. The GC analyses were conducted every 30 min for 3 h in order to reach the equilibrium. The permeate rate of CO_2 was obtained from the volume fraction of the mixed gas at the permeate side analyzed by GC. The GC was carried out under the conditions that are given below:

Injection volume	2 ml
Column material	SUS 314
Column length	2 m
Column stationary phase	Porapak T (Mesh range 50-80)

Column temperature	30 °C
Carrier gas	He gas
Pressure of carrier gas	201.3 kPa

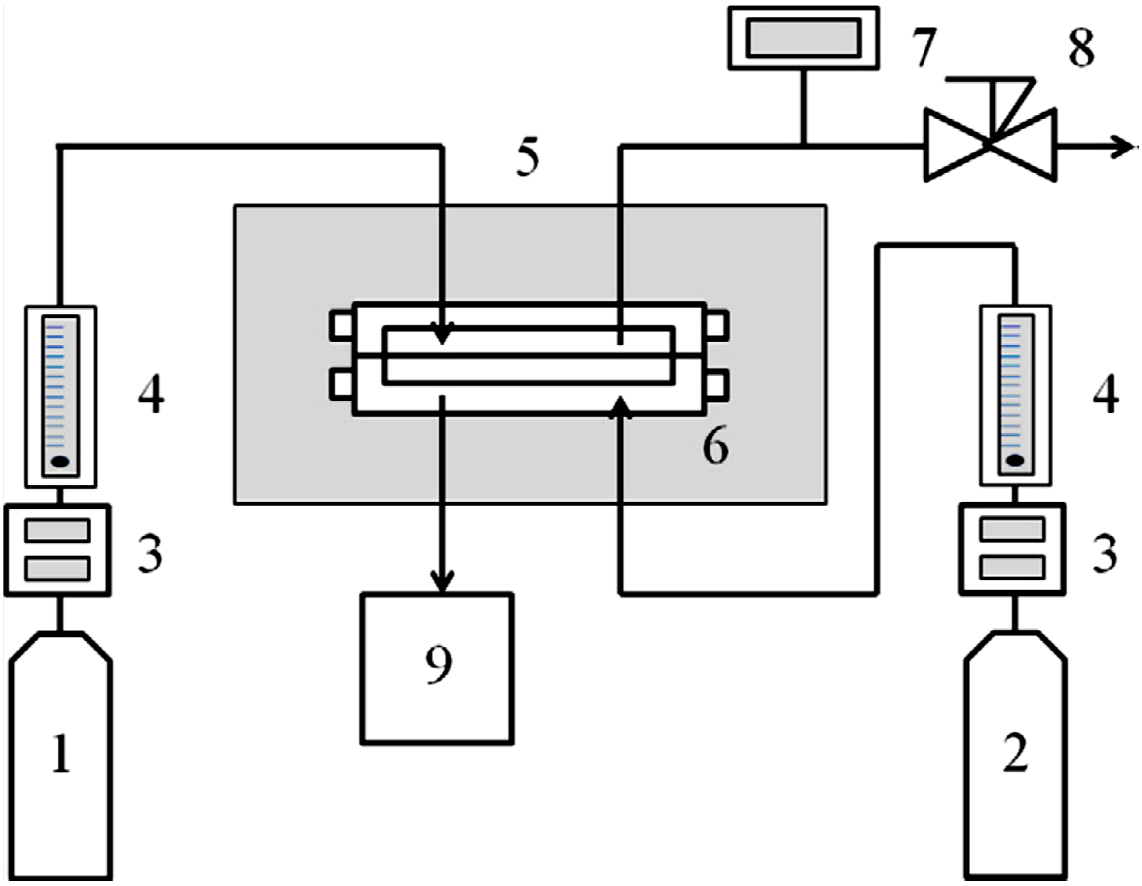

Fig. 3.2 Schematic diagram of experimental apparatus for CO_2 permeability. 1: CO_2 cylinder, 2: N_2 cylinder, 3: mass flow controller, 4: gas flow meter, 5: water bath, 6: membrane module, 7: pressure gauge, 8: back-pressure regulator, 9: gas chromatograph.

The permeability of the CO_2 was determined from the permeate rate as follows:

$$Q = \frac{F\delta}{\Delta pA} \tag{3.2}$$

where Q, F and Δp mean permeability of gas in Barrer (1 Barrer = 10^{-10} cm^3(STP; standard temperature and pressure, 273.15 K and 1 atm)cm cm^{-2} s^{-1} $cmHg^{-1}$), permeation rate in cm^3(STP)s^{-1} and partial pressure difference between feed and permeate sides in cmHg, respectively. The CO_2 permeability was measured at temperatures from (303.15 to 343.15) K. The CO_2 permeability measurements were carried out twice time for all experiments.

3.2.4 Measurement of selectivity between CO_2/N_2

The selectivity between CO_2/N_2 through ionic liquids was measured by a sweep gas method. The schematic diagram of the experimental apparatus for the selectivity is shown in Fig. 3.3. The mixed gas of CO_2 and N_2 was supplied into the feed side of membrane module.The flow rates were controlled at (12 and 108) cm^3 min^{-1} for CO_2 and N_2, respectively. The volume fraction of CO_2 at the feed side was 0.10. The pressure at feed side of the membrane module was 103 cmHg. At the permeate side, He gas was used as the sweep gas. The flow rate of He was controlled at 10 cm^3 min^{-1}. The permeate side was at atmospheric pressure. The permeated mixed gas of CO_2 and N_2 was injected into a GC with He gas. The compositions of the permeated gas were analyzed by GC every 30 min in 3 h. In this work, the selectivity was defined as the ratio of permeability for CO_2 and N_2 by the following equation:

$$S = \frac{Q_{CO2}}{Q_{N2}} = \left(\frac{F_{CO2}\delta}{\Delta p_{CO2} A} \right) \Big/ \left(\frac{F_{N2}\delta}{\Delta p_{N2} A} \right) = \frac{F_{CO2}}{F_{N2}} \times \frac{\Delta p_{N2}}{\Delta p_{CO2}} \qquad (2.3)$$

The ratio of permeate flux for CO_2 and N_2 was obtained from the volume fraction the mixed gas at the permeate side analyzed by GC. The partial pressure differences for CO_2 and N_2 between feed and permeated sides were (10.3 and 92.7) cmHg, respectively. The selectivity between CO_2/N_2 was measured at temperatures from (303.15 to 343.15) K.

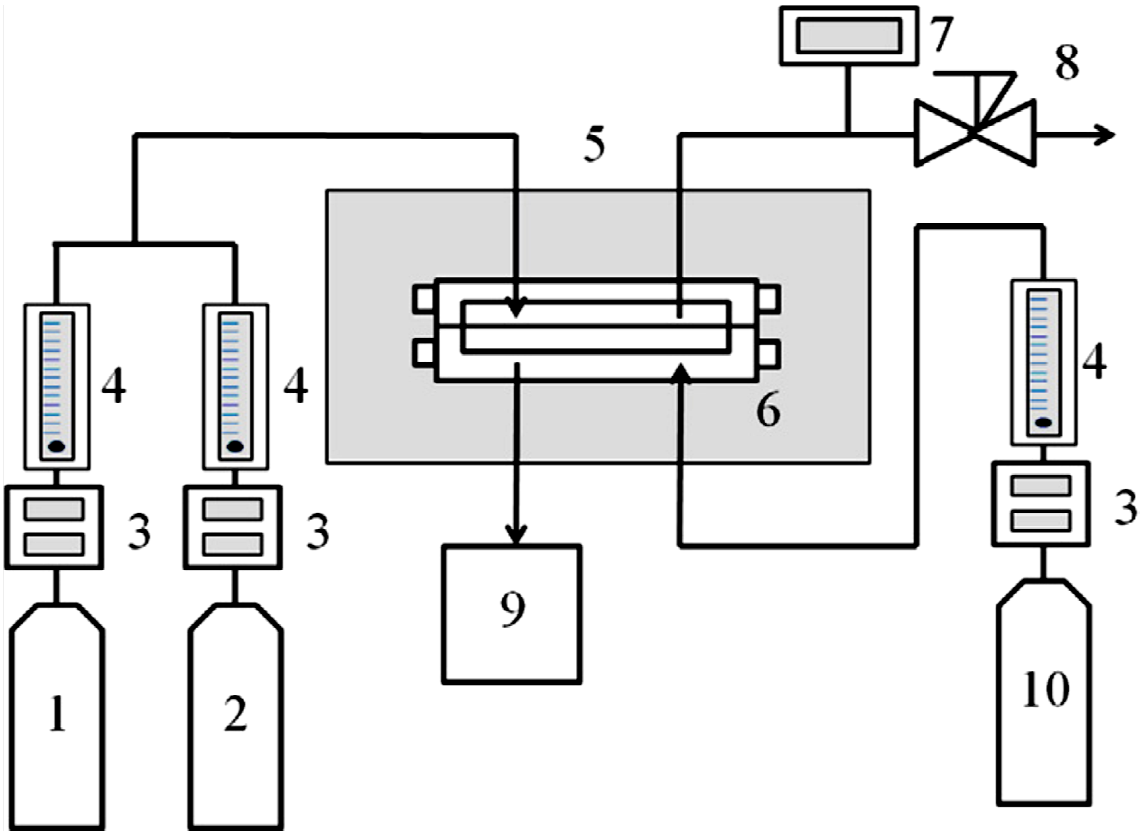

Fig. 3.3 Schematic diagram of experimental apparatus for CO_2/N_2 selectivity. 1: CO_2 cylinder, 2: N_2 cylinder, 3: mass flow controller, 4: gas flow meter, 5: water bath, 6: membrane module, 7: pressure gauge, 8: back-pressure regulator, 9: gas chromatograph, 10: He cylinder.

3.3 Results and discussion

3.3.1 Gel-membrane structure

To prepare the gel type membrane for CO_2 single gas separation, two samples of microporous polymer PVDF and PTFE with the similar pore size 0.2 μm were used to test the blending ability between the ionic liquid and polymer fibers. The impregnated PVDF and PTFE membranes are shown in Fig. 3.4. The results showed that after impregnation, PVDF became transparent membrane along its whole membrane cross section while PTFE was unchanged. This result indicated that the mixing between the ionic liquid and porous membrane occurred in only PVDF.

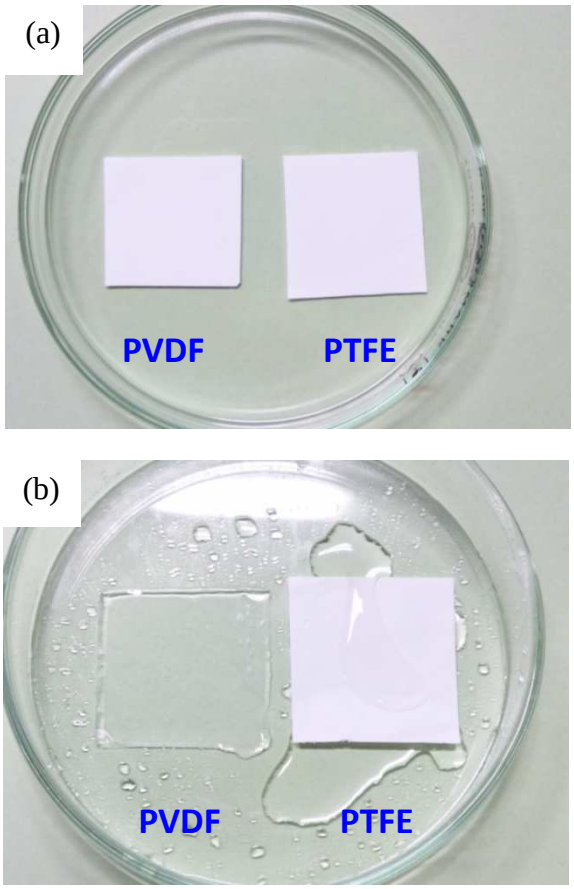

Fig. 3.4 PVDF and PTFE membranes (a) unprocessed and (b) impregnated with [bmim][PF_6]

To ensure that the PVDF membrane was more suitable than PTFE for the membrane preparation, the scanning electron microscope (SEM) was used to observe the surface morphology of the PVDF and PTFE membranes as shown in Fig. 3.5. It was found that the PVDF membrane demonstrates the highly porous material (Fig. 3.5a) whereas the fiber of PVDF membrane with ionic liquid became swelling, structure changed to the gel type and the size of pore turn into the smallness (Fig. 3.5b). Conversely, PTFE membrane after impregnation still showed non-swollen fiber and the porosity more than that of PVDF. There is no doubt that PVDF was selected to use for gel membrane preparation.

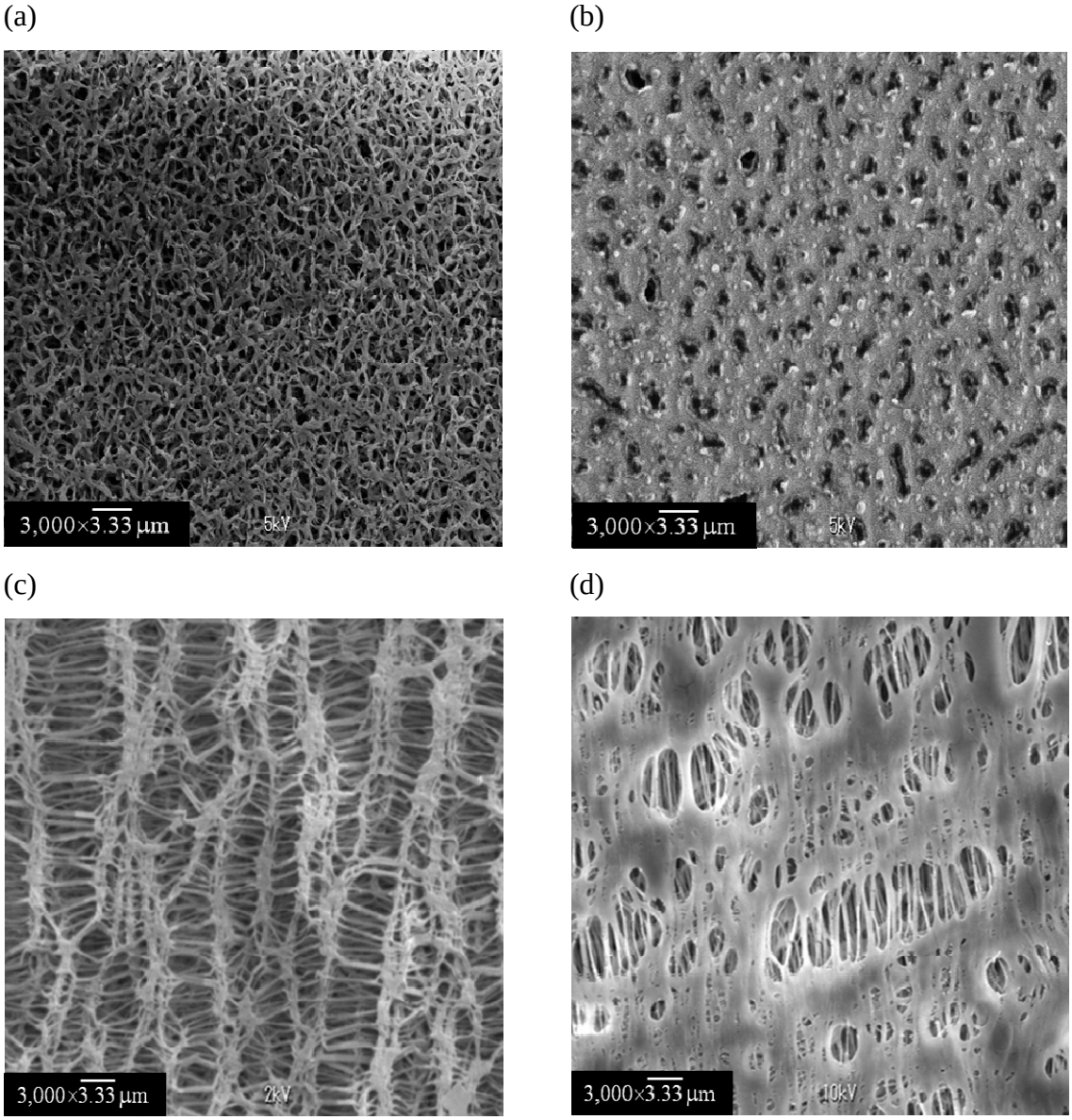

Fig. 3.5 Scanning electron microscope of the membrane surface morphology (a) the unprocessed PVDF, (b) the impregnated PVDF membrane with [bmim][PF_6], (c) the unprocessed PTFE and (d) the impregnated PTFE membrane with [bmim][PF_6]

3.3.2 Permeability and selectivity investigation

The experimental results of CO_2 permeability through [emim][BF_4], [bmim][BF_4], and [bmim][Tf_2N] membranes at T = 303.15 K were compared with the literature data [28, 74] at room temperature. The comparisons are presented in Table 3.2.

The results in this work are in agreement with the literature data within the order of the permeability.

Table 3.2 Comparisons of CO_2 permeability data through [emim][BF_4], [bmim][BF_4], and [bmim][Tf_2N] membranes at T = 303.15 K with literature data.

Ionic liquid	Q (Barrer) (in this work)	Q_{Ref} (Barrer)
emim[BF_4]	189	482*[74], 968[28]
bmim[BF_4]	200	462*[74]
bmim[TF_2N]	349	984*[74]

*Literature data are at room temperature.

The temperature dependences of CO_2 permeability through ionic liquid membranes are shown in Table 3.3 and Fig. 3.6. As presented in Table 3.3 and Fig. 3.6, the permeability of CO_2 through the all ionic liquid membranes increases with temperature. It is found that the [bmim][Tf_2N] membrane gives the highest value of permeability, while [bmim][PF_6] yields the lowest. The [emim] cation results in a higher CO_2 permeability than that with the [bmim] cation as given the comparison between [emim][BF_4] and [bmim][BF_4]. For [emim][BF_4] and [bmim][dca] membranes, the values of the permeability at T = (303.15 and 313.15) K are the almost same. The larger differences of permeability are given at the higher temperature at (323.15 to 343.15) K. The values of the permeability through [bmim][BF_4] and [bmim][OTf] are the almost same at the all temperatures in this work.

Table 3.3 Experimental results of CO_2 permeability through ionic liquid membranes.

Ionic liquid	Q_{CO2} (Barrer)				
	303.15 K	313.15 K	323.15 K	333.15 K	343.15 K
[emim][BF_4]	189 ± 0.0	218 ± 1.3	250 ± 0.0	278 ± 2.6	301 ± 1.3
[bmim][BF_4]	200 ± 1.3	214 ± 0.0	233 ± 0.0	250 ± 0.0	266 ± 1.3
[bmim][PF_6]	121 ± 0.0	143 ± 0.0	166 ± 1.3	203 ± 0.0	221 ± 1.3
[bmim][Tf_2N]	349 ± 1.3	376 ± 0.0	396 ± 0.0	437 ± 1.3	446 ± 0.0
[bmim][OTf]	205 ± 1.3	218 ± 0.0	234 ± 0.0	250 ± 0.0	266 ± 0.0
[bmim][dca]	199 ± 1.3	211 ± 0.0	226 ± 0.0	232 ± 0.0	242 ± 0.0

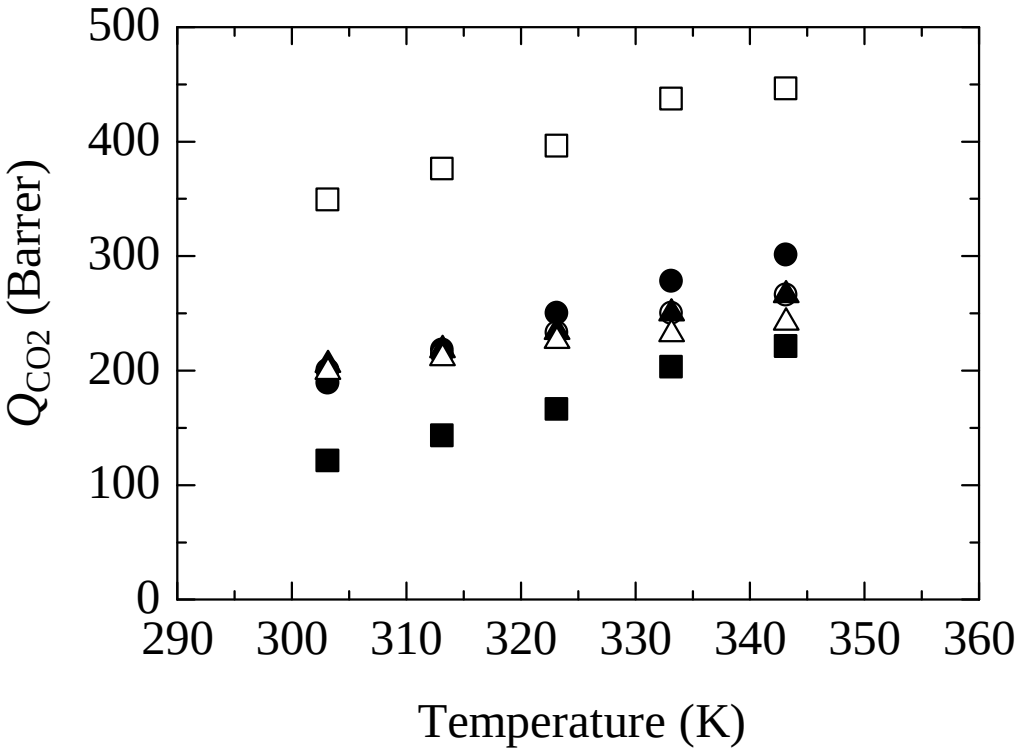

Fig. 3.6 Plot of CO_2 permeability against temperature through ionic liquid membranes, (●) [emim][BF_4], (○) [bmim][BF_4], (■) [bmim][PF_6], (□) [bmim][Tf_2N], (▲) [bmim][OTf], (△) [bmim][dca].

Based on solution-diffusion theory, the permeant dissolves into the liquid membrane, then diffuses through the membrane to the permeate side. The permeability of CO_2 through the ionic liquid membrane can be represented from solubility, C_{CO2}, and diffusion coefficients, D_{CO2}, as follows:

$$Q_{CO2} = C_{CO2} D_{CO2} \tag{3.4}$$

The diffusion coefficient of CO_2 in ionic liquids was obtained by an equation proposed by Morgan et al [75] as follows:

$$D_{CO2} = 3.7 \times 10^{-3} \left(\frac{1}{\eta_{IL}^{0.59} V_{CO2} \rho_{IL}^{2}} \right) \tag{3.5}$$

where η and V represent the viscosity of ionic liquid in cP and molar volume at the normal boiling temperature in $cm^3\ mol^{-1}$, respectively. The molar volume of CO_2 is available from the literature [76]. The viscosity and density of ionic liquids studied in this work are obtained from the literature data [54, 61, 77, 78]. The results of diffusion coefficients of CO_2 in ionic liquids at T = (303.15 to 343.15) K are listed in Table 3.4.

Table 3.4 Diffusion coefficient of CO_2 into ionic liquid membranes

Ionic liquid	$D \times 10^5$ ($cm^2\ s^{-1}$)				
	303.15 K	313.15 K	323.15 K	333.15 K	343.15 K
[emim][BF_4]	7.84	9.29	10.88	12.62	14.52
[bmim][BF_4]	5.18	6.30	7.57	8.92	10.38
[bmim][PF_6]	2.97	3.57	4.29	5.13	6.02
[bmim][Tf_2N]	5.49	6.71	8.09	9.65	11.39
[bmim][OTf]	5.19	6.29	7.45	8.78	10.32
[bmim][dca]	13.39	16.69	19.97	24.28	28.97

The diffusion coefficients of CO_2 through the ionic liquid membrane at operating temperature of 303.15 and 343.15 K are illustrated in Fig. 3.7. It is known that the higher temperature causes the more diffusivity. Furthermore, the result shows apparently that [bmim][PF_6] has the lowest diffusivity compared to those the other ionic liquids. Hence, it can be said that the cause of the lowest CO_2 permeability using [bmim][PF_6] as liquid membrane comes from the lowest diffusivity of CO_2 into this ionic liquid specie. As mentioned before, the results of [bmim][Tf_2N] liquid membrane gives the highest CO_2 permeability but the diffusivity has not presented the highest. It may cause from the solubility has a stronger effect than diffusivity. For [bmim][OTf], its diffusivity and permeability are comparable with [bmim][BF_4]. In the case of [bmim][dca], it shows the highest diffusion coefficient but the permeability is in the second rank from the minimum. For all the ionic liquid species, it can be indicated that the diffusivity has significant effect on CO_2 permeability.

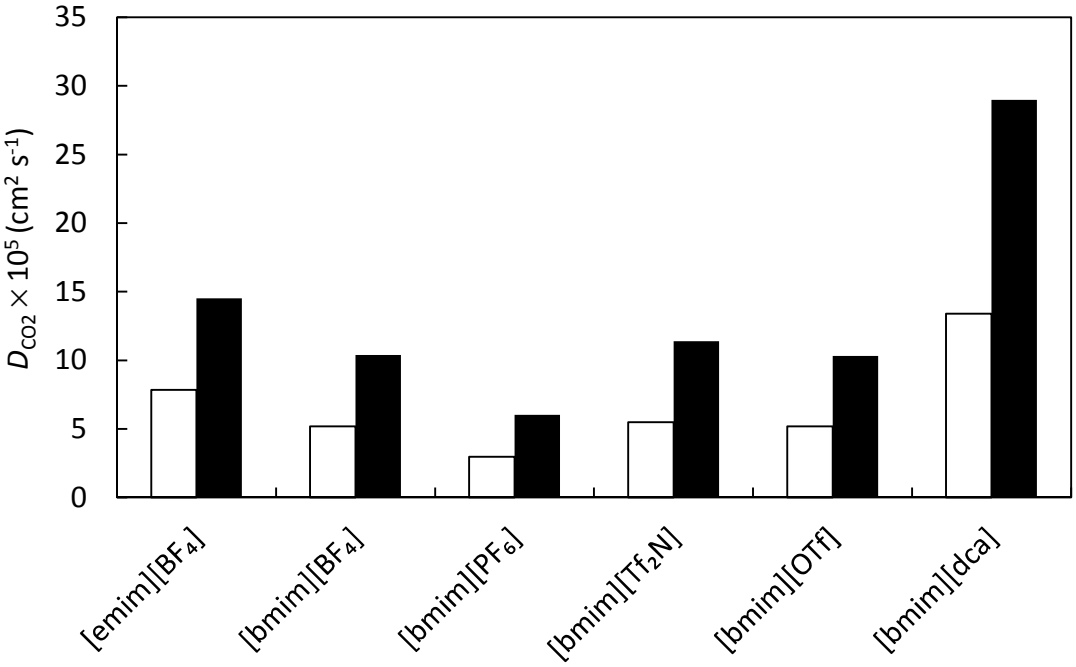

Fig. 3.7 Diffusion coefficient of CO_2 in six ionic liquid membranes at temperature, (□) 303.15 K, (■) 343.15 K.

The effects of six ionic liquids species which difference species of five anions and two cations on the CO_2 permeabilities were investigated. As pointed out above, based on solution-diffusion theory, permeability is controlled by both solubility and diffusivity. The diffusivity of gas depends on temperature while solubility hinges on the types of chemicals. The values of the solubility coefficient of CO_2 in ionic liquids were obtained from the permeability and diffusion coefficient using Eq. (3.4). The calculation results for all temperature are shown in Table 3.5. Fig. 3.8 illustrates the comparison of solubility coefficient of CO_2 in ionic liquid membranes between temperature of 303.15 and 343.15 K. When increased the temperature, the solubility coefficient decreased. This is because the increase in temperature leads to raise the vapor pressure of CO_2, and then resulting in the decrease in solubility.

Table 3.5 Solubility coefficient of CO_2 into ionic liquid membranes

Ionic liquid	$C \times 10^{-5}$ (cm^3(STP)cm^{-3} $cmHg^{-1}$)				
	303.15 K	313.15 K	323.15 K	333.15 K	343.15 K
[emim][BF_4]	24.17	23.51	22.98	22.00	20.75
[bmim][BF_4]	38.61	34.04	30.77	28.03	25.61
[bmim][PF_6]	40.76	40.17	38.65	39.50	36.72
[bmim][Tf_2N]	63.51	56.08	48.96	45.27	39.16
[bmim][OTf]	39.55	34.73	31.44	28.47	25.75
[bmim][dca]	14.84	12.61	11.33	29.54	8.36

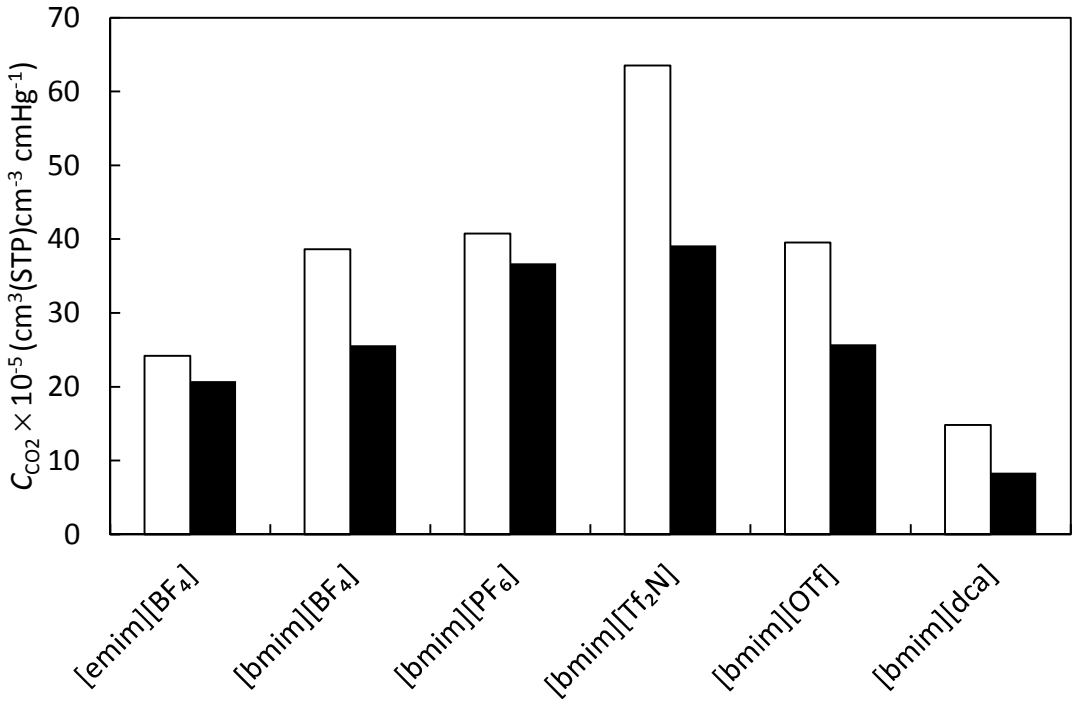

Fig. 3.8 Solubility coefficient of CO_2 in six ionic liquid membranes at temperature, (□) 303.15 K, (■) 343.15 K.

For the all ionic liquid species, the degrees by which the diffusion coefficient increases with temperature are greater than those by which the solubility coefficient decreases. These phenomena result in the increase of CO_2 permeability with temperature.

The experimental values for the selectivity between CO_2/N_2 through ionic liquid membrane are given in Table 3.6 and Fig. 3.9. The values of the selectivity between CO_2/N_2 through the all ionic liquid membranes decrease with increase of temperature. The selectivity through [emim][BF_4], [bmim][BF_4], and [bmim][dca] membranes are higher than those through the other ionic liquid membranes. It is interesting to observe the lowest selectivity at constant temperature is obtained with the [bmim][Tf_2N] membrane which shows the highest value of permeability for CO_2.

Table 3.6 Experimental results of selectivity of CO_2/N_2 through ionic liquid membranes.

Ionic liquid	$S = Q_{CO2}/Q_{N2}$				
	303.15 K	313.15 K	323.15 K	333.15 K	343.15 K
[emim][BF_4]	83.2 ± 0.8	75.6 ± 0.8	73.5 ± 1.1	64.1 ± 0.4	49.6 ± 0.8
[bmim][BF_4]	86.5 ± 0.1	75.6 ± 0.1	66.8 ± 0.1	59.4 ± 0.1	52.6 ± 0.8
[bmim][PF_6]	60.0 ± 0.7	55.1 ± 0.9	56.5 ± 0.2	47.0 ± 0.5	43.3 ± 0.8
[bmim][Tf_2N]	56.8 ± 0.2	56.6 ± 0.2	48.9 ± 0.5	44.9 ± 0.1	42.2 ± 0.8
[bmim][OTf]	60.6 ± 1.1	56.0 ± 0.9	55.8 ± 0.1	50.5 ± 0.4	45.0 ± 0.8
[bmim][dca]	78.9 ± 0.9	70.6 ± 0.3	62.6 ± 0.3	60.4 ± 0.0	53.7 ± 0.8

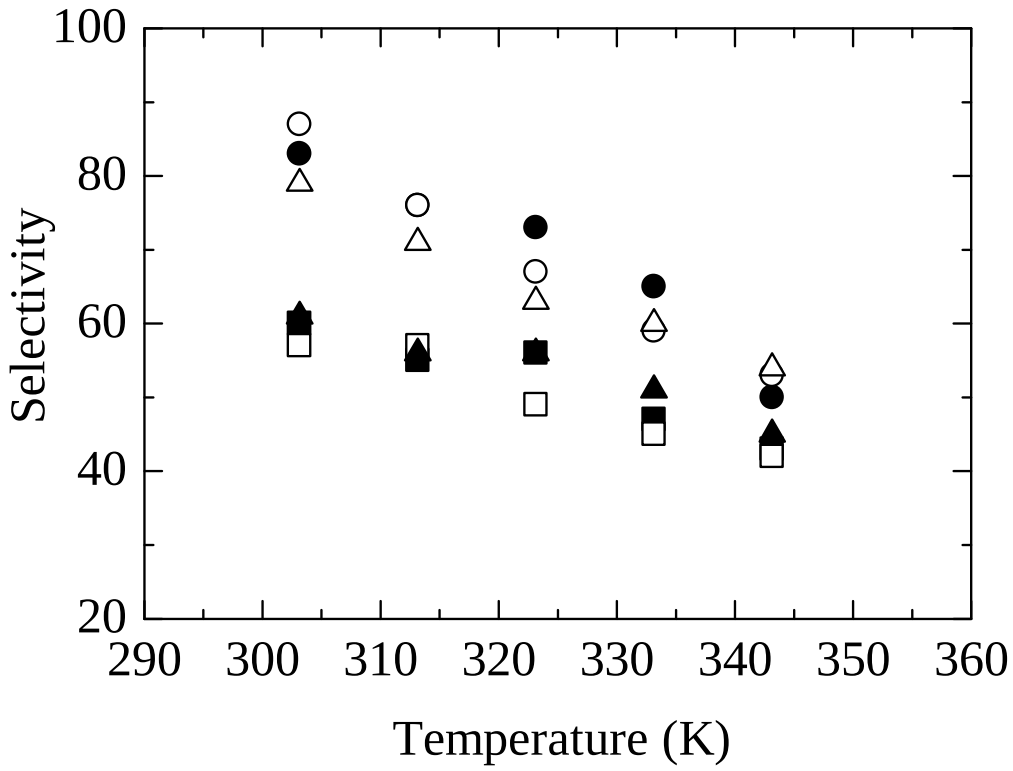

Fig. 3.9 Plot of CO_2/N_2 mixed gas selectivity against temperature through ionic liquid membranes, (●) [emim][BF_4], (○) [bmim][BF_4], (■) [bmim][PF_6], (□) [bmim][Tf_2N], (▲) [bmim][OTf], (△) [bmim][dca].

3.4 Conclusions

PTFE membrane was not capable to be employed as ionic liquid gel membrane because heterogeneous phase occurred during preparation. PVDF was successful to be impregnated with ionic liquid and its fiber became swollen and transparent. CO_2 permeabilities were tested by using six well-known types of ionic liquids as the liquid membranes under the various operating temperatures from 303.15 to 343.15 K. The increase in temperature results in the enhancement of CO_2 permeabilities due to the rise of diffusivity. The higher temperature causes the lower viscosity and the higher diffusivity. It can be explained by solution-diffusion theory that the diffusion coefficient has the stronger effect more than solubility coefficient on CO_2 permeability through liquid membrane because the degrees of diffusion coefficient increases with temperature

are larger than those of the decrease of solubility coefficient. The greatest permeability is given with the [bmim][Tf_2N] membrane in which CO_2 solubility coefficient is the highest. The membrane with [bmim][PF_6] presents the lowest permeability due to the lowest diffusion coefficient. It is very important for the design of ionic liquid membrane to understand not only the solubility but also diffusion coefficients of CO_2 in ionic liquids. In addition, the different anion species of ionic liquids have the major effects on CO_2 permeabilities as well.

The mixed gas selectivity between CO_2/N_2 through the ionic liquid membranes decreases with the increase of temperature. Unlike the results of CO_2 permeability, the lowest selectivity is given with the [bmim][Tf_2N] membrane in which the permeability of CO_2 is the highest.

Chapter 4

Separation of CO_2 from the CO_2/N_2 mixed gas through ionic liquid membranes at the high feed concentration

4.1 Statement of problem and objectives

Chapter 3 has studied the effects of temperature and anion species of ionic liquid membrane on CO_2 permeability with the low volume fraction of CO_2 at feed stream. The supported membrane was hydrophobic PVDF. The highest permeability of CO_2 single gas was obtained from [bmim][Tf_2N] liquid membrane while the lowest was obtained from [bmim][PF_6]. The permeability of CO_2 increases with temperature for all the experimental conditions. The results of CO_2/N_2 selectivity presented the opposite trends with permeability. However, the CO_2 permeability and separation phenomena with high CO_2 feed concentration are very doubtful. The results of our ongoing attempt to investigate and develop the separation of CO_2 through ionic liquid membranes are introduced in this Chapter.

This Chapter presents the results of the experimental investigation of CO_2 permeability and separation with high CO_2 volume fraction at the feed stream [55]. The separation of CO_2 with the volume fraction of 0.3 to 0.5 through ionic liquid membranes was examined. The total pressure difference between feed and permeate sides was varied from 0.05 to 0.21 atm. The operating temperature was controlled at 313.15 K for all the experiments. Two species of ionic liquid with different anion, 1-butyl-3-methylimidazolium hexafluorophosphate ([bmim][PF_6]) and 1-butyl-3-methylimidazolium bis(trifluoromethylsulfonyl)imide ([bmim][Tf_2N]), were used in this study. The supported microporous PVDF membrane was similar as in the previous work [12]. The selectivity of the mixed gas CO_2/N_2 and the permeability of CO_2 through ionic liquid membrane were measured using the sweep gas method. The effects of the total pressure difference, the total flow rate of the gases and the CO_2 concentration at the feed side on both selectivity and gas permeability were investigated.

4.2 Experimental

4.2.1 Materials

Ionic liquids, 1-butyl-3-methylimidazolium hexafluorophosphate ([bmim][PF_6]) and 1-butyl-3-methylimidazolium bis(trifluoromethylsulfonyl)imide ([bmim][Tf_2N]) were purchased from MerckKGaA, with purity higher than 98%. The chemical structures of ionic liquids are shown in Fig. 4.1. The physical properties; molecular weight, melting point, surface tension, density, and viscosity are listed in Table 4.1. A microporous polymer membrane, hydrophobic polyvinylidene fluoride (PVDF), with the pore size 0.2 μm and the thickness 95 μm was supplied from Wako Pure Chemical Industries, Ltd. Carbon dioxide (CO_2), nitrogen (N_2) and helium (He) gases were provided from Fuji Bussan Co. Ltd. Their purities were 99.95%, 99.95% and 99.9995%, respectively.

(a)

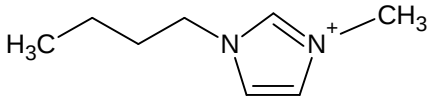

[bmim]

(b)

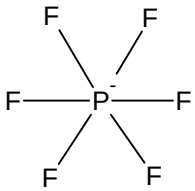

[PF_6]

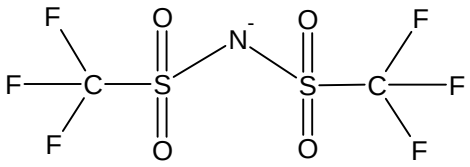

[Tf_2N]

Fig. 4.1 Chemical structures of (a) cation and (b) anions of ionic liquids in this study

Table 4.1 Physical property of ionic liquids in this study

Short name	M (g mol^{-1})	T_m (K)	γ (mN m^{-1})	ρ (g cm^{-3})*	η (cP)*
[bmim][PF_6]	284.18	283.2 [57]	48.8 [79]	1.37 [57]	182 [57]
[bmim][Tf_2N]	419.36	270.2 [57]	37.5 [79]	1.43 [57]	40 [57]

* Temperatures of density and viscosity at 303.15 K

4.2.2 Ionic liquid membrane preparation

A microporous PVDF membrane with diameter 5 cm and area 19.6 cm^2 was employed as a support membrane. The liquid membrane preparation method was similar with Chapter 2.

The membrane thickness, δ, was obtained from the amount of ionic liquid in the membrane by the following equation:

$$\delta = \frac{m_{IL}}{A\rho_{IL}} \tag{4.1}$$

where m, A and ρ are membrane mass in g, membrane area in cm^2 and density in g cm^{-3}, respectively. The subscript IL represents ionic liquid. The results of membrane thickness for each operating condition are shown in Table 4.2

Table 4.2 Thickness of ionic liquid membrane in this study

Ionic liquid	CO_2 volume fraction	Total feed flow rate (ml min^{-1})	Membrane thickness (μm)
[bmim][PF_6]	0.3	100	183.7
		300	215.6
[bmim][Tf_2N]		100	199.7
		300	189.8
[bmim][PF_6]	0.4	100	188.8
		300	215.4
[bmim][Tf_2N]		100	191.7
		300	189.8
[bmim][PF_6]	0.5	100	184.2
		300	215.6
[bmim][Tf_2N]		100	199.7
		300	199.7

4.2.3 CO_2 separation experiment

The experimental apparatus for gas separation measurement is shown in Fig. 4.2. The CO_2 volume fraction was varied from 0.3 to 0.5. The CO_2/N_2 mixed gas was supplied into the feed side of membrane module at the total flow rates 100 and 300 ml min^{-1}.The pressure at the feed side was changed from 1.05 to 1.21 atm. The pressure of the permeate side was atmospheric pressure. The permeate mixed gases were carried into gas chromatograph (GC) by sweep gas method with the injection volume of 5 ml, using He gas with flow rate 10 ml min^{-1}.The samples were taken and analyzed every 30 min until steady state was reached. The operating temperature was kept constant at 313.15 K by air bath for all the experiments. All the experiments were conducted in duplicate runs. The average absolute deviations were used to calculate the reproducibility. The volume flow rate at the permeate side was measured by using the soap film gas flow meter. The gas permeate rate was determined from the volume flow rate and GC analysis for the mixed gas at permeate side.

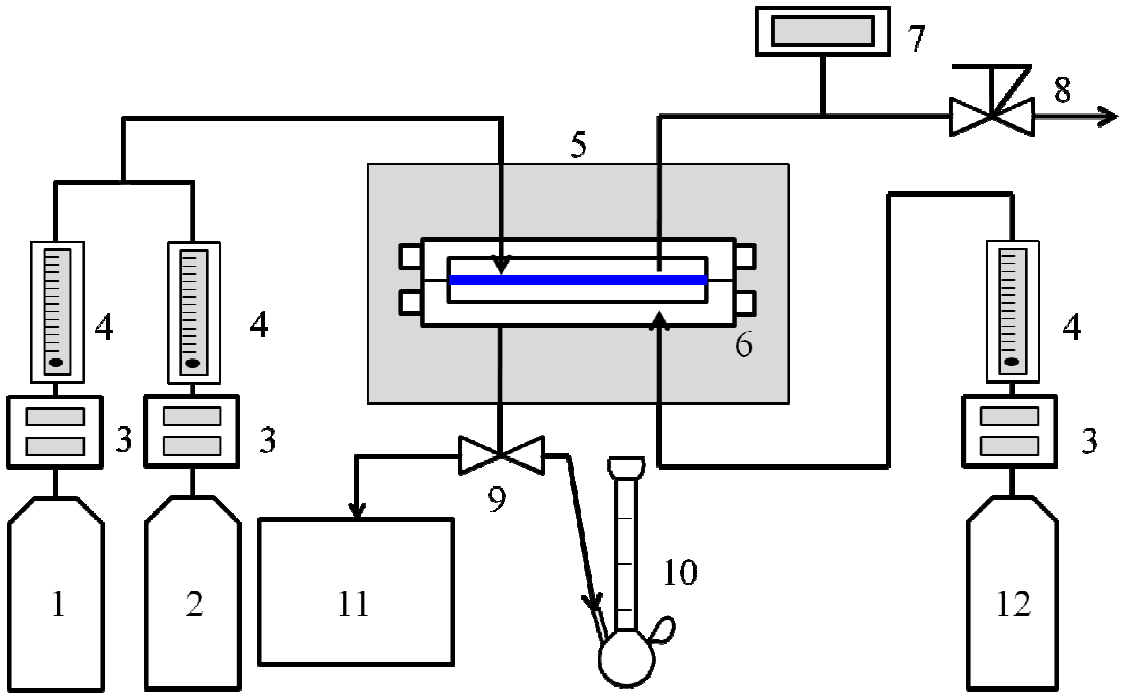

Fig. 4.2 Schematic diagram of experimental apparatus for CO_2/N_2 selectivity, 1: CO_2 cylinder, 2: N_2 cylinder, 3: mass flow controller, 4: gas flow meter, 5: air bath, 6: membrane module, 7: pressure gauge, 8: back-pressure regulator, 9: three parts valve, 10: soap film gas flow meter, 11: gas chromatograph, 12: He cylinder

The gas permeabilities, Q in Barrer (1 Barrer = 10^{-10} cm^3(STP)cm cm^{-2} s^{-1} $cmHg^{-1}$), were obtained by the following equation:

$$Q = \frac{F\delta}{\Delta pA} \tag{4.2}$$

where F, Δp and A are permeate rate in cm^3(STP)s^{-1}, partial pressure difference in cmHg and membrane area in cm^2, respectively.

The selectivity of mixed gas denoted by S, can be obtained from the ratio of the permeability of CO_2 to that of N_2 as follows:

$$S = \frac{Q_{CO_2}}{Q_{N_2}} \tag{4.3}$$

4.3 Results and discussion

4.3.1 Effect of total pressure difference

The mixed gas of CO_2/N_2 was used as the feed gas. The total pressure differences were varied from 0.05 to 0.21 atm while the pressure at the permeate side was at atmospheric pressure. The experimental results of the effect of the total pressure differences at the feed side on CO_2 selectivity and permeability are shown in Tables 4.3 and 4.4, respectively. The selectivity at the CO_2 volume fraction at feed side (X_{CO2}), X_{CO2} = 0.5 through [bmim][PF_6] and [bmim][Tf_2N] liquid membranes are pretty similar. The larger differences of selectivity are given at the lower CO_2 concentration, X_{CO2} = 0.3, and 0.4.The differences of permeability can be obviously seen at the lower CO_2 concentration, especially at X_{CO2} = 0.3 while the permeability of CO_2 do not differ significantly at higher CO_2 concentration. The CO_2 permeability which obtained from [bmim][Tf_2N] membrane is higher than that of [bmim][PF_6] except for X_{CO2} = 0.3 with the total feed flow rate of 300 ml min^{-1}. According to the previous work in Chapter 3, the permeabilities of low CO_2 concentration at feed side were investigated using six species of ionic liquid membranes including [bmim][PF_6] and [bmim][Tf_2N] membranes. The [bmim][Tf_2N] liquid membrane performed the highest CO_2 permeability while [bmim][PF_6] presented the lowest for single gas permeation. The results from this study strongly explain that this phenomenon in mixed gas corresponds with single gas permeation.

Table 4.3 Selectivity of mixed gas between CO_2/N_2 through ionic liquid membranes

Ionic liquid	CO_2 volume fraction	Total feed flow rate (ml min^{-1})	$S = Q_{CO2}/Q_{N2}$			
			0.05 atm	0.10 atm	0.15 atm	0.21 atm
[bmim][PF_6]	0.3	100	21.8 ± 0.5	21.2 ± 0.4	22.1 ± 0.0	21.5 ± 0.9
		300	16.9 ± 0.1	16.8 ± 0.1	16.9 ± 0.2	17.2 ± 0.2
[bmim][Tf_2N]		100	18.3 ± 0.1	18.0 ± 0.1	17.6 ± 0.1	18.0 ± 0.2
		300	17.5 ± 0.1	17.4 ± 0.1	17.1 ± 0.1	18.5 ± 0.0
[bmim][PF_6]	0.4	100	15.8 ± 0.2	15.4 ± 0.2	15.4 ± 0.2	15.5 ± 0.2
		300	13.7 ± 0.0	13.7 ± 0.1	13.6 ± 0.7	13.8 ± 0.7
[bmim][Tf_2N]		100	13.5 ± 0.1	13.3 ± 0.1	12.9 ± 0.0	12.5 ± 0.0
		300	14.1 ± 0.0	14.1 ± 0.1	14.1 ± 0.0	14.0 ± 0.2
[bmim][PF_6]	0.5	100	11.5 ± 0.0	11.4 ± 0.0	11.2 ± 0.1	11.5 ± 0.0
		300	11.1 ± 0.1	11.1 ± 0.1	10.9 ± 0.1	10.4 ± 0.3
[bmim][Tf_2N]		100	11.9 ± 0.1	11.7 ± 0.1	12.0 ± 0.1	12.0 ± 0.2
		300	11.3 ± 0.1	11.3 ± 0.0	11.3 ± 0.0	11.2 ± 0.2

Table 4.4 Permeability of CO_2 through ionic liquid membranes

Ionic liquid	CO_2 volume fraction	Total feed flow rate (ml min^{-1})	$Q_{CO2} \times 10^{-3}$ (Barrer)			
			0.05 atm	0.10 atm	0.15 atm	0.21 atm
[bmim][PF_6]	0.3	100	9.1 ± 0.5	7.6 ± 1.2	6.4 ± 0.3	6.2 ± 0.9
		300	19.8 ± 0.5	9.2 ± 0.7	6.8 ± 0.5	4.9 ± 0.6
[bmim][Tf_2N]		100	11.4 ± 0.3	9.4 ± 0.2	8.8 ± 0.4	4.9 ± 0.3
		300	13.4 ± 0.6	3.2 ± 0.6	1.3 ± 0.3	3.2 ± 0.3
[bmim][PF_6]	0.4	100	12.8 ± 0.4	1.8 ± 0.4	0.5 ± 0.2	0.3 ± 0.1
		300	17.2 ± 0.4	6.5 ± 0.3	6.1 ± 0.4	3.3 ± 0.5
[bmim][Tf_2N]		100	12.6 ± 0.3	11.0 ± 0.6	6.7 ± 0.1	3.0 ± 0.1
		300	17.5 ± 0.7	5.1 ± 0.0	5.0 ± 0.1	4.9 ± 0.2
[bmim][PF_6]	0.5	100	17.1 ± 0.5	6.3 ± 0.5	5.6 ± 0.8	5.3 ± 0.8
		300	16.4 ± 0.1	5.7 ± 0.2	5.6 ± 0.6	5.0 ± 0.3
[bmim][Tf_2N]		100	17.9 ± 0.2	7.7 ± 0.2	6.4 ± 0.2	5.4 ± 0.1
		300	16.1 ± 0.4	5.5 ± 0.7	5.5 ± 0.2	4.6 ± 0.3

Fig. 4.3 shows the effect of total pressure difference on the selectivity of CO_2/N_2 and the permeability of CO_2 through ionic liquid membranes at the constant total flow rate at the feed side of 300 ml min^{-1}. From these results, it was demonstrated that the selectivity insignificantly changed with the decrease in the total pressure difference as shown in Fig. 4.3a. Fig. 4.3b shows the relationship between permeabilities of CO_2 and the total pressure difference. The permeabilities of CO_2 decrease by increasing the total pressure difference. These results imply that the facilitated transport took place at the operating pressure region. The carriers for the CO_2 molecules in the ionic liquid membrane should be the anion species of the ionic liquid, especially fluorine atom. Hasib-ur-Rahman et al [80] reported that the ionic liquid, which contained fluorine atom, had stronger affinity with CO_2 than that of non-fluorine atom. At higher total pressure difference, the saturation of the carrier is limiting factor on the CO_2 permeation through ionic liquid membrane. It is thought that the reductions of the carrier potential result in the decrease in CO_2 permeability through ionic liquid membranes [81-83].

(a)

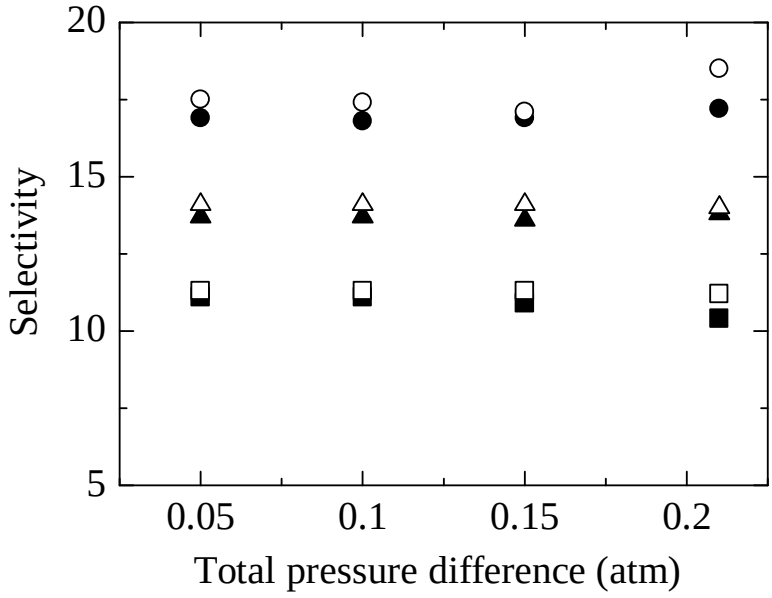

(b)

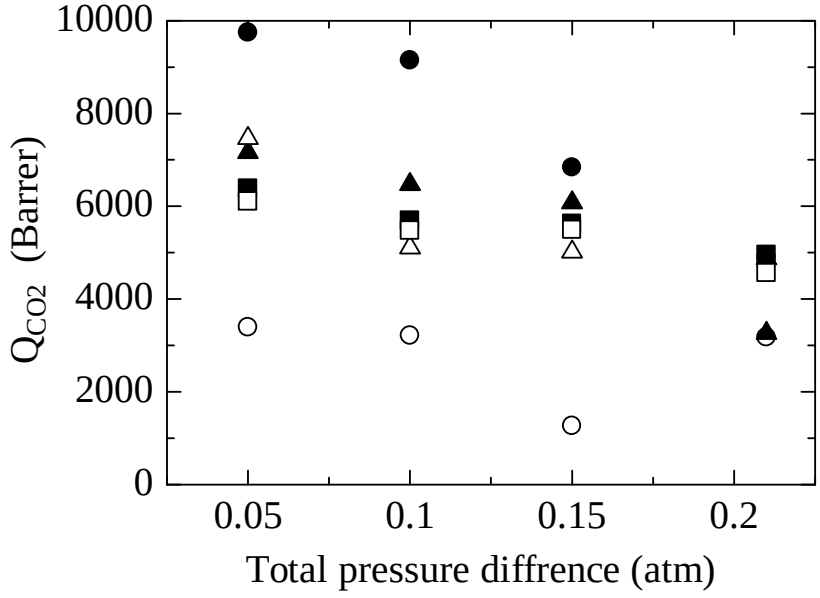

Fig. 4.3 Effect of total pressure difference on (a) selectivity of CO_2/N_2 and (b) permeability of CO_2 through ionic liquid membranes in difference CO_2 volume fraction at the constant total flow rate at the feed side of 300 ml min^{-1}; (●) [bmim][PF_6], X_{CO2} = 0.3, (○) [bmim][Tf_2N], X_{CO2} = 0.3, (▲) [bmim][PF_6], X_{CO2} = 0.4, (△) [bmim][Tf_2N], X_{CO2} = 0.4, (■) [bmim][PF_6], X_{CO2} = 0.5, (□) [bmim][Tf_2N], X_{CO2} = 0.5

Fig 4.4 shows the effect of total pressure difference on the selectivity of CO_2/N_2 and the permeability of CO_2 through ionic liquid membranes at the constant total flow rate at the feed side of 100 ml min^{-1}. The selectivity shows the similar tendency with the total flow rate at the feed side of 300 ml min^{-1}. The change of total pressure difference has not affected the selectivity as shown in Fig. 4.4a. The highest selectivity can be obtained from [bmim][PF_6] membranes. Fig. 4.4b illustrates the permeabilities of CO_2 also increase by decreasing the total pressure difference which corresponds to the facilitated transport mechanism. The reasons have already explained above.

(a)

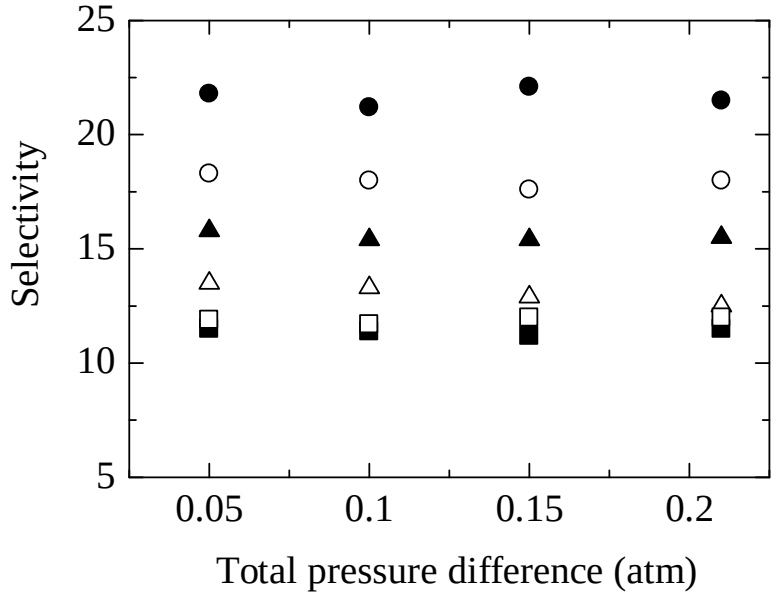

(b)

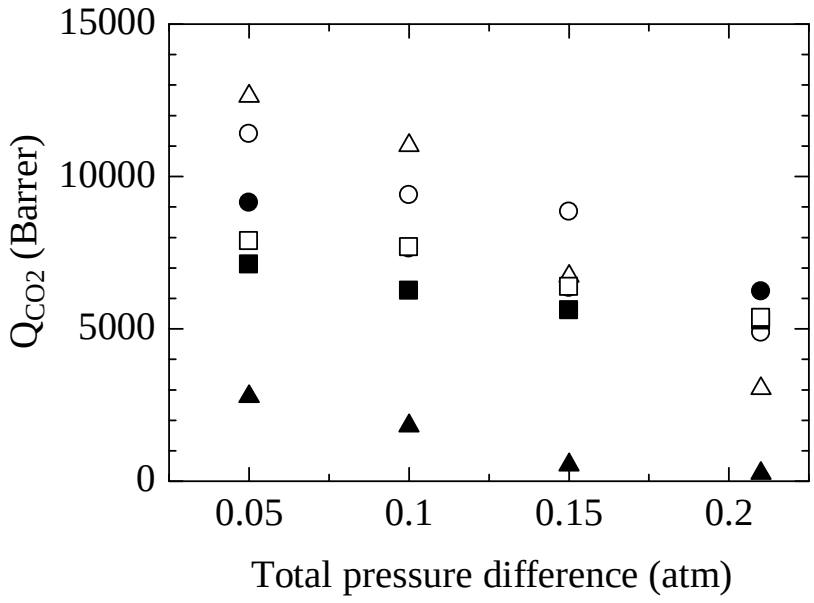

Fig. 4.4 Effect of total pressure difference on (a) selectivity of CO_2/N_2 and (b) permeability of CO_2 through ionic liquid membranes in difference CO_2 volume fraction at the constant total flow rate at the feed side of 100 ml min^{-1}; (●) [bmim][PF_6], X_{CO2} = 0.3, (○) [bmim][Tf_2N], X_{CO2} = 0.3, (▲) [bmim][PF_6], X_{CO2} = 0.4, (△) [bmim][Tf_2N], X_{CO2} = 0.4, (■) [bmim][PF_6], X_{CO2} = 0.5, (□)[bmim][Tf_2N], X_{CO2} = 0.5

4.3.2 Effect of total flow rate at feed side

To examine the effect of total flow rates of the mixed gas at the feed side, the measurements of CO_2 permeability and selectivity were conducted at the flow rate of 100 and 300 ml min^{-1}. The overall results of selectivity and permeability of CO_2 are also listed in Tables 4.3 and 4.4, respectively. The higher selectivity was obtained from the lower total feed flow rate 100 ml min^{-1} at X_{CO2} = 0.3, but the equivalence of the selectivity in the case of 100 and 300 ml min^{-1} was presented at X_{CO2} = 0.5. The CO_2 permeabilities through [bmim][PF_6] increase with the total feed flow rate at X_{CO2} = 0.3 and 0.4, while those through [bmim][Tf_2N] decrease. The CO_2 permeability results were extremely interesting because they were similar for both [bmim][PF_6] and [bmim][Tf_2N] liquid membranes at X_{CO2} = 0.5 even though the total flow rate was changed. Fig. 4.5 shows the examples of the effect of total flow rates at the feed side on the CO_2/N_2 selectivity and CO_2 permeability through [bmim][Tf_2N] liquid membranes. As it can be seen, the selectivity between two feed flow rates is slightly different at high CO_2 concentration. By increasing the total flow rate, the CO_2 permeability greatly decreased.

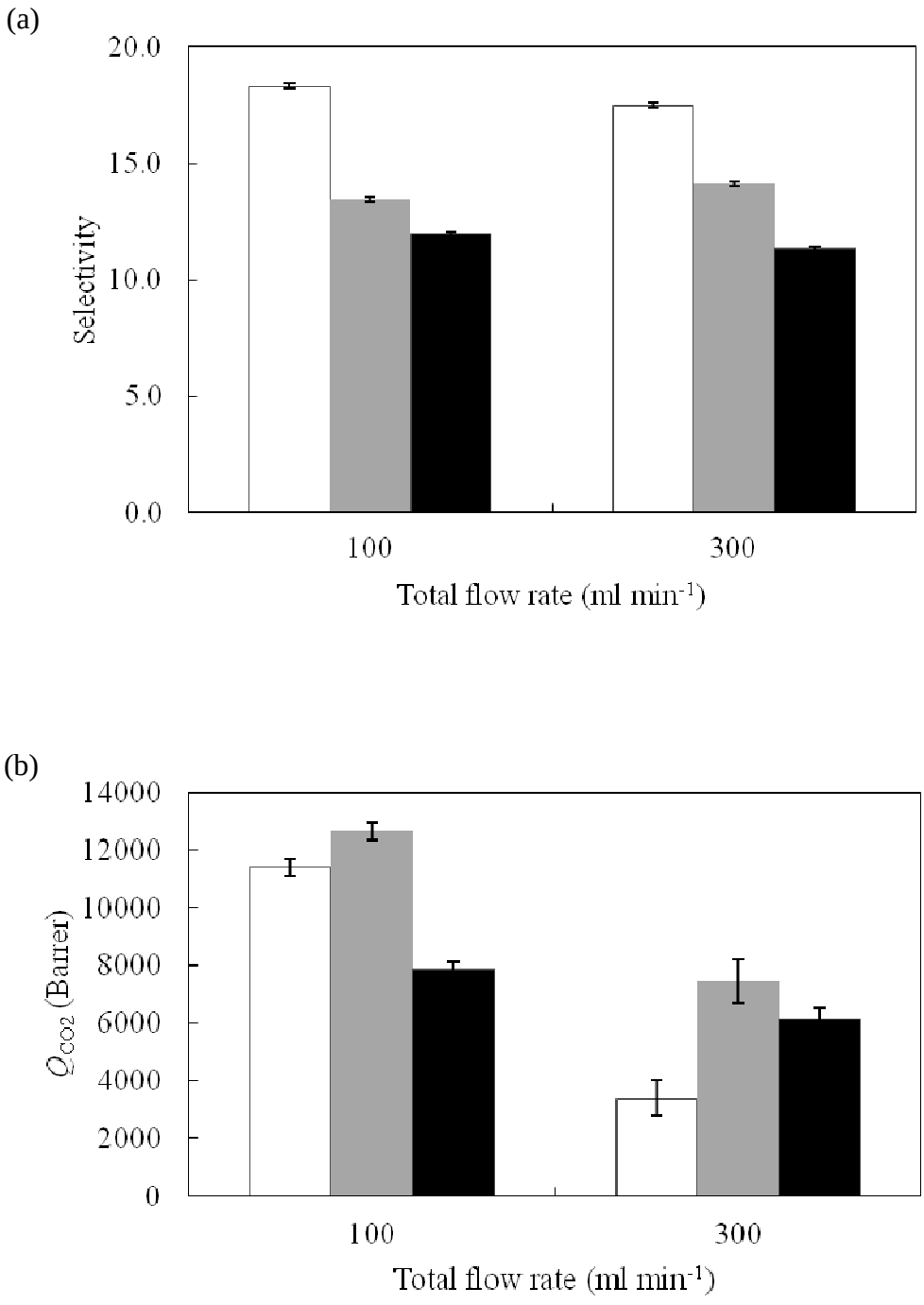

Fig. 4.5 Effect of total flow rate at feed side on CO_2 permeability trough [bmim][Tf_2N] liquid membrane at constant pressure at feed side 1.05 atm and X_{CO2} = (□) 0.3, (■) 0.4 and (■) 0.5

Fig. 4.6 shows the effect of total flow rate at the feed side on permeability of CO_2 and N_2 through [bmim][Tf_2N] liquid membrane at the constant the pressure feed at feed side 1.05 atm. The changes of the total flow rate insignificantly affected the N_2 permeabilities as presented in Fig. 4.6.

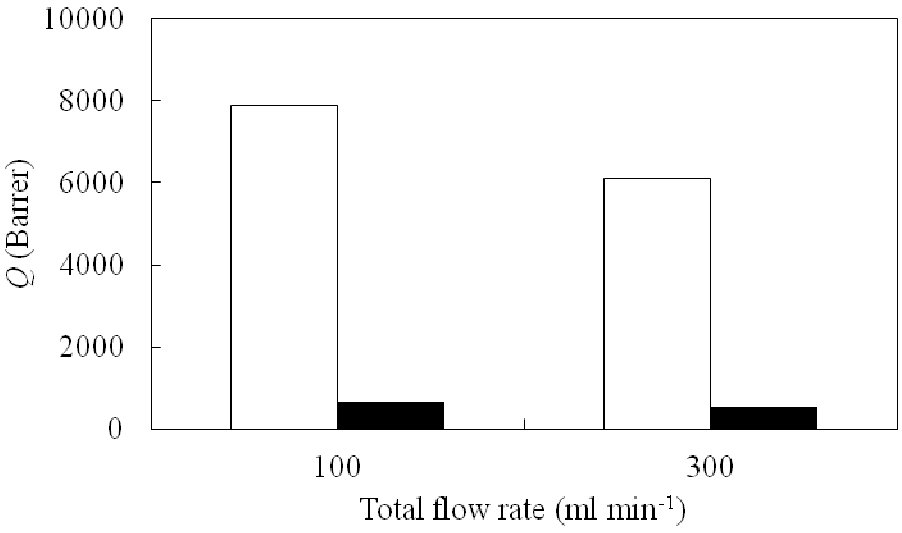

Fig. 4.6 Effect of total flow rate at feed side on permeability of gases trough [bmim][Tf_2N] liquid membrane at constant CO_2 volume fraction of 0.5 with the pressure at feed side 1.05 atm for (□) CO_2, (■) N_2

4.3.3 Effect of CO_2 concentration

The effect of CO_2 concentration on selectivity and permeability of CO_2 permeability were also investigated. The volume fractions of CO_2 (X_{CO2}) at the feed side were varied from 0.3 to 0.5. Fig. 4.7 shows the effect of CO_2 concentration on selectivity of CO_2/N_2 and CO_2 permeability through [bmim][PF_6] membrane with the total flow rate at the feed side 300 ml min^{-1} and the total pressure different of 0.05 atm. As shown in Fig. 4.7a, it was found that the lower CO_2 volume fraction showed the higher selectivity. The permeability of CO_2 shows the corresponding trend with selectivity as shown in Fig. 4.7b.

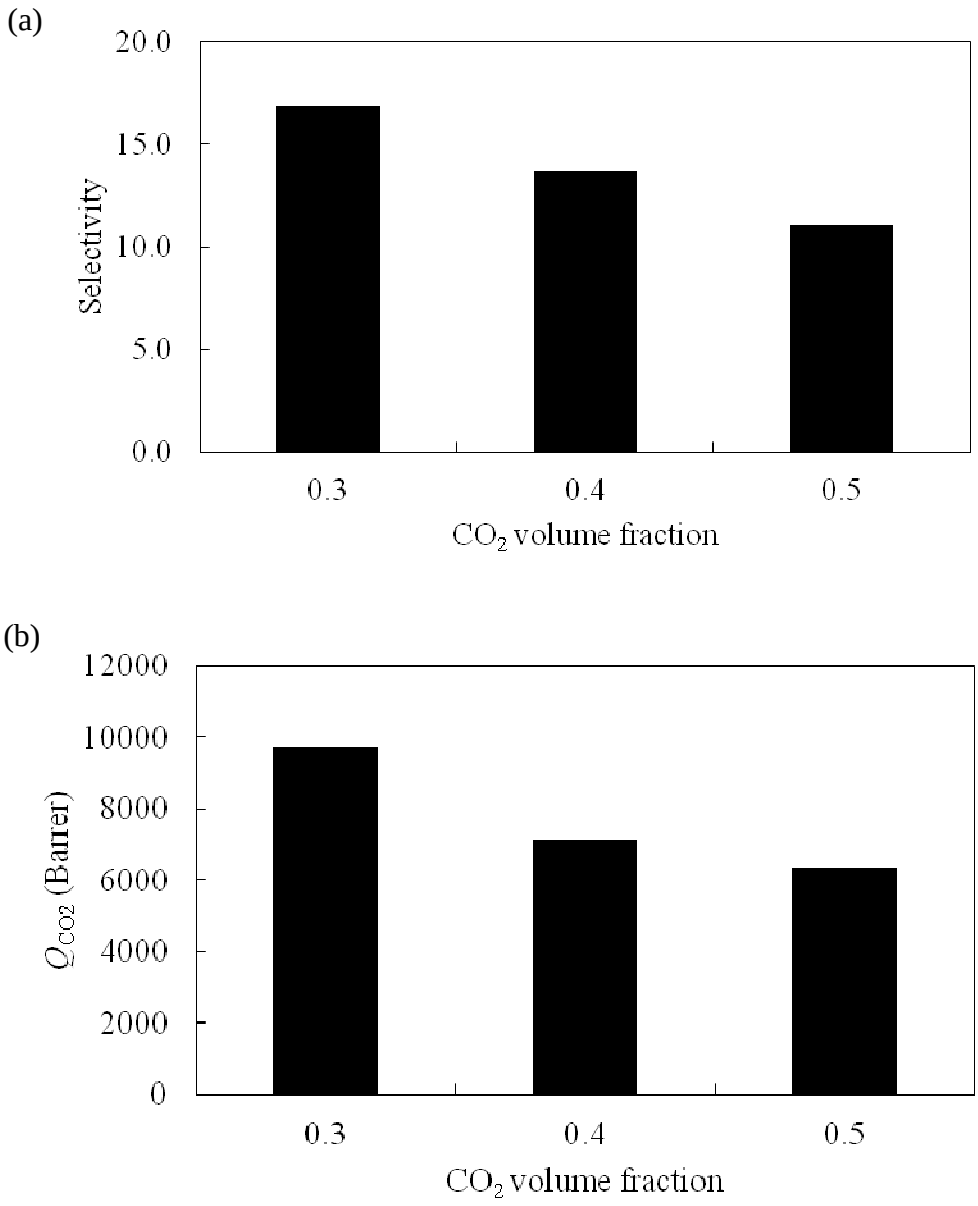

Fig. 4.7 Effect of CO_2 concentration on (a) selectivity of mixed gas CO_2/N_2 and (b) permeability of CO_2 though [bmim][PF_6] ionic liquid membrane with the pressure at feed side 1.05 atm and total flow rate at the feed side 300 ml min^{-1}

Fig. 4.8 illustrates the facilitated transport mechanism of liquid membrane. Regarding the limited occupancies of CO_2 on the carrier, especially fluorine atom of anion species inside the ionic liquid membrane, it is thought that the lower CO_2 concentration presents the easy movement of CO_2 molecules from the feed side to the

permeate side via the carriers as shown in Fig 4.8a. On the other hand, the higher CO_2 concentration shows the lower permeability. As mentioned above, the carriers inside the ionic liquid membrane are saturated by CO_2 molecules in the case of high CO_2 volume fraction at feed side. The occupied carriers hardly release and capture the CO_2 molecules to the nearby carriers because there are no empty carriers (see Fig 4.8b). The CO_2 difficultly permeates to the permeate side.

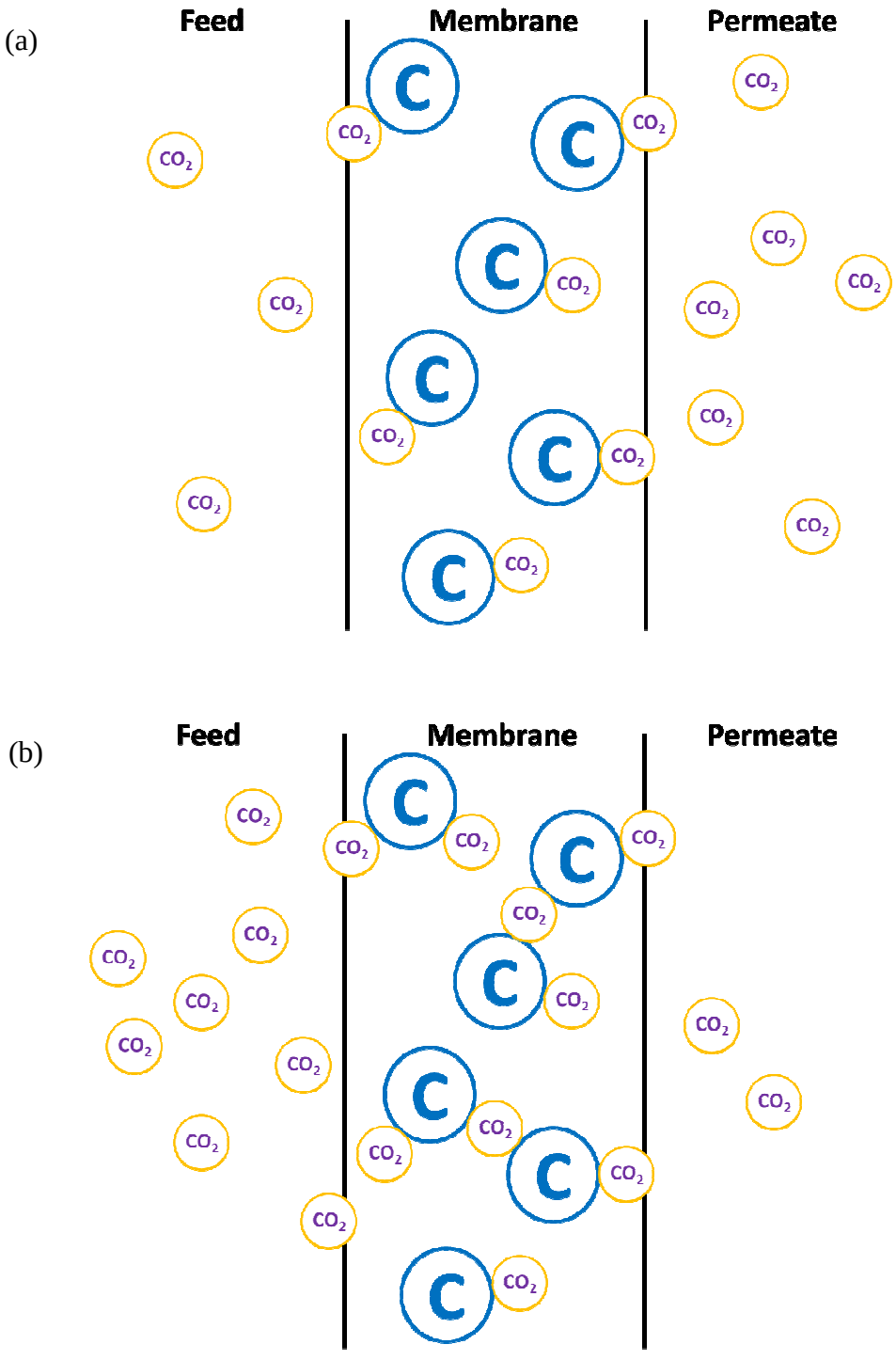

Fig. 4.8 Facilitated transport mechanism of liquid membrane; © = carrier, (a) low CO_2 concentration and (b) high CO_2 concentration

4.4 Conclusions

Carbon dioxide (CO_2) separation from nitrogen (N_2) through ionic liquid membrane with high feed CO_2 concentration was investigated. Regarding to the increase in permeability of CO_2 with the decrease in the total pressure difference, the results strongly pointed out that the facilitated transport play a key role at the 1.05 to 1.21 atm of the total pressure at the feed side. The fluorinated anions of ionic liquid acted as the carriers, which were immobilized inside the ionic liquid membrane. At higher total pressure difference, the saturation of the carrier was the limiting factor leading to lower efficiency of carrier resulting in the decrease of CO_2 permeabilities. At the feed volume fraction of CO_2, 0.3 and 0.4, and total pressure difference, 0.05 to 0.15 atm, the permeabilities increase and decrease with increasing total feed flow rate through [bmim][PF_6] and [bmim][Tf_2N] membranes, respectively. In the case of N_2 permeability, the effect of feed gas flow rate was relatively small. Concentration of CO_2 at the feed side also affected both the CO_2 permeability and selectivity. At high CO_2 concentration, the permeabilities of CO_2 were limited by the carrier saturation also. The results from this study may be used to apply for the CO_2 separation process design using ionic liquid membrane in the future.

Chapter 5

Effect of water vapor at feed and permeate streams on CO_2 permeabilities through ionic liquid membranes

5.1 Statement of problem and objectives

CO_2 permeabilities and selectivities through ionic liquid membrane with dry feed stream have been investigated in Chapters 3 and 4 varying operating factors. The previous works [27, 28, 35, 55] have studied dry feed CO_2 while the additions of water in ionic liquid membranes are few. The presence of water in ionic liquid is interesting owing to the change of the properties such as surface tension [84, 85], density and viscosity [77]. Zhang et al [86] reported that that small amount of water (1 mass%) in the ionic liquids can absorb equimolar ratio of CO_2 and generate zwitterion resulting in the change of absorption mechanism of aqueous ionic liquid solution and pure ionic liquid. The effect of ion and solvent of the aqueous solution of [bmim][PF_6] was examined by Raju et al [87]. They found that cation diffused slower than anion in the aqueous [bmim][PF_6] solution which is totally different from pure [bmim][PF_6]. Fortunato et al [88] have examined the influence of water on the solute transport through ionic liquid membrane. The presence of water affected the solute transport mechanism between amino acids (initial phase) and deionized water. Kasahara et al [67] have investigated the effect of water in amino acid ionic liquid membrane on CO_2/N_2 separation. They obtained the pinnacle of CO_2 permeability through tetrabutylphosphonium proline of 14000 Barrer. Their results imply that amount of water has a serious impact on the CO_2 permeation.

This Chapter focuses on the presence of water in ionic liquid membrane at the feed and permeate sides of the CO_2 separation process. Two species of ionic liquids, 1-butyl-3-methylimidazolium hexafluorophosphate ([bmim][PF_6]) and 1-butyl-3-methylimidazolium bis(trifluoromethylsulfonyl)imide ([bmim][Tf_2N]) were used in this study. The effects of water vapor at feed and permeate side on CO_2 permeabilities were discussed in term of the permeation mechanism based on the solution-diffusion theory. The water permeabilities were also examined.

5.2 Experimental

5.2.1 Materials

Two species of ionic liquid used in this study were alike with Chapter 4 those were [bmim][PF_6] and [bmim][Tf_2N]. The microporous polymer membrane with the pore size 0.2 μm, hydrophobic polyvinylidene fluoride (PVDF) were supplied from Wako Pure Chemical Industries, Ltd. Ultrapure water was purchased from Wako Pure Chemical Industries, Ltd. Carbon dioxide (CO_2) and nitrogen (N_2) gases were provided from Fujii Bussan Co. Ltd. with the similar purities 99.95 %.

5.2.2 Preparation of liquid gel membrane

Liquid gel membrane preparation method was explained in the previous Chapter. The membrane diameter and area used in this work were also same as the previous Chapter as well. In this study, the thickness of the membrane was observed by Microscope (Yashima Tokyo) with the six hundred magnifications. Three points in difference position of the gel membrane were measured. The thickness was obtained by the average of all points. This method would give more accurate values than the calculation by density of ionic liquid. The gel membrane thickness for this work was approximately 133 to 142 μm. The observation results are shown in Table 5.1. The results implied that the calculation values show higher thickness than the observation values.

Table 5.1 The ionic liquid membrane thickness for each operating condition in this study

Ionic liquid membrane	Membrane thickness (μm)			
	303.15 K	313.15 K	323.15 K	333.15 K
[bmim][PF_6] [27]*	152	152	152	152
[bmim][PF_6] (humid feed)	137	139	142	140
[bmim][PF_6] (humid permeate)	146	135	138	145
[bmim][Tf_2N] [27]*	173	173	173	173
[bmim][Tf_2N] (humid feed)	144	133	137	134

*The thickness of liquid membranes were obtained from the calculation by density of ionic liquid

5.2.3 Experimental set-up

In this study, the effects of the water vapor at feed and permeate streams on both CO_2 and water permeabilities were investigated. The experimental set-up for humid feed and permeate streams are shown in Figs. 5.1 and 5.2, respectively. The CO_2 flow rate at the feed side was controlled by the flow control valve at 100 ml min^{-1}. Carbon dioxide was flowed into water saturator and then passed through the membrane module. The pressure difference between the feed and permeated sides was adjusted at 0.2 atm by back-pressure regulator while the permeate side was discharged to atmosphere. Nitrogen (N_2) gas was supplied to the membrane module at the permeate side as a sweep gas and its flow rate 100 ml min^{-1}. The temperature of this experiment was kept the constant by air bath. The permeabilities of CO_2 was investigated at temperatures from (303.15 to 333.15)K in 10 K intervals. All the experiments were carried out twice times. The experiment of the humid permeate stream was conducted in the similar way as humid feed stream experiment except for the position of water saturator. The water saturator was installed before N_2 gas was flowed into membrane module as shown in Fig. 5.2. The water traps were collected the amount water at permeate side. The permeate rate was measured by a soap film gas flow meter. To analyzed the composition of the permeated gas, the permeate gas was switched from the soap film gas flow meter to a gas chromatograph by three pathway valve. The sweep and

permeate gases were directly injected into the gas chromatograph every 30 min until reach the steady state.

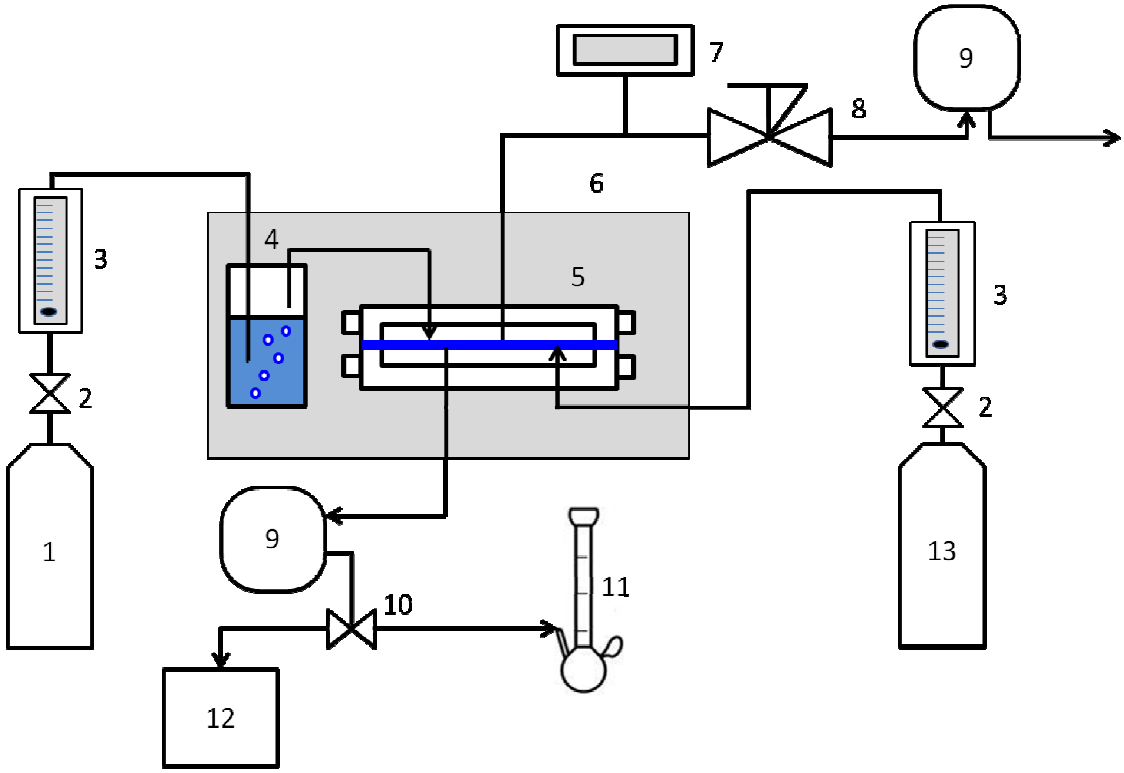

Fig. 5.1 Schematic diagram of experimental apparatus of humid feed stream for CO_2 permeabilities measurement, 1: CO_2 cylinder, 2: flow control valve, 3: gas flow meter, 4: water saturator, 5: membrane module, 6: air bath, 7: pressure gauge, 8: back-pressure regulator, 9: water trap 10: three parts valve, 11: soap film gas flow meter, 12: gas chromatograph, 13: N_2 cylinder

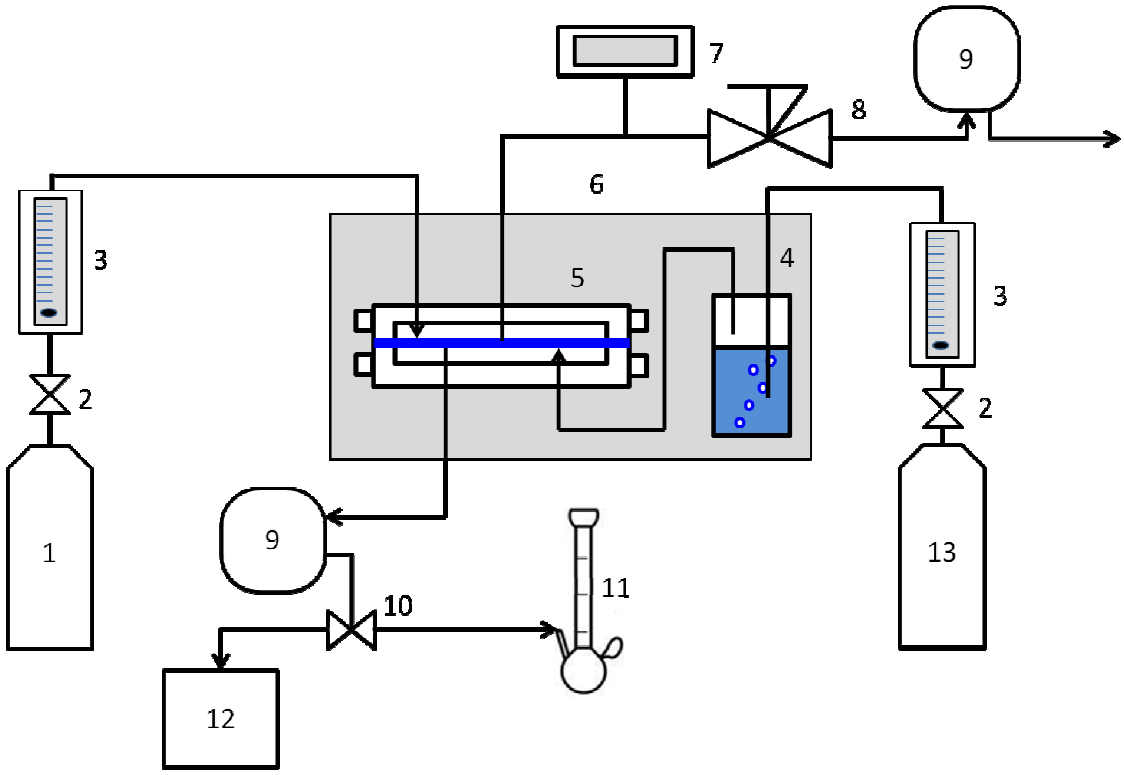

Fig. 5.2 Schematic diagram of experimental apparatus of humid permeate stream for CO_2 permeabilities measurement, 1: CO_2 cylinder, 2: flow control valve, 3: gas flow meter, 4: water saturator, 5: membrane module, 6:air bath, 7: pressure gauge, 8: back-pressure regulator, 9: water trap 10: three parts valve, 11: soap film gas flow meter, 12: gas chromatograph, 13: N_2 cylinder

The permeabilites, Q in Barrer (1 Barrer = 10^{-10} cm^3(STP)cm cm^{-2} s^{-1} $cmHg^{-1}$) of CO_2 were obtained by the following equation:

$$Q = \frac{F\delta}{\Delta pA} \tag{5.1}$$

where F, δ, Δp and A are permeate rate in cm^3(STP)s^{-1}, membrane thickness in cm, partial pressure difference in cmHg and membrane area in cm^2, respectively. The water permeabilities were measured simultaneous with CO_2 permeabilities.

5.3 Results and discussion

The effects of water vapor at feed and permeate sides on CO_2 permeabilities through [bmim][PF_6] and [bmim][Tf_2N] membranes were investigated. The experimental results are shown in Fig. 5.3 and Table 5.2. The rise of operating temperature resulted in the increase of CO_2 permeabilities because of the increase of the mobility of polymeric fibers [80]. The structure of ionic liquid gel membrane is more relaxed. The higher mass transfer of CO_2 can be obtained. The permeabilities of CO_2 through ionic liquid membrane with water vapor increase the slope of temperature dependence both humid feed and permeate streams compared with those without water vapor in our previous work [27]. From these results, the presence of water in the system leads to the significant increase of CO_2 permeabilities.

(a)

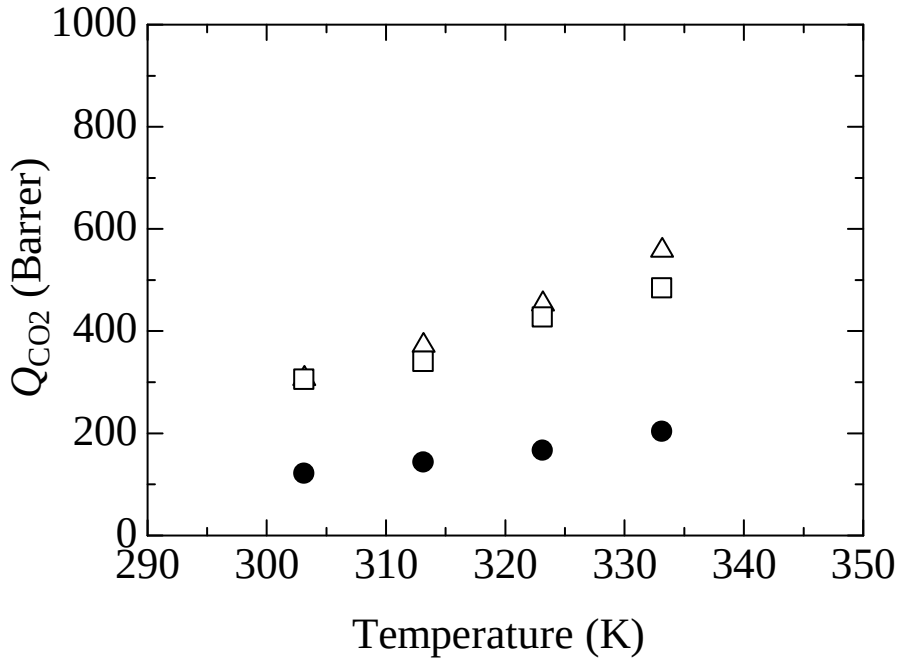

(b)

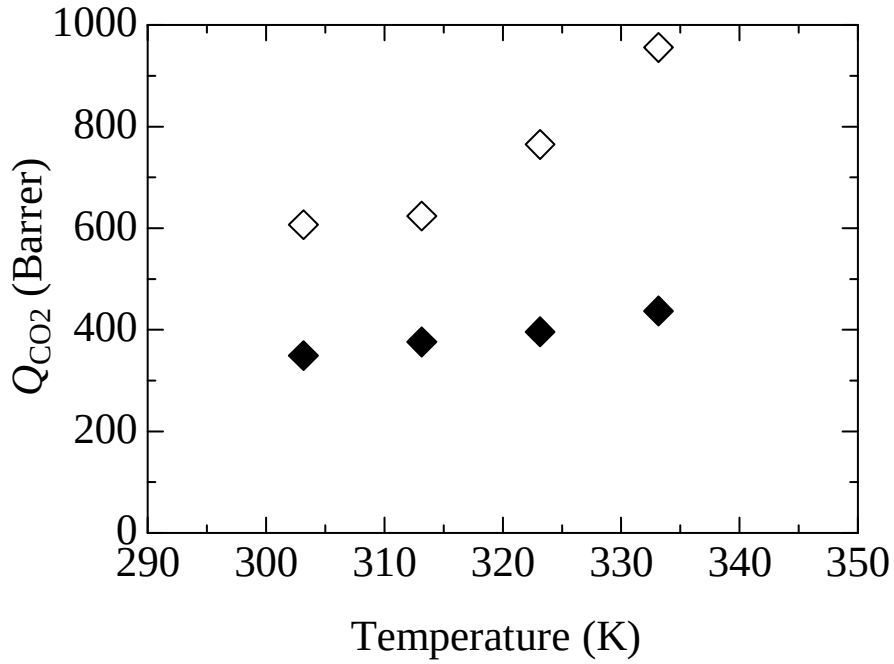

Fig. 5.3 Experimental results of CO_2 permeabilities through ionic liquid membranes with temperature dependence, (a) [bmim][PF_6] (●) dry feed [27], (△) humid feed, (□) humid permeate, (b) [bmim][Tf_2N] (◆) dry feed [27], (◇)humid feed

Table 5.2 Experimental results of CO_2 permeabilities with temperature dependence

Ionic liquid membrane	Q_{CO2} (Barrer)			
	303.15 K	313.15 K	323.15 K	333.15 K
[bmim][PF_6] [27]	121 ± 1	143 ± 1	166 ± 1	203 ± 1
[bmim][PF_6] (humid feed)	307 ± 3	372 ± 3	453 ± 7	558 ± 13
[bmim][PF_6] (humid permeate)	305 ± 3	340 ± 1	427 ± 8	484 ± 4
[bmim][Tf_2N] [27]	349 ± 1	376 ± 1	396 ± 1	437 ± 1
[bmim][Tf_2N] (humid feed)	607 ± 5	624 ± 8	765 ± 3	956 ± 10

Kasahara et al [67] reported that the increase of CO_2 absorption in ionic liquids with amount of water may cause from the modification of the absorption phenomena which corresponds with our work. The humid feed stream gave the permeabilities of CO_2 higher than those of humid permeate stream. This phenomenon can be explained by solution-diffusion theory which the permeability of gas through a dense membrane was controlled by solubility and diffusivity. The suggestion of water and CO_2 concentration profile through the ionic liquid membranes for both streams are shown in Fig. 5.4. In the case of the humid feed stream in Fig. 5.4a, the concentration of water at the interphase between vapor and gel phases is high. CO_2 concentration profile shows the rapid diffusion in gel membrane at the water effect region and getting slow near the permeate side. In the case of humid permeate stream in Fig. 5.4b, water concentration at the feed side is very low resulting in the amount of CO_2 concentration slowly diffuse in gel phase. Comparison the solubility of CO_2 in ionic liquid membrane with water vapor at feed and permeate streams found that the solubility of CO_2 at the feed stream is lower than that of permeate stream as seen in Fig. 5.4. Kerlé et al [89] have reported the decrease of CO_2 solubility in ionic liquid due to the increase of water. From this knowledge, it can be explained that the permeability with the humid feed stream is lower than that with the humid permeate stream. However, the results of CO_2 permeability through the ionic liquid membrane with water vapor obtained in this work are contrary to this explanation. The possible reason is that the diffusion plays an important role for both humid feed and permeate streams.

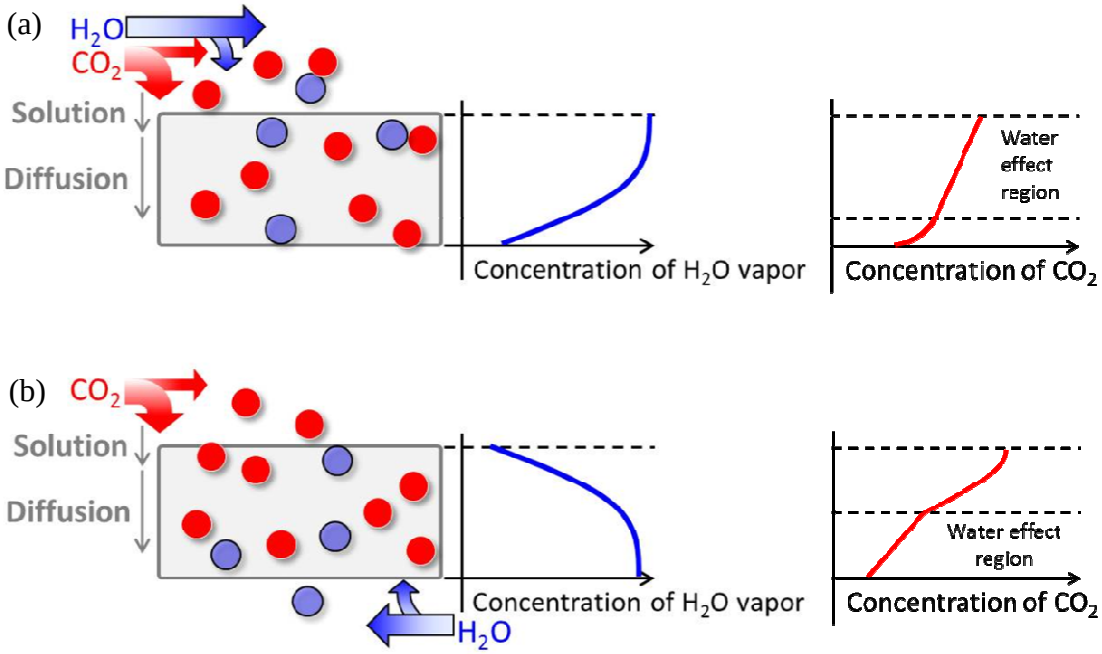

Fig. 5.4 Concentration profile of H_2O and CO_2 in the liquid membrane, (a) humid feed, (b) humid permeate

The rate of the CO_2 permeability enhancement was also considered in this study and defined by following equation:

$$R = \frac{Q_{IL+w}}{Q_{IL}} \tag{5.2}$$

where R and Q refer to rate of the enhancement and permeabilities of the compound, respectively. Subscripts IL and w mean ionic liquid and water, respectively. The enhancement rates of CO_2 permeabilities with water vapor are given in Fig. 5.5. The rate of the CO_2 permeabilities enhancement increased with temperature. It is found that [bmim][PF_6] liquid membrane with both the humid feed and permeate streams give the higher enhancement rate than that of [bmim][Tf_2N].

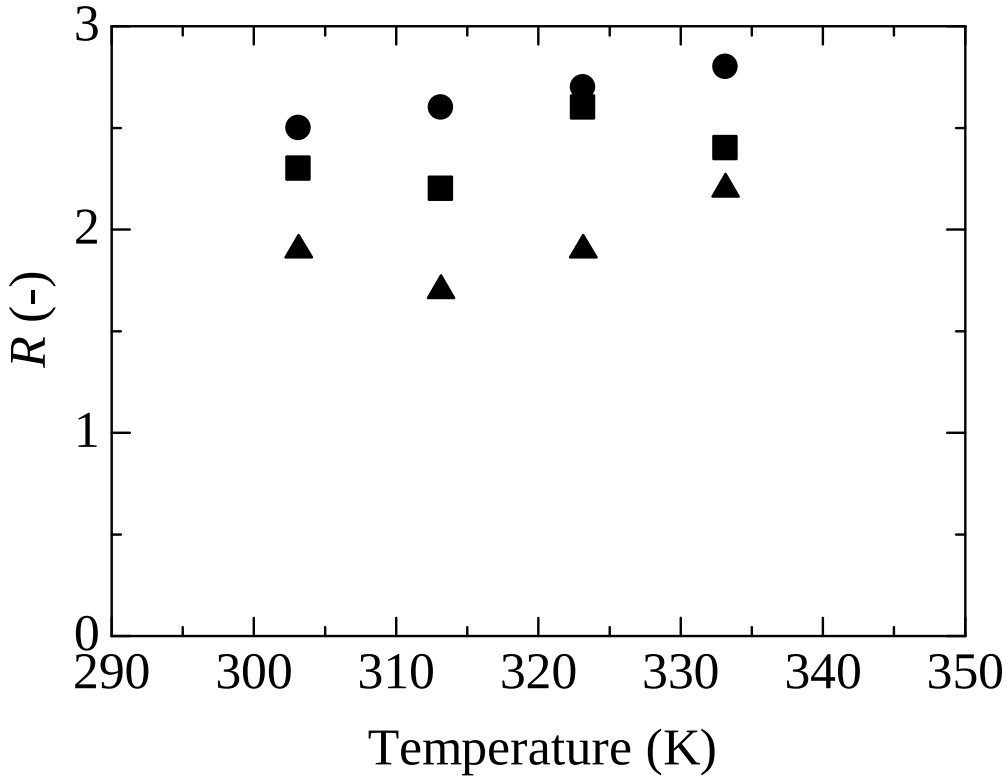

Fig. 5.5 Rate of the enhancement of CO_2 permeabilities, (●) [bmim][PF_6] with humid feed, (■) [bmim][PF_6] with humid permeate, (▲) [bmim][Tf_2N] with humid feed

The knowledges of the solubility and diffusion coefficients of CO_2 are very important to understand the permeation mechanism through ionic liquid membrane with and without water vapor. Vapor liquid equilibrium relationship is considered for the calculation of the solubility of CO_2, x_{CO2}, in ionic liquid as presented follows:

$$x_{CO2} = \frac{p_{CO2}}{\gamma_{CO2} f_{CO2}^{ref}} \tag{5.3}$$

where p_{CO2}, γ_{CO2} and f_{CO2}^{ref} stand for partial pressure, activity coefficient and fugacity of CO_2 in liquid at the standard state, respectively.

The fugacity of CO_2 at the standard state can be obtained from the equation that was proposed by Shimoyama et al [65]:

$$\ln f_{CO2}^{ref} = 10.752 - \frac{1787.8}{T} \tag{5.4}$$

where f_{CO2}^{ref} and T are fugacity at standard state and temperature, respectively.

Solubility coefficient of CO_2 in the ionic liquid is calculated from substitution solubility x_{CO2} in mole fraction from Eq. (5.3) into Eq. (5.5) as follows:

$$C_{CO2} = \frac{T}{273.15} \cdot \frac{\rho_{\mathrm{IL}} \times 22.4 \times 10^3}{M_{\mathrm{IL}} p_{\mathrm{CO_2}}} \cdot \frac{x_{\mathrm{CO_2}}}{1 - x_{\mathrm{CO_2}}} \tag{5.5}$$

where C, T, ρ_{IL}, M_{IL} and $p_{\mathrm{CO_2}}$ mean the solubility coefficient in $cm^3(STP)cm^{-3}\ cmHg^{-1}$, temperature in K, density of ionic liquid in g ml^{-1}, molar mass in g mol^{-1} and partial pressure of CO_2 in cmHg, respectively. In the case of water vapour, molar mass of the mixture, $M_{\mathrm{IL+w}}$, was computed by following equation:

$$M_{IL+w} = \left(M_{IL} \times \frac{n_{IL}}{n_{IL} + n_w} \right) + \left(M_w \times \frac{n_w}{n_{IL} + n_w} \right) \tag{5.6}$$

where n is mole of the component. The mixture density, $\rho_{\mathrm{IL+w}}$, was obtained from Li et al [90].

The diffusion coefficient of CO_2 in the ionic liquid is given from the correlation proposed by Morgan et at [75].

$$D_{CO2} = \frac{3.7 \times 10^{-3}}{\eta_{\mathrm{IL}}^{0.59} V_{\mathrm{CO_2}} \rho_{\mathrm{IL}}^{2}} \tag{5.7}$$

where D, η_{IL}, V and ρ_{IL} are the diffusion coefficient in $cm^2 s^{-1}$, viscosity of ionic liquid in cP, molar volume at normal boiling point in $cm^3 mol^{-1}$ and density of ionic liquid in g ml^{-1}. The solubility and diffusion coefficients of CO_2 in [bmim][PF_6] with and without water vapour were calculated. Their density and viscosity were obtained from literature [90]. The results of solubility and diffusion coefficients of CO_2 in [bmim][PF_6] gel membrane with dry and humid streams at feed and permeate sides were given in Table 5.3 and Fig. 5.6. The rise of temperature affected the decrease of solubility coefficient as presented in Fig. 5.6a. In this study, the assumption for humid permeate stream is no water concentration at the interphase between CO_2 and liquid membrane. Therefore, the solubility coefficient of humid permeate stream is similar with dry feed stream. The highest solubility coefficient was obtained from both dry feed and humid permeate streams while the humid feed stream gave the lowest for all temperature. Fig. 5.6b shows the increase of diffusion coefficient with temperature. The results are adverse with solubility coefficient that is humid feed and permeate streams show the similar diffusion coefficient but still higher than dry feed stream.

Table 5.3 Solubility and diffusion coefficients of CO_2 in [bmim][PF_6] gel membrane

Temperature (K)	$C\times10^3$ (cm^3(STP)cm^{-3} $cmHg^{-1}$)			$D\times10^6$ (cm^2 s^{-1})		
	Dry feed	Humid feed	Humid permeate	Dry feed	Humid feed	Humid permeate
303.15	2.37	2.37	2.02	2.43	2.59	2.58
313.15	1.96	1.96	1.84	3.39	3.75	3.75
323.15	1.68	1.68	1.61	5.14	5.74	5.74
333.15	1.48	1.48	1.49	6.54	7.24	7.25

(a)

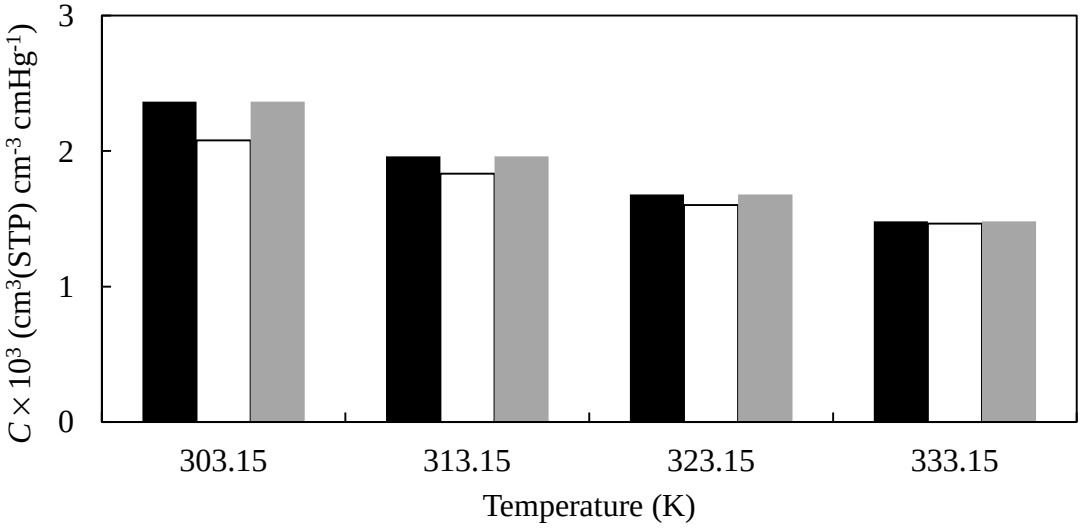

(b)

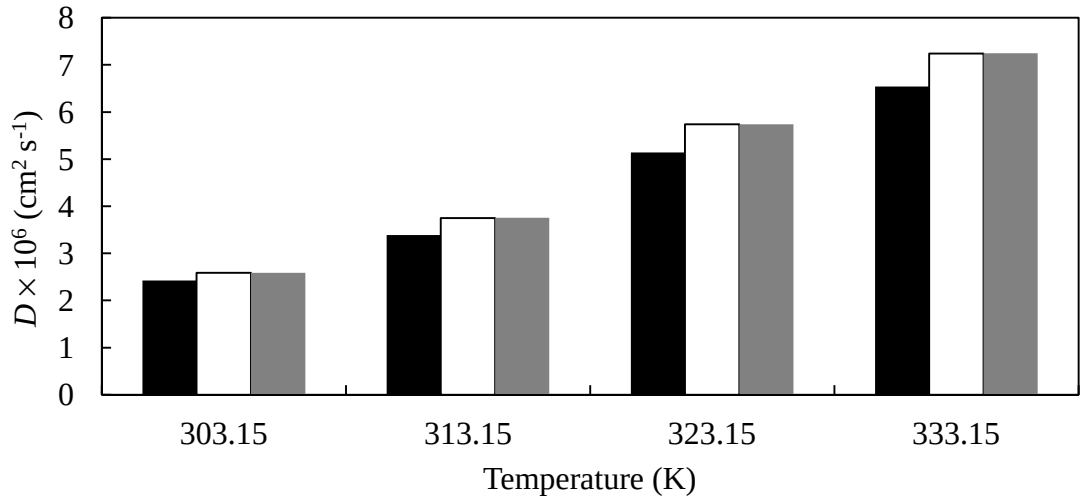

Fig.5.6 Plot of solubility and diffusion coefficients (■) dry feed, (□) humid feed, (■) humid permeate (a) solubility coefficient, (b) diffusion coefficient

To make the clear understanding of the effect of the addition of water into ionic liquid membrane on CO_2 permeabilities, the enhancement rate of solubility and diffusion coefficients of CO_2 were calculated as follows:

$$\frac{Q_{IL+w}}{Q_{IL}} = \frac{C_{IL+w}}{C_{IL}} \times \frac{D_{IL+w}}{D_{IL}} \times \alpha \qquad (5.8)$$

where α is the additional parameter which present difference of enhancement ratio between experiment and theoretical data. The calculation results of feed and permeate streams are shown in Tables 5.4 and 5.5, respectively. The α parameters of humid feed and permeate insignificantly change with temperature. At humid feed and humid permeate streams, the enhancement rate of diffusion coefficient is higher than solubility coefficient for all temperature. The supported reason should be the presence of water vapor resulting in the decrease of viscosity of ionic liquid. Fig. 5.7 shows the molecular interaction of CO_2 water and $[PF_6]^-$ molecules. In case of pure ionic liquid, CO_2 molecules are fastened with $[PF_6]^-$ as shown in Fig. 5.7a. In contrast, the presence of water in ionic liquid shows that water molecules intervene between the CO_2 and $[PF_6]^-$. The $[PF_6]^-$ has pair correlation functions with water molecule above the unity [87]. It suggests that the pair of water-$[PF_6]^-$ is rather stable leading to comfortable moving of CO_2 molecules as given in Fig. 5.7b.

Table 5.4 Enhancement rate of permeability, solubility, diffusion coefficients and α of CO_2 by addition of water at feed stream

Temperature (K)	Q_{IL+w}/Q_{IL}	C_{IL+w}/C_{IL}	D_{IL+w}/D_{IL}	α
303.15	2.54	0.88	1.07	2.70
313.15	2.60	0.93	1.11	2.52
323.15	2.73	0.95	1.12	2.57
333.15	2.75	0.99	1.11	2.50

Table 5.5 Enhancement rate of permeability, solubility, diffusion coefficients and α of CO_2 by addition of water at permeate stream

Temperature (K)	Q_{IL+w}/Q_{IL}	C_{IL+w}/C_{IL}	D_{IL+w}/D_{IL}	α
303.15	2.52	1.00	1.07	2.36
313.15	2.38	1.00	1.11	2.14
323.15	2.57	1.00	1.12	2.29
333.15	2.38	1.00	1.11	2.14

(a)

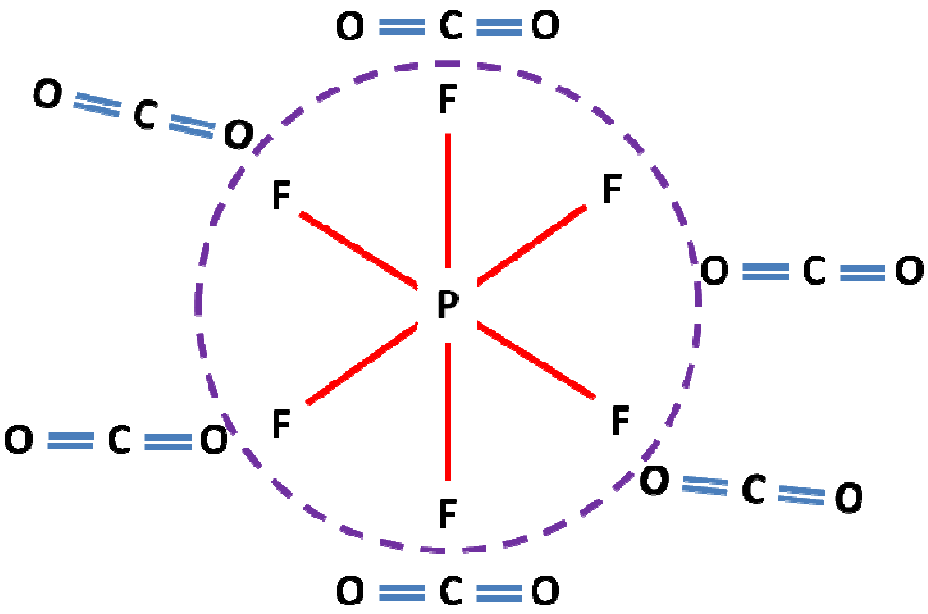

(b)

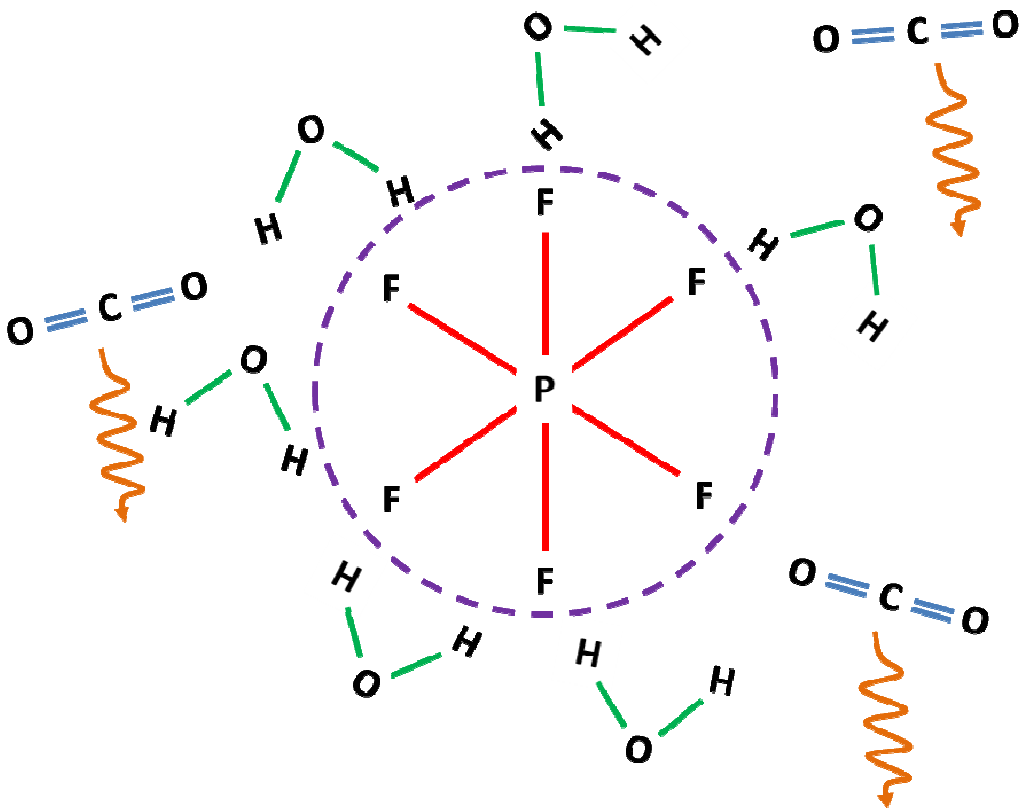

Fig. 5.7 Molecular interaction, (a) CO_2 - $[PF_6]^-$, (b) CO_2 - H_2O - $[PF_6]^-$

In addition, the permeation of water was measured in this study. Table 5.6 and Fig. 5.8 show the results of water permeabilities through ionic liquid membrane. Permeabilities of water decreased with temperature in case of [bmim][PF_6] membrane while this phenomenon could not be found in [bmim][Tf_2N] membrane. It is very interesting results that the poor water permiablities was obtained from [bmim][Tf_2N] membrane which presented the higher CO_2 permeabilities while [bmim][PF_6] membrane presented the contradictory phenomena. It is confirmed our hypothesis $[PF_6]^-$ anion has stronger affinity with water molecules than $[Tf_2N]^-$. However, the further study is required for more discussion.

Table 5.6 Experimental results of H_2O permeabilities with temperature dependence

Ionic liquid membrane	$Q_{H2O} \times 10^{-2}$ (Barrer)			
	303.15 K	313.15 K	323.15 K	333.15 K
[bmim][PF_6] (humid feed)	712	652	424	426
[bmim][PF_6] (humid permeate)	850	590	470	669
[bmim][Tf_2N] (humid feed)	340	499	373	351

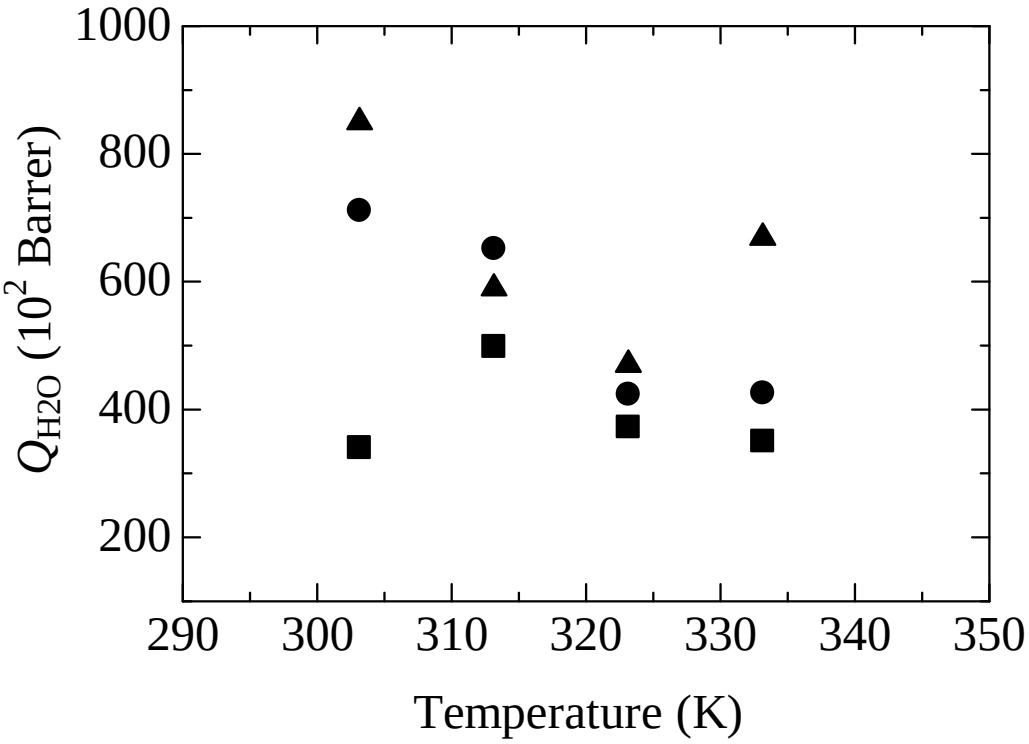

Fig. 5.8 Permeabilities of water through ionic liquid membranes, (●) [bmim][PF_6] at humid feed, (▲) [bmim][PF_6] at humid permeate, (■) [bmim][Tf_2N] at humid feed

5.4 Conclusions

The increase of temperature caused the relaxation of the gel membrane structure owing to the higher CO_2 mass transfer. The presence of water in ionic liquid membrane is able to enhance the CO_2 permeabilities due to the change of absorption of CO_2 mechanism. The freedom movement of CO_2 molecules occurs in the gel phase. The humid permeate stream gave the lower CO_2 permeabilities than that of humid feed stream due to the low water concentration and low CO_2 solubility. When consideration of two species of ionic liquid membranes found that [bmim][PF_6] membrane gave higher the rate of CO_2 permeabilities enhancement than that of [bmim][Tf_2N] membrane. These results also suggested that $[PF_6]^-$, which was more hygroscopic, presented the stronger interaction with water molecules than that of $[Tf_2N]^-$. The addition of water in ionic liquid results in the decrease of solubility coefficient whereas

the increase of diffusivity coefficient is observed. It is clear that the presence of water in ionic liquid membrane can improve of CO_2 permeabilities. Water permeabilities were also measured in this study. Low water permeabilities is obtained from [bmim][Tf_2N] membrane which present high CO_2 permeabilities. That means the affinity of the molecular pair between water and $[Tf_2N]^-$ is weaker than that of $[PF_6]^-$. This work may be applied to CO_2 separation process design in the industrial scale such as power plant without the removal of water vapor from the feed and permeate streams. The system which contains amount of water vapor is able to operate without concern.

Chapter 6

Prediction of the membrane area and amount of CO_2 mole fraction at permeate for CO_2 separation process

6.1 Statement of problem and objective

Chapters 3 to 5 reported the experimental data of the study of CO_2 capture through ionic liquid membranes. In the Chapter 3, CO_2 permeabilities and selectivities were studied monitoring the impact of anion species of ionic liquid membranes and operating temperature. The separation of CO_2/N_2 mixed gas through ionic liquid membrane were investigated by changing gas concentration at feed side, total pressure difference involved the flow rate of gas as elucidated in Chapter 4. Finally, in the Chapter 5, the effects of water vapor streams at feed and permeate on single gas CO_2 separation through ionic liquid membrane were examined. The results from experiments in these three Chapters would be analyzed and predicted the trend in order to broaden the knowledge of gas separation by membrane technique. Therefore, the predictions of other essential variables such as the size of membrane, percent reduction of membrane area and the CO_2 capacity at permeate without performing the experiments are necessary.

In this study, the results from the experiments in Chapters 3 to 5 were introduced and used in the computational simulation which proposed in a literature [91]. The estimations of desired membrane area for CO_2 separation, the percent decrease of membrane area and the amount of CO_2 mole fraction at permeate side were investigated. The simulation results would supposed to be an alternative for designing the CO_2 separation process using ionic liquid membrane.

6.2 Theory

CO_2 separation process in our study was based on the simple model was proposed by Sui et al. [91]. They separated volatile organic compounds (VOCs) from air through triethylene glycol liquid membrane. Air and VOCs were mixed in the

chamber with the volume of 1 m^3. Feed side was considered as a perfect mixing while a plug flow model was applied for the permeate side. In our case, CO_2 and N_2 mixed gas at the feed side were regarded as the perfect mixing and the permeate side was the plug flow also. The schematic of CO_2 separation simulation using ionic liquid membrane process is shown in Fig. 6.1.

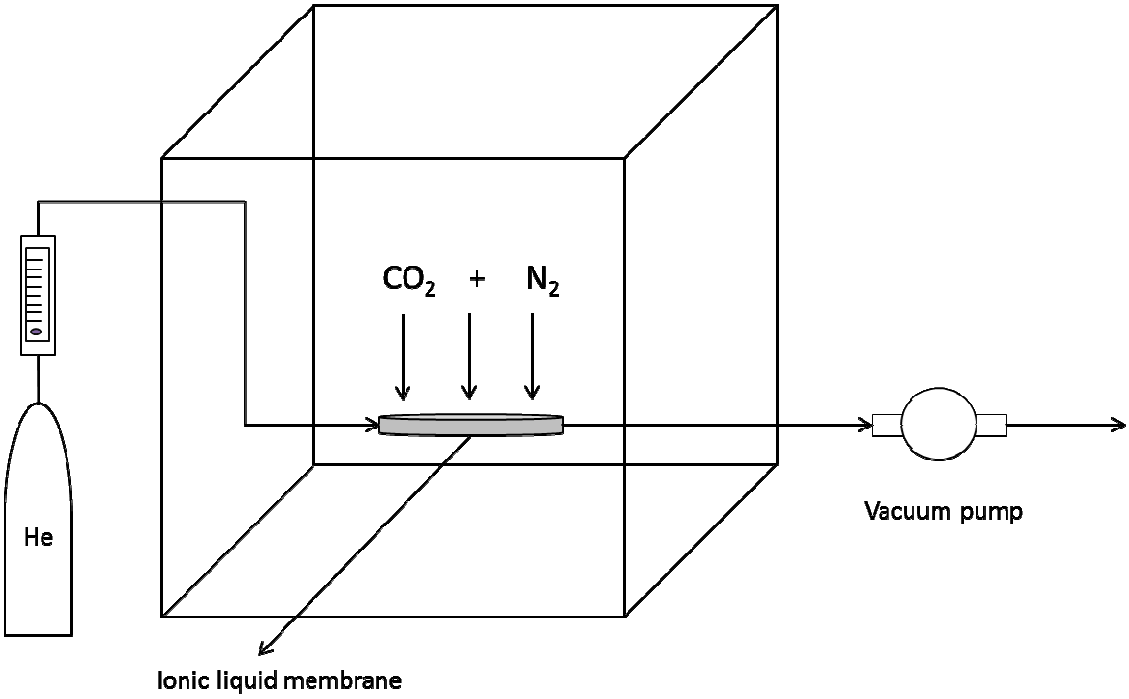

Fig. 6.1 Schematic of CO_2 separation simulation through ionic liquid membranes

The concentration of CO_2 over the ionic liquid membrane in the chamber, *x*, was constant whereas the amount of CO_2 at permeate side, *y*, increased along the membrane area due to the driving force of CO_2 partial pressure across the ionic liquid membrane given by following equation:

$$G\frac{dy}{dA}=\frac{Q}{\delta}\left(p_f x-p_p y\right) \tag{6.1}$$

where *G*, *A*, *Q* and δ represent sweep gas flow rate at permeate side in $cm^3(STP)s^{-1}$, membrane area in cm^2, permeability of CO_2 in $cm^3(STP)cm\ cm^{-2}\ s^{-1}\ cmHg^{-1}$ and membrane thickness in cm, respectively. Total pressure at feed and permeate in cmHg are p_f and p_p, respectively.

In order to predict the reduction of membrane area when changing the affecting operating conditions, the calculation can be evaluated by following equation:

$$\%reduction\,of\ \ membrane\,area = \frac{H - L}{H} \times 100 \qquad (6.2)$$

where H and L are higher and lower membrane area values, respectively.

6.3 Computational details

The simulation of the desired membrane area for CO_2 separation through ionic liquid membrane and the prediction of CO_2 concentration at permeate side was performed using the results from the experiments in Chapters 3-5. The operating conditions are difference in each Chapter. The variables, operating temperatures (T = 303.15 to 343.15 K) and species of ionic liquids ([emim][BF_4], [bmim][BF_4], [bmim][PF_6], [bmim][Tf_2N], [bmim][OTf] and [bmim][dca]), affected CO_2 permeation were studied in Chapter 3. In Chapter 4, the experiments were performed under the constant temperature of 313.15 K. The pressure difference (Δp = 0.05, 0.10, 0.15 and 0.21 atm), CO_2 volume fractions at feed side (X_{CO2} = 0.3, 0.4 and 0.5) and total flow rate at feed side were investigated. These variables made the effect on CO_2 permeability and selectivity. For Chapter 5, presence of water at feed and permeate streams were determined and compared the results of CO_2 permeation with the dry feed streams by varying temperatures (T = 303.15 to 333.15 K). The membrane area used in this study was 19.6 cm^2 for whole experiments. The summaries of experimental conditions of Chapters 3, 4 and 5 are listed in Tables 6.1, 6.2 and 6.3, respectively.

Table 6.1 Detail of experimental conditions of Chapter 3

Variable	Detail
Ionic liquid	Six species: [emim][BF_4], [bmim][BF_4], [bmim][PF_6], [bmim][Tf_2N], [bmim][OTf] and [bmim][dca]
x	1
δ	Listed in Table 3.1
Q_{CO2}	Listed in Table 3.3
G	1.66667 $cm^3(STP)s^{-1}$
p_f	92 cmHg
p_p	76 cmHg

Table 6.2 Detail of experimental conditions of Chapter 4

Variable	Detail
Ionic liquid	Two species: [bmim][PF_6] and [bmim][Tf_2N]
x	0.3, 0.4 and 0.5
δ	Listed in Table 4.2
Q_{CO2}	Listed in Table 4.4
G	0.16667 $cm^3(STP)s^{-1}$
p_f	Depended on the conditions of total pressure difference
p_p	76 cmHg

Table 6.3 Detail of experimental conditions of Chapter 5

Variable	Detail
Ionic liquid	Two species: [bmim][PF_6] and [bmim][Tf_2N]
x	1
δ	Listed in Table 5.1*
Q_{CO2}	Listed in Table 5.2
G	1.66667 $cm^3(STP)s^{-1}$
p_f	92 cmHg
p_p	76 cmHg

*The membrane thickness of humid feed stream was used for the simulation of dry feed stream in order to prevent the discrepancy between humid and dry thicknesses.

6.4 Results and discussion

The simulations of CO_2 separation through ionic liquid membranes were conducted using Eq. 6.1 based on the various conditions of the experiments in Chapters 3 to 5. The simulations were focused on the prediction of permeate quantity of CO_2 and the desired membrane area. The results of simulations using experimental results from Chapter 3 which specify the membrane area at A = 20, 100, 1000 cm^2 are shown in Figs. 6.2a, 6.2b and 6.2c, respectively. From Fig. 6.2, the increase in operating temperatures resulted in the enhancement of CO_2 mole fraction at permeate. Moreover, the increase in membrane area is able to absorb more CO_2 concentration for all prediction. The raise of membrane area 50 times presents the permeate amount of CO_2 concentration around 4 to 5 times while increase the membrane to 500 times, the CO_2 mole fraction at permeate approximately gains around 34 to 42 times.

(a)

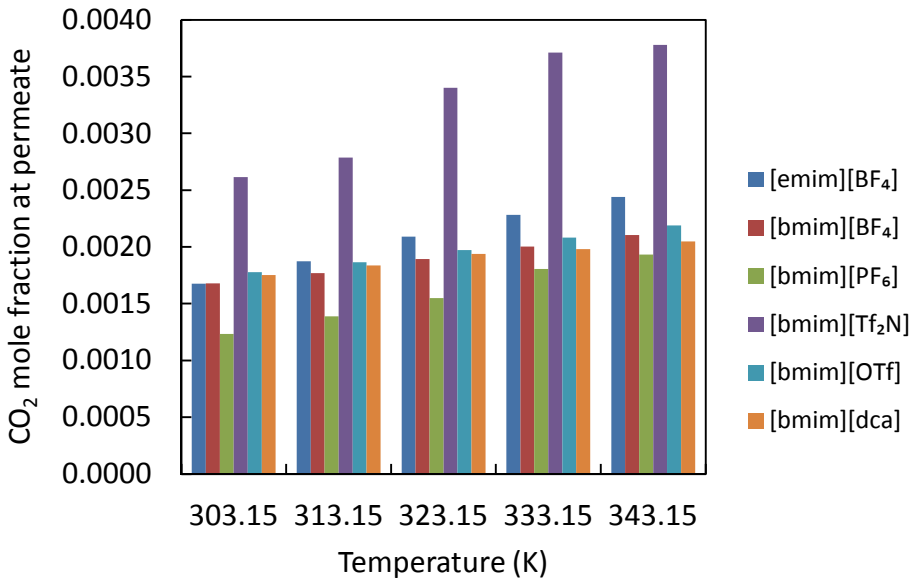

(b)

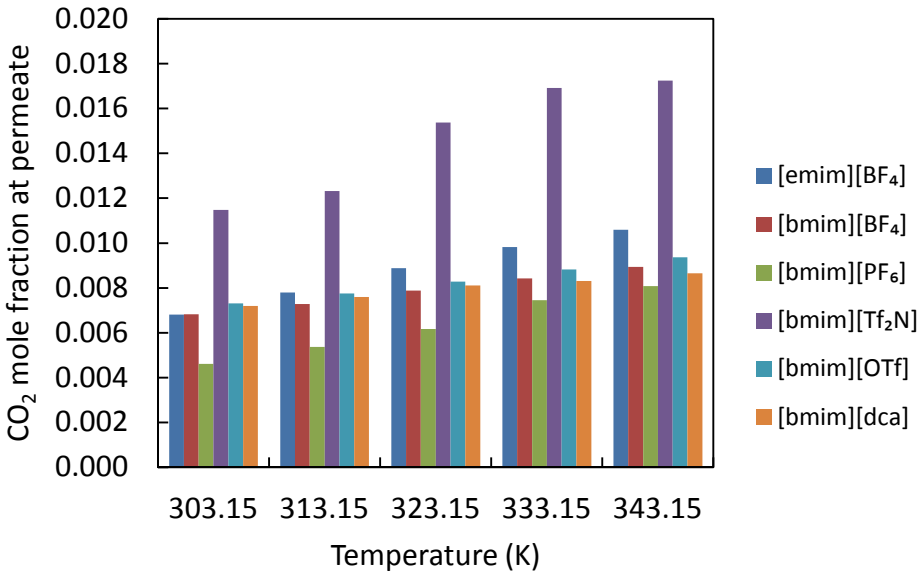

(c)

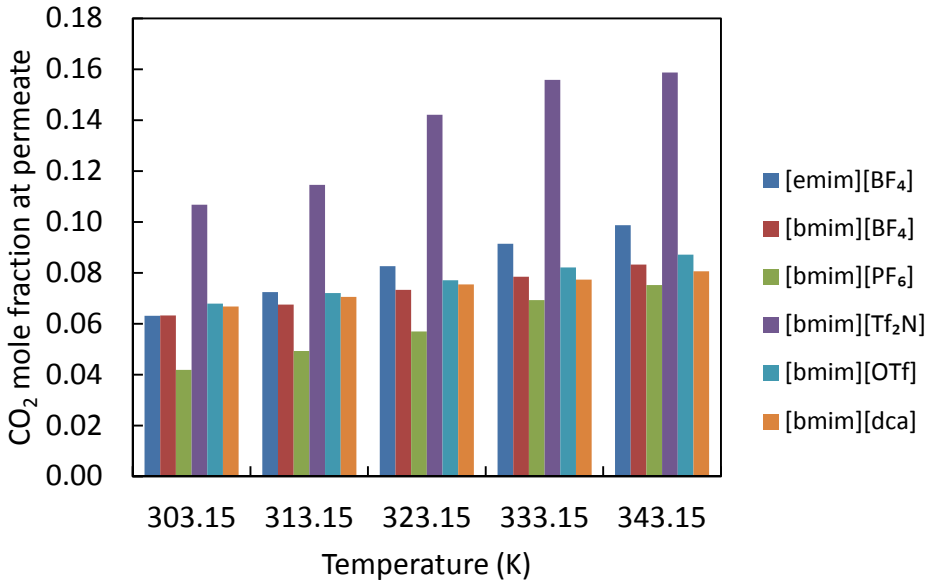

Fig. 6.2 Comparison of different species of ionic liquid membranes with temperature dependence, (a) membrane area = 20 cm^2, (b) membrane area = 100 cm^2, (c) membrane area = 1000 cm^2

To predict the required membrane area, the mole fraction of CO_2 at permeate was defined at 0.001, 0.01, 0.1, 0.25, 0.50, 0.75 and 1. Fig. 6.3 shows the comparison of required membrane area between the difference of operating temperature (303.15 and 343.15)K. As shown in Fig. 6.3a, to obtain the equimole fraction, [bmim][Tf_2N] liquid membrane used the lowest membrane area of 19050 cm^2 whereas [bmim][PF_6] liquid membrane required the highest membrane area of 50500 cm^2 at unity of CO_2 mole fraction. For other ionic liquid species ([emim][BF_4], [bmim][BF_4], [bmim][OTf] and [bmim][dca]), the requirement of membrane area shows the insignificant change. When increasing operating temperature to 343.15 K and the mole fraction of CO_2 at permeate keep the constant for all species of ionic liquid membranes, the required membrane area reduced. The [bmim][Tf_2N]and [bmim][PF_6] membranes still remain the similar trend with T = 303.15 K by giving the required membrane area of 14900 and 27500 cm^2, respectively at equimole fraction of unity as shown in Fig. 6.3b. The [emim][BF_4], [bmim][BF_4], [bmim][OTf] and [bmim][dca] membranes demonstrate the significant difference of membrane area. The ranking of the smallest to the highest membrane area is [emim][BF_4] < [bmim][OTf] < [bmim][BF_4] < [bmim][dca] which correspond with experimental results of CO_2 permeabilities.

(a)

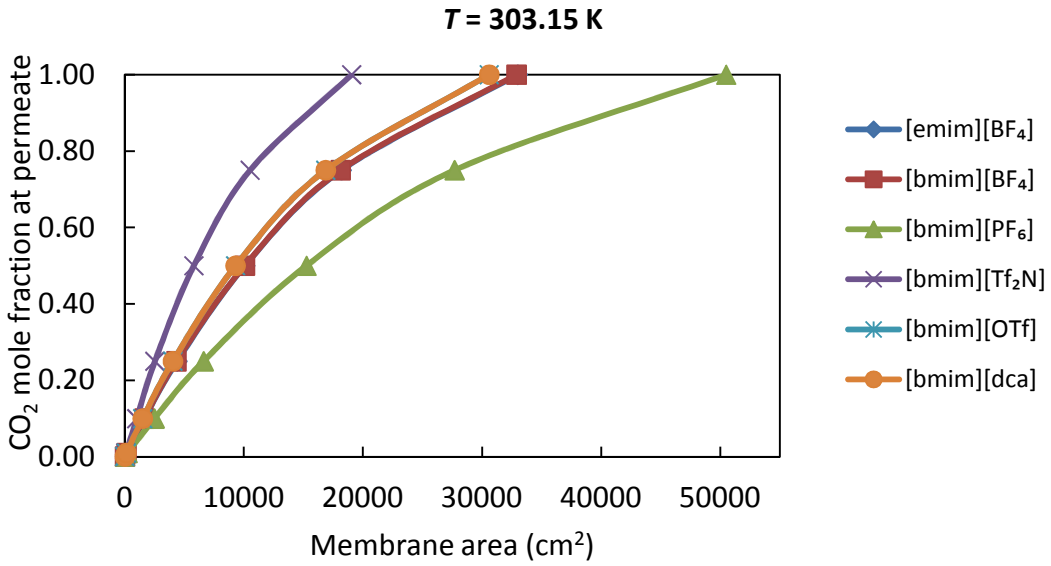

(b)

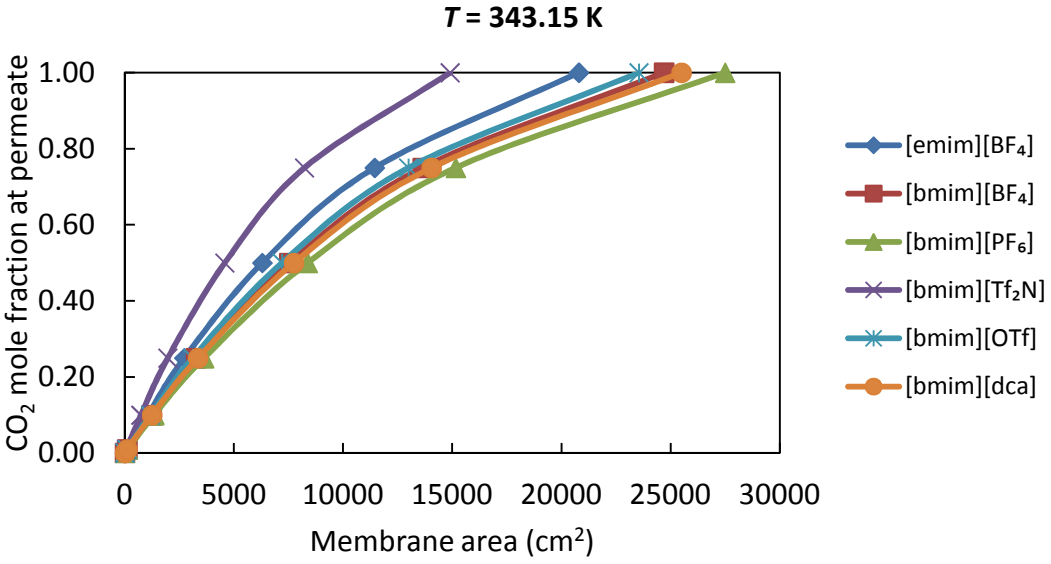

Fig. 6.3 Simulated results of required membrane area when specified the CO_2 mole fraction at permeate, (a) T = 303.15 K and (b) T = 343.15 K

As mentioned above, when increase in operation temperature from T = 303.15 to 343.15 K, the membrane area for CO_2 separation process decreased. To estimate the percent reduction of membrane area, Eq. (6.2) were used to calculate. The calculation results are illustrated in Fig. 6.4. The concentration of CO_2 at permeate was plotted in the logarithm scale against %reduction of membrane area. The simulation results show that when the increase in temperature, [bmim][PF_6] membrane shows the prominent decrease of membrane area around 45%. On the other hand, the smallest reduction of membrane area was obtained from [bmim][dca] membrane with the average value of 14%. The possibility explanation would be the effect of temperature dependence of [bmim][dca] membrane. It is quite interesting results that [bmim][Tf_2N] membrane did not show the lowest membrane area as expected.

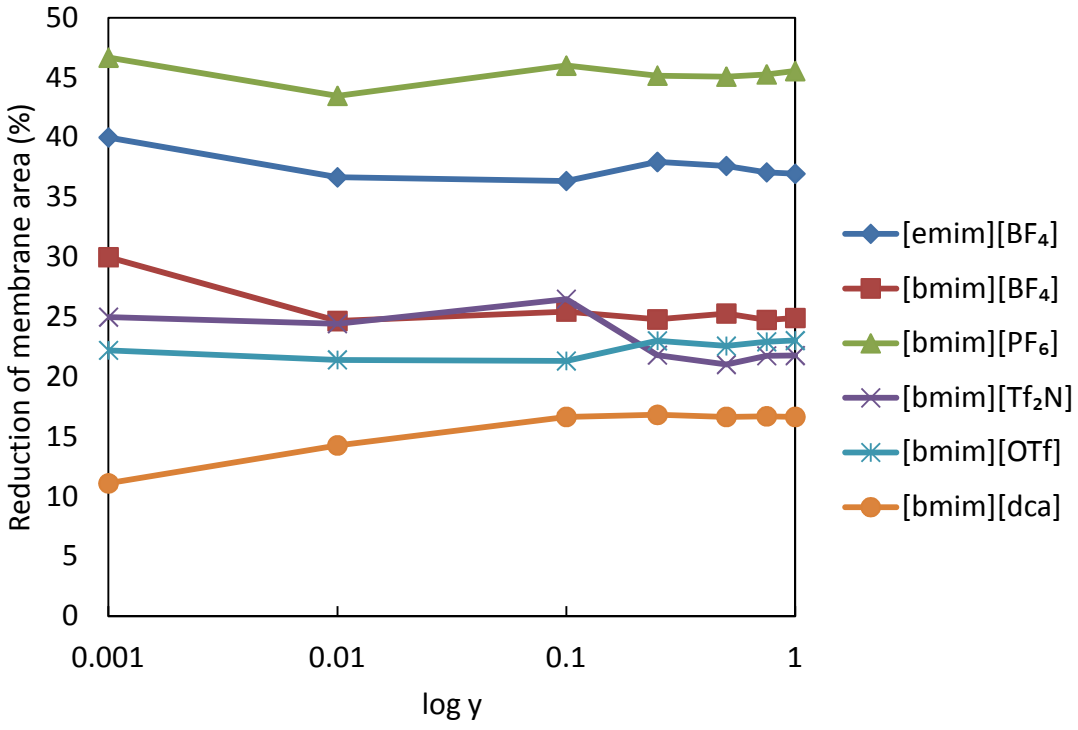

Fig. 6.4 Comparison of percent reduction of membrane area with different ionic liquid membranes

The simulation results using the conditions from Chapter 4 to optimize the membrane area are shown in Fig. 6.5. These simulations focused on the efficiency of

the membrane for CO_2 separation from CO_2/N_2 mixed gas until reach the steady state. The membrane area were fixed at 20, 50, 100, 500, 1000 and 2500 cm^2. The volume fractions of CO_2 at feed side, X_{CO2}, are varied from 0.3 to 0.5. The simulations are compared among total pressure difference of 0.05, 0.10, 0.15 and 0.21 atm and the difference of flow rate at the feed stream (F = 100 and 300 ml min^{-1}). The maximum capability of the liquid membrane for each condition and their optimum points of the membrane area to separate CO_2 from CO_2/N_2 can be seen in the graphes. As shown in Fig. 6.5, the optimum membrane areas were in the range of 2000 cm^2 for all simulation results excepted for [bmim][PF_6] membrane at X_{CO2} = 0.4 with Δp = 0.15 and 0.21 atm which required higher.

All simulation results demonstrate that the increase in total pressure difference leads to the enhancement of the absorption amount of CO_2 at permeate side which shows the unlike phenomena with the experimental results. The results strongly indicated that this simulation was not successful to predict CO_2 concentration at permeate when the total pressure difference changed because of the carrier saturation by the facilitated transport in this particular pressure range. The effects of the change of flow rate at feed side (F = 100 and 300 ml min^{-1}) on CO_2 absorption were compared each other. There simulation results show that there were no consequent changes between lower and higher flow rate at feed stream for whole simulation results.

(a)

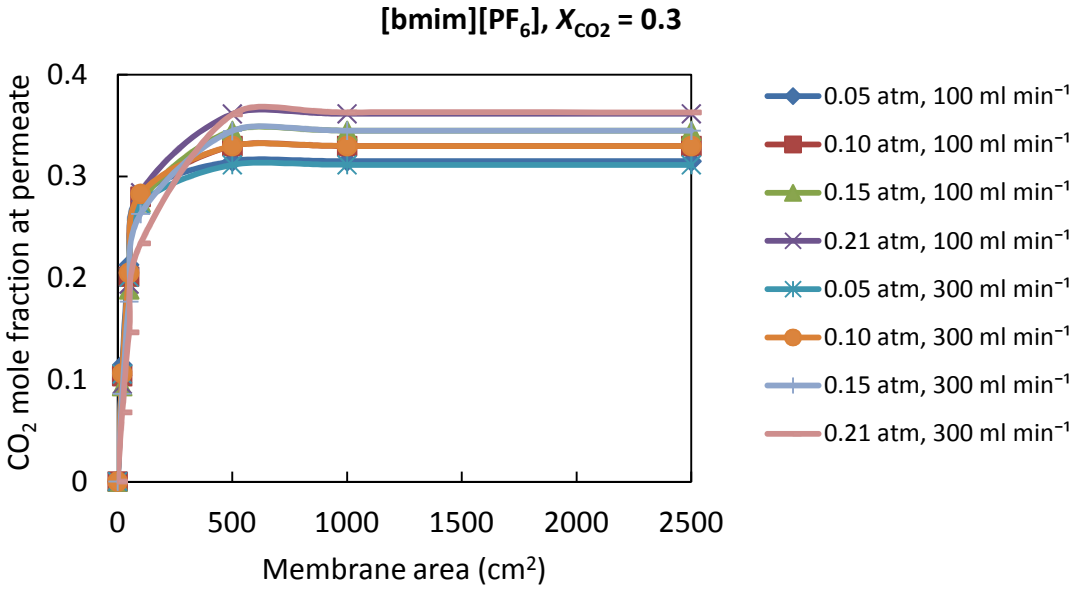
[bmim][PF6], XCO2 = 0.3
CO2 mole fraction at permeate
0.4
0.3
0.2
0.1
0
0
500
1000
1500
2000
2500
Membrane area (cm2)
0.05 atm, 100 ml min−1
0.10 atm, 100 ml min−1
0.15 atm, 100 ml min−1
0.21 atm, 100 ml min−1
0.05 atm, 300 ml min−1
0.10 atm, 300 ml min−1
0.15 atm, 300 ml min−1
0.21 atm, 300 ml min−1

(b)

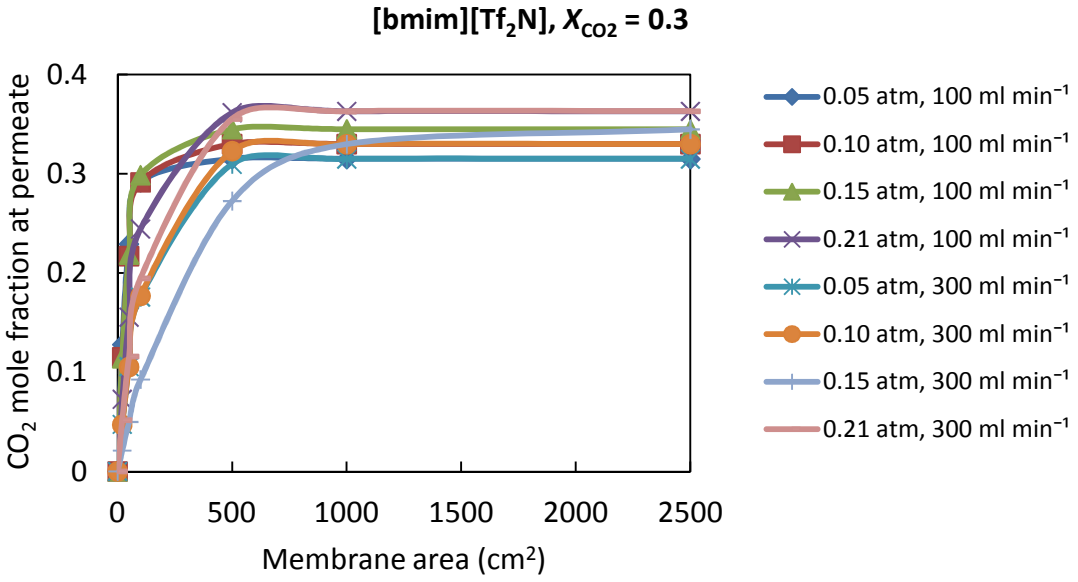
[bmim][Tf2N], XCO2 = 0.3
CO2 mole fraction at permeate
0.4
0.3
0.2
0.1
0
0
500
1000
1500
2000
2500
Membrane area (cm2)
0.05 atm, 100 ml min−1
0.10 atm, 100 ml min−1
0.15 atm, 100 ml min−1
0.21 atm, 100 ml min−1
0.05 atm, 300 ml min−1
0.10 atm, 300 ml min−1
0.15 atm, 300 ml min−1
0.21 atm, 300 ml min−1

(c)

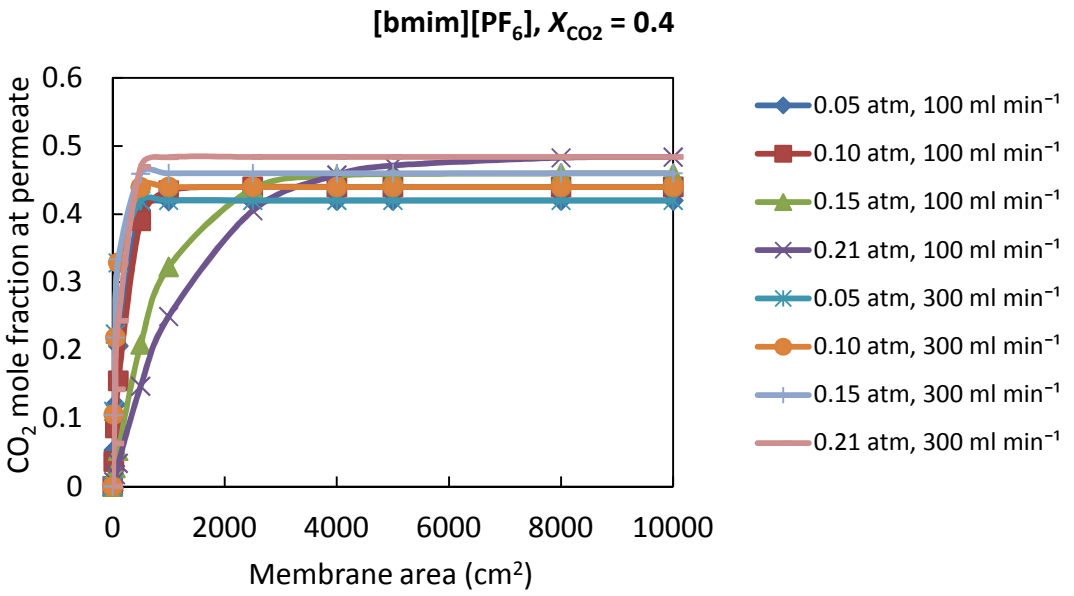
[bmim][PF6], XCO2 = 0.4
CO2 mole fraction at permeate
0
0.1
0.2
0.3
0.4
0.5
0.6
0
2000
4000
6000
8000
10000
Membrane area (cm2)
0.05 atm, 100 ml min-1
0.10 atm, 100 ml min-1
0.15 atm, 100 ml min-1
0.21 atm, 100 ml min-1
0.05 atm, 300 ml min-1
0.10 atm, 300 ml min-1
0.15 atm, 300 ml min-1
0.21 atm, 300 ml min-1

(d)

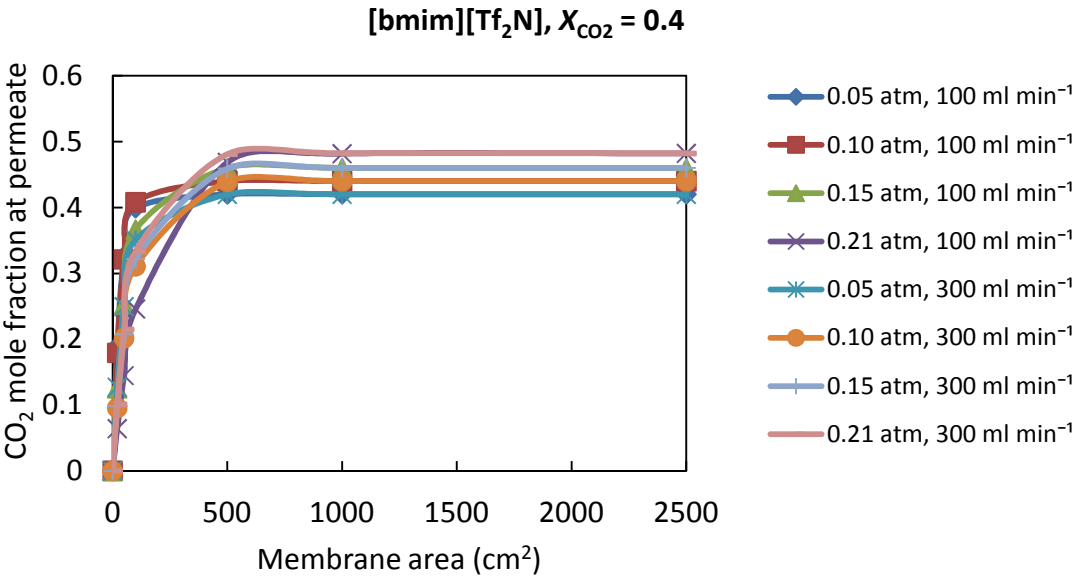
[bmim][Tf2N], XCO2 = 0.4
CO2 mole fraction at permeate
0
0.1
0.2
0.3
0.4
0.5
0.6
0
500
1000
1500
2000
2500
Membrane area (cm2)
0.05 atm, 100 ml min-1
0.10 atm, 100 ml min-1
0.15 atm, 100 ml min-1
0.21 atm, 100 ml min-1
0.05 atm, 300 ml min-1
0.10 atm, 300 ml min-1
0.15 atm, 300 ml min-1
0.21 atm, 300 ml min-1

(e)

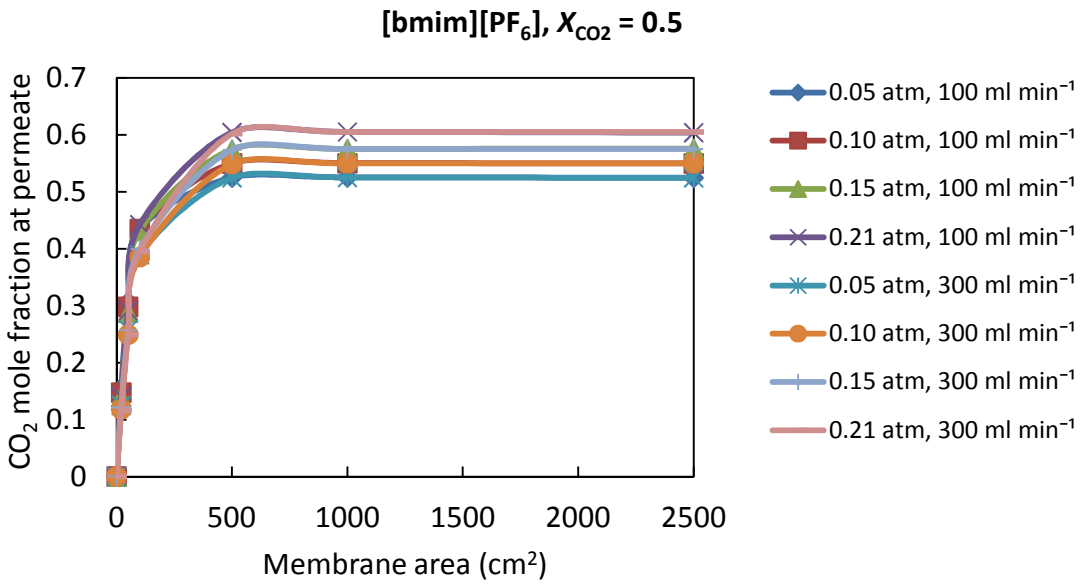

(f)

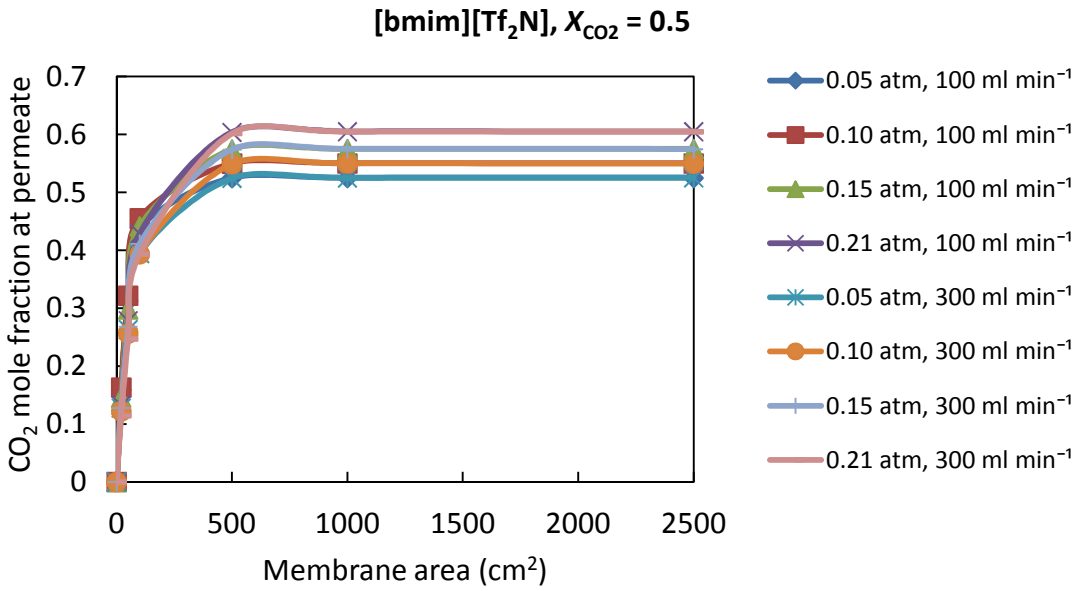

Fig. 6.5 Optimization of membrane area for CO_2 separation from CO_2/N_2 mixed gas, (a) [bmim][PF_6] membrane at X_{CO2} = 0.3, (b) [bmim][Tf_2N] membrane at X_{CO2} = 0.3, (c) [bmim][PF_6] membrane at X_{CO2} = 0.4, (d) [bmim][Tf_2N] membrane at X_{CO2} = 0.4, (e) [bmim][PF_6] membrane at X_{CO2} = 0.5, (f) [bmim][Tf_2N] membrane at X_{CO2} = 0.5

The presence of water in the feed and permeate streams were studied in Chapter 5. The simulation results using the conditions from Chapter 5 are illustrated in Figs. 6.6-6.8. The membrane area was defined as 20, 50, 100, 200, 300, 400, 500, 600, 800, 1000 and 2500 cm^2. The absorption amount of CO_2 at permeate was examined. Fig. 6.6 shows the comparison of CO_2 concentration at permeate of dry and humid feed streams using [bmim][PF_6] membrane. The increase in operating temperature resulted in the enhancement of amount of CO_2 mole fraction as seen in Figs 6.6a and b. At the similar membrane area, the results pointed out that CO_2 cooperated with water at feed side at lower temperature show the enhancement of CO_2 concentration at permeate than dry feed stream around 2.1 to 2.5 times as shown in Fig. 6.6a. Fig. 6.6b presents the increase in CO_2 mole fraction at permeate of humid feed stream around 2.4 to 2.7 times when equated with dry feed stream.

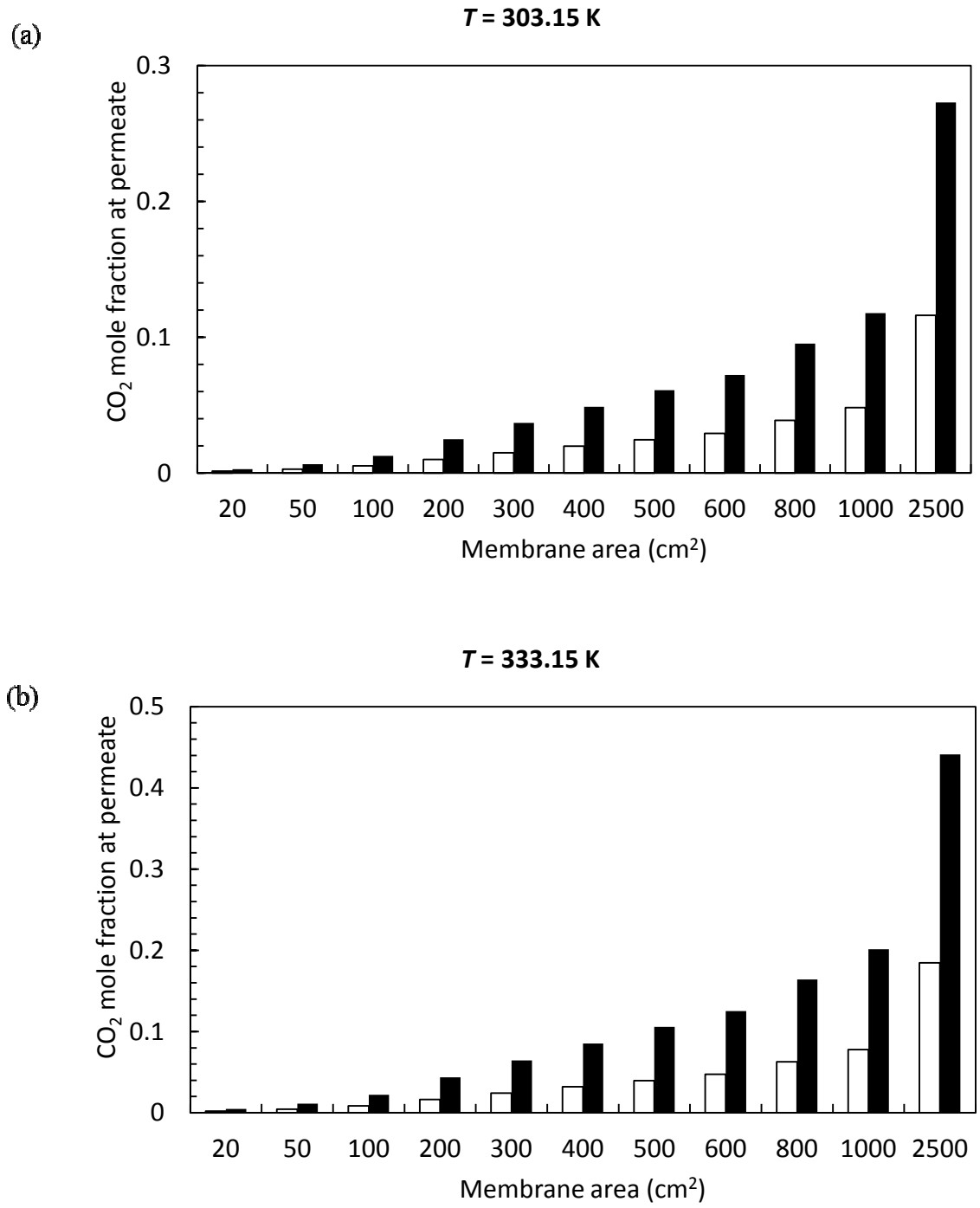

Fig. 6.6 Effect of (□) dry and (■) humid feed streams of CO_2 permeabilities through [bmim][PF_6] membrane on CO_2 mole fraction at permeate, (a) T = 303.15 K and (b) T = 343.15 K

Fig. 6.7 illustrates the comparison of amount of CO_2concentration at permeate through [bmim][PF_6] membrane of humid feed and permeate streams when the membrane areas were specified. At the similar membrane area, humid feed stream conditions gave higher CO_2 concentration at permeate than humid permeate stream around 1.1 times for T = 303.15 K and 1.2 times for T = 333.15 K.

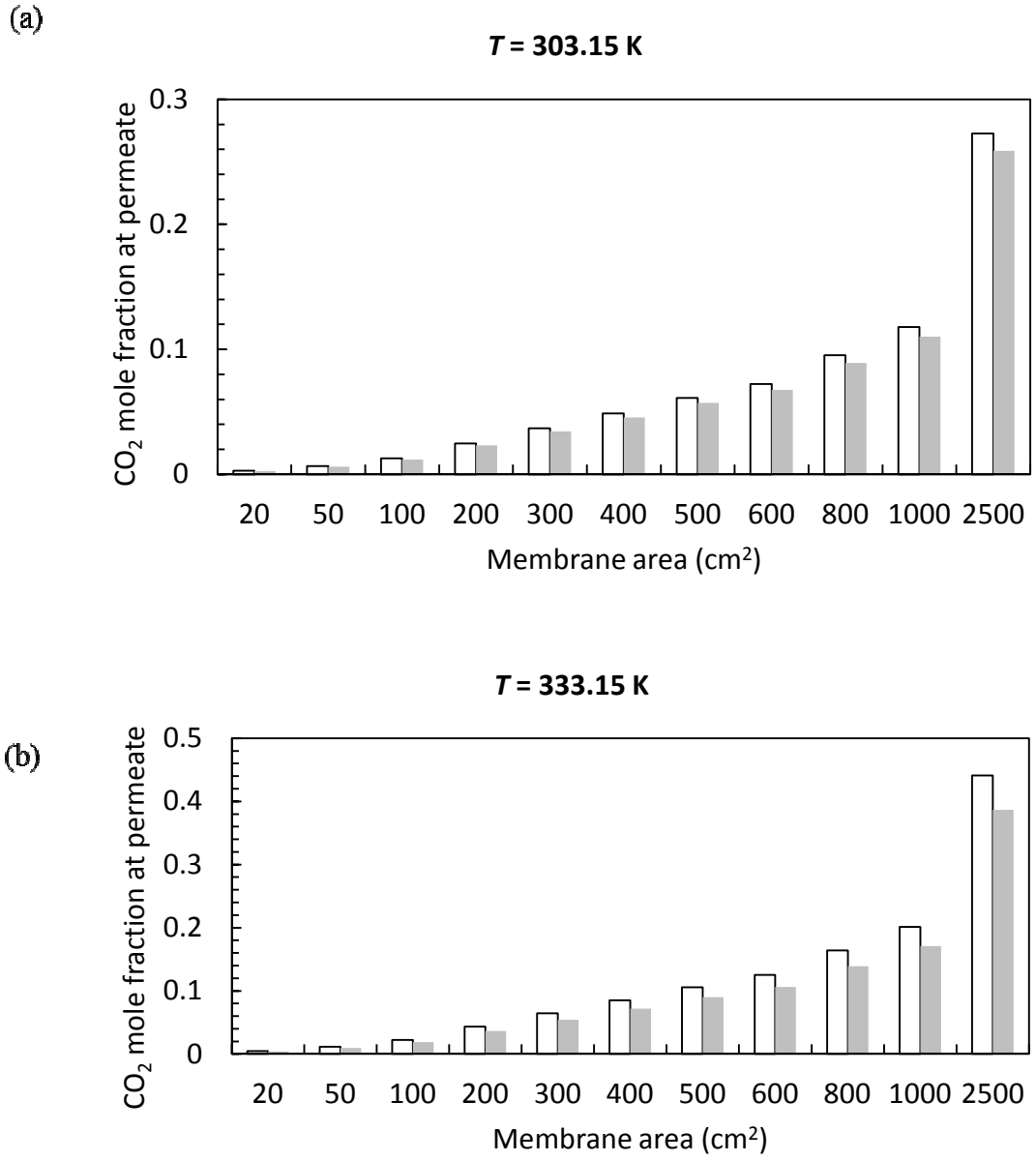

Fig. 6.7 Effect of (□) humid feed and (▒) humid permeate streams of CO_2 permeabilities through [bmim][PF_6] membrane on CO_2 mole fraction at permeate, (a) *T* = 303.15 K and (b) *T* = 343.15 K

Fig. 6.8 shows the amount of CO_2 concentration at permeate through [bmim][Tf_2N] membrane with and without water at feed streams when the membrane areas were kept constant. The results show the equivalent trend with the use of [bmim][PF_6]. As seen in Figs. 6.8a and b, the humid feed stream present higher CO_2

mole fraction than that of dry feed stream 1.6 to 1.7 and 1.8 to 2.1 times for T = 303.15 and 333.15 K, respectively.

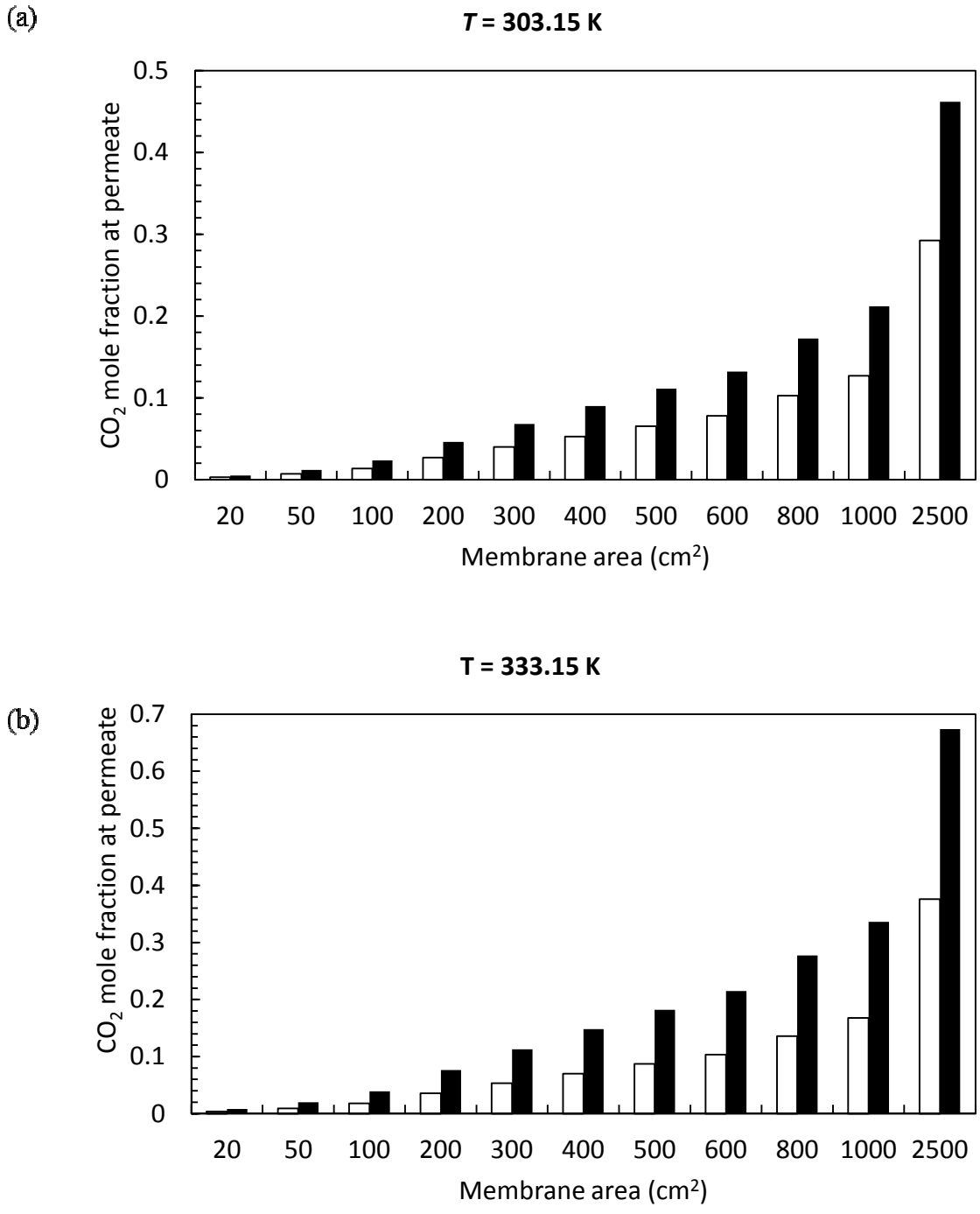

Fig. 6.8 Effect of (□) dry and (■) humid feed streams of CO_2 permeabilities through [bmim][Tf_2N] membrane on CO_2 mole fraction at permeate, (a) T = 303.15 K and (b) T = 343.15 K

To identify how large the membrane sizes for CO_2 capture process, CO_2 mole fractions at permeate side were fixed at 0.001, 0.01, 0.1, 0.25, 0.50, 0.75 and 1. The size of membrane could be estimated as shown in Fig. 6.9. Figs. 6.9a and b show the simulation results of membrane area for [bmim][PF_6] and [bmim][Tf_2N] membranes, respectively. This graph compared between dry and humid feed streams at T = 303.15 and 333.15 K. The results robustly indicated that smaller size of membrane was obtained from the humid feed stream as illustrated in Figs 6.9a and b. The [bmim][Tf_2N] membrane consume smaller membrane area than that of [bmim][PF_6] membrane. If the dry feed stream was changed to humid stream, the membrane area of [bmim][PF_6] would be reduced 2.5 to 2.6 and 2.7 to 2.8 times at T = 303.15 and 333.15 K, respectively. In addition, size of [bmim][Tf_2N] membrane would be decreased 1.7 and 2.2 to 2.3 times at T = 303.15 and 333.15 K, respectively by changing the dry to humid feed stream.

(a)

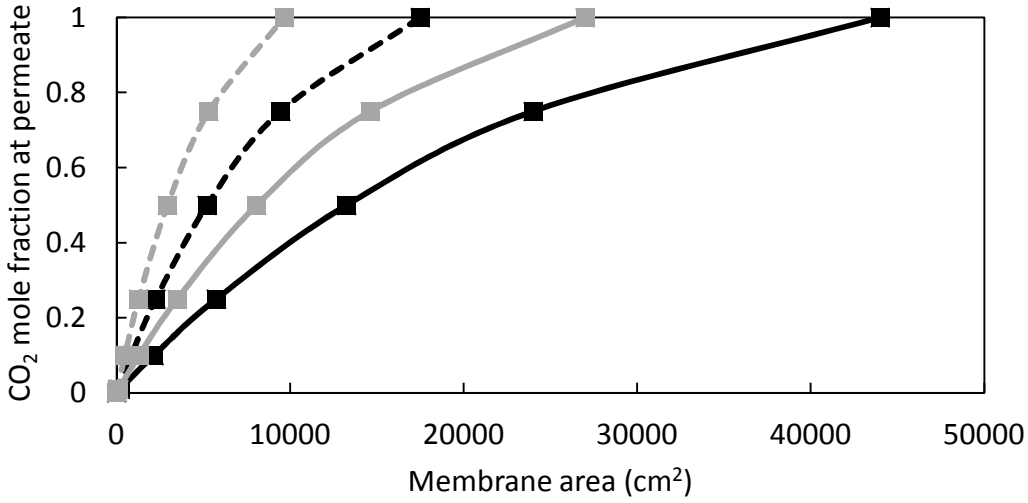

(b)

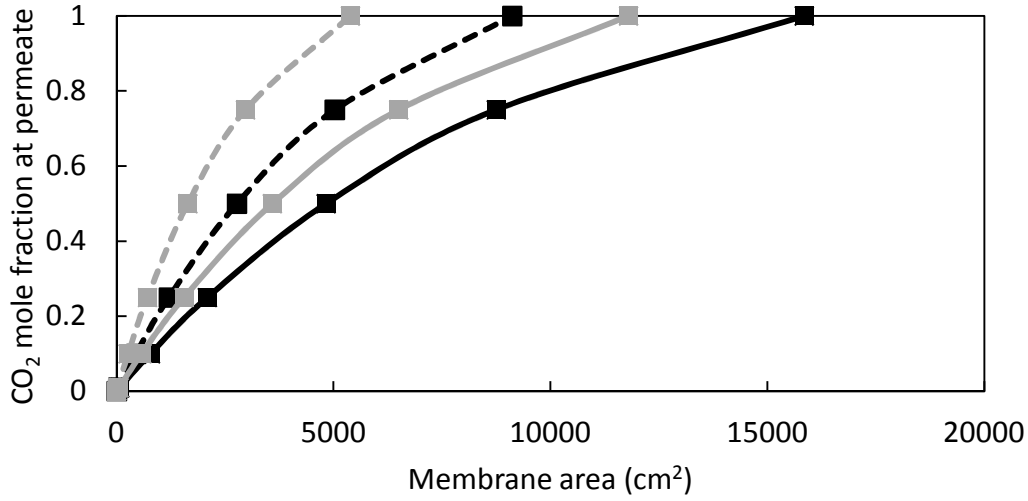

Fig. 6.9 Simulated results of required membrane area when specified the CO_2 mole fraction at permeate: —— dry feed at T = 303.15 K, – – – humid feed at T = 303.15 K, —— dry feed at T = 333.15 K, – – – humid feed at T = 333.15 K, (a) [bmim][PF_6] and (b) [bmim][Tf_2N]

As mentioned before, the size of membrane could be reduced by additional water into feed stream. The percent reduction of membrane area was also evaluated.

The calculation was computed by Eq. (6.2). The comparison of two species of ionic liquid membranes is shown in Fig. 6.10. At the constant temperature of 303.15 K, [bmim][PF_6] and [bmim][Tf_2N] membranes show the reduction of membrane size around 61 and 42%, respectively as shown in Fig. 6.10a. From Fig. 6.10b, at T = 333.15 K, 64 and 54% of membrane area reduction could be obtained from [bmim][PF_6] and [bmim][Tf_2N] membranes, respectively. When increasing in operating temperature from 303.15 to 333.15 K and changing dry to humid feed stream, the reduction of [bmim][PF_6] and [bmim][Tf_2N] membrane area were approximate 3 and 12%, respectively.

(a)

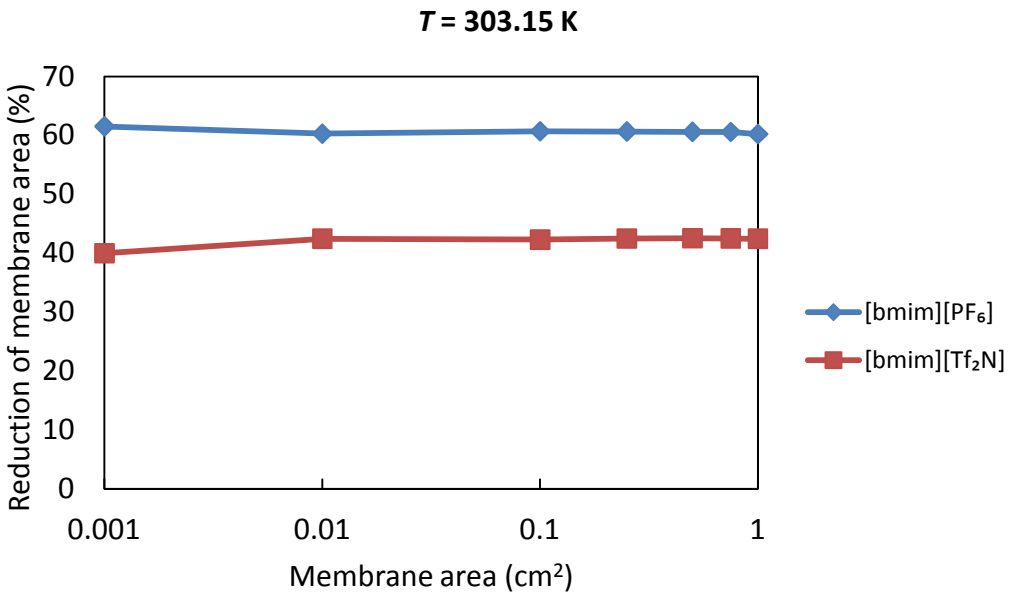
T = 303.15 K
Reduction of membrane area (%)
70
60
50
40
30
20
10
0
0.001
0.01
0.1
1
Membrane area (cm²)
[bmim][PF₆]
[bmim][Tf₂N]

(b)

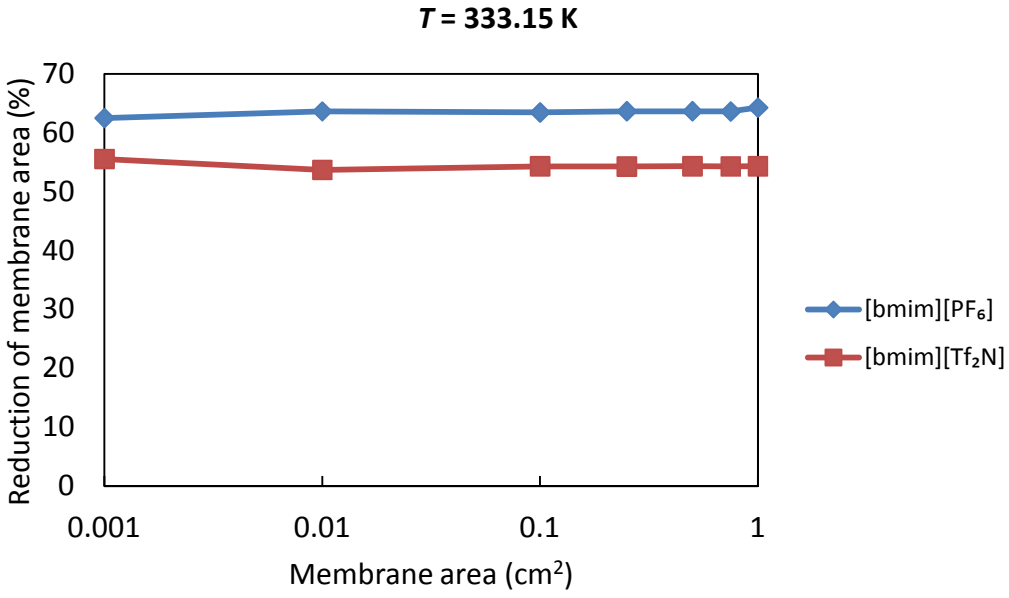
T = 333.15 K
Reduction of membrane area (%)
70
60
50
40
30
20
10
0
0.001
0.01
0.1
1
Membrane area (cm²)
[bmim][PF₆]
[bmim][Tf₂N]

Fig. 6.10 Comparison of percent reduction of membrane area by additional water into feed stream with different ionic liquid membranes, (a) T = 313.15 K and (b) T = 333.15 K

6.5 Conclusions

The simulations for prediction membrane area, CO_2 mole fraction at permeate and the percent reduction of membrane size were carried out using the conditions from experiments in Chapter 3 to 5. The conclusions were divided in three parts as follows:

1.) A model simulation of Chapter 3: An increase in operating temperature results in the less membrane area and the rise of CO_2 concentration amount at permeate side. [bmim][PF_6] and [bmim][Tf_2N] membranes show the highest and the smallest membrane size when fixing CO_2 concentration at permeate, respectively. When enlarging the membrane area 50 and 500 times, the amount of CO_2 concentration at permeate increased around 4 to 5 and 34 to 42 times, respectively. The permeability results from experiments by varying species of ionic liquid membrane corresponded with the simulation results. The highest and the lowest reduction of membrane area were obtained from [bmim][PF_6] and [bmim][dca], respectively.

2.) A model simulation of Chapter 4: the simulation results show disagreement with the experiment because the facilitated transport phenomena took place these pressure regions (0.05 to 0.21 atm). It implies that this model was suitable for the simulation of the CO_2 concentration at permeate side with constant pressure. Additionally, there was no significant difference of CO_2 mole fraction at permeate between lower and higher flow rate at feed stream for all simulation results. The optimum membrane depended on the conditions case by case.

3.) A model simulation of Chapter 5: amount of CO_2 mole fraction at permeate increase 2.1 to 2.5 and 2.4 to 2.7 times at T = 303.15 and 333.15 K, respectively when adding water into feed stream for [bmim][PF_6] membrane. CO_2 mole fraction at permeate obviously increases when changing humid feed to humid permeate streams around 1.1 to 1.2 times by using [bmim][PF_6] membrane. [bmim][Tf_2N] membrane would be decreased 1.7 to 2.3 times when increasing temperature and changing the dry to humid feed stream. The reduction of

[bmim][PF_6] membrane area were approximate 3% and [bmim][Tf_2N] were about 12% by increasing of operating temperature from 303.15 to 333.15 K and changing dry to humid feed.

Chapter 7

Summary of the research

7.1 Conclusions

The goal of this study is to design the CO_2 separation process by investigating the key parameters that affect the CO_2 permeability and selectivity through liquid membrane. Firstly, an amine/glycol membrane was used as a permeability study to recovery CO_2 from air. The results show good CO_2 permeability but the short duration of membrane is a big problem. Thus, ionic liquids are promoted to be novel chemical for CO_2 capture due to low vapor pressure and high affinity with CO_2. Therefore, this study mainly focuses on the application of ionic liquid membranes. The highlights of this research are divided into two categories; experiments and simulations as listed follows:

Experiments

- Amine/glycol liquid membrane can be used to recovery CO_2 from air.
- CO_2 separation through ionic liquid membrane is successful to operate near room temperature.
- An increase in operating temperature resulting in the enhancement of CO_2 permeabilities unlike the selectivity.
- CO_2 permeabilities increase with the decrease of total pressure difference due to facilitated transport.
- Low flow rate at feed side gives higher CO_2 permeabilities but selectivity presents the similar for both low and high flow rate at feed.
- At high CO_2 concentration, CO_2 permeabilities were limited by the carrier saturation.
- The CO_2 permeation rises around twice when changing dry to w humid stream.

- CO_2 permeabilities from [bmim][PF_6] and [bmim][Tf_2N] membranes slightly differed when operating with humid feed stream.
- The humid permeate stream gave CO_2 permeabilities lower than that of humid feed stream because of the low water concentration and low CO_2 solubility.
- High CO_2 and low water permeabilities were obtained from [bmim][Tf_2N] membrane due to the weak affinity of molecular pair between water and $[Tf_2N]^-$.

Simulation

- This model is useful for the optimization of membrane area.
- At constant membrane area, the increase in operating temperature leads to the increase in CO_2 concentration at permeate side.
- At constant amount of CO_2 concentration at permeate, [bmim][PF_6] and [bmim][Tf_2N] presents the highest and the smallest membrane size.
- The rise of operating temperature results in the less membrane area.
- [bmim][PF_6] and [bmim][dca] show the highest and the lowest reduction of membrane area when increasing temperature.
- The simulation fails to predict the effect of pressure due to facilitated transport phenomena.
- The increase in flow rate at feed side shows insignificant change of CO_2 mole fraction at permeate.
- At the alike membrane size, CO_2 mole fraction at permeate obtained from humid feed stream is higher than that of humid permeate stream around 1.1 to 1.2 times when using [bmim][PF_6] membrane.
- At the permeate equimole fraction, [bmim][Tf_2N] membrane with water vapor at feed stream and high temperature requires smallest membrane area.

7.2 Recommendations for future works

This work has carried out both experiments and simulation in order to find out the optimization conditions and parameters for CO_2 separation process design. However, this work should be extended the ideas with the combination of knowledge to apply for practical process in the future study. The recommendations and suggestions are listed as follows:

1.) Improve the impregnation of ionic liquid into porous membrane

The impregnation of membrane with ionic liquid has not been perfect because of high viscosity of ionic liquid. Even though the homogeneous phase can be seen with the naked eye, the heterogeneous phase still appears as observed by SEM. It is necessary to improve the mixing method. The suggestion is to use the solvent which dissolve ionic liquid. The solvent should be easy to evaporate or low boiling point and do not dissolve with polymer membrane. Other alternative is the use of supercritical CO_2. Pressure, temperature and flow rate affect the morphology of the membrane. The dominant advantage of this method is that it will not destroy the membrane structure.

2.) Prediction of gel membrane viscosity

Generally, the solution-diffusion mechanism is used for the calculation of permeability of gas. In this mechanism equation, a diffusion coefficient of ionic liquid was proposed by Morgan et al as described in the previous Chapter. The viscosity that uses for calculation is obtained from only ionic liquid. In this work, although diffusion coefficient was calculated from only viscosity of ionic liquid, the viscosity of porous membrane should be concerned as well. From this concept, it would be considered that the viscosity of the mixture between ionic liquid and porous membrane may give more accuracy of calculation. Therefore, in order to improve the accuracy of calculation, the viscosity term should be modified by using both the viscosity of porous membrane and ionic liquid.

3.) Fundamental study for SO_2 removal unit in the industry

SO_2 from the combustion process (e.g. incineration plant, biomass power plant, cogeneration plant) should be also reconsidered as an environmental issue due to the cause of global warming phenomena. Ionic liquid is not only able to capture CO_2 but also other acid gas i.e. sulfur dioxide (SO_2). The existing SO_2 removal method is to inject the limestone into the fuel gas stream. The existing problem is that the bag filter often clogs and need to clean up or install the new unit. In the future, the study should focus on the SO_2 permeability and selectivity in several parameters such as new species of ionic liquids, the types of supported porous membranes, temperature dependence and so on.

References

[1] P. Li, D.R. Paul, T.-S. Chung, High performance membranes based on ionic liquid polymers for CO_2 separation from the flue gas, Green Chemistry, 14 (2012) 1052-1063.

[2] J.-S. Lee, J.-H. Kim, J.-T. Kim, J.-K. Suh, J.-M. Lee, C.-H. Lee, Adsorption equilibria of CO_2 on zeolite 13X and zeolite X/activated carbon composite, Journal of Chemical & Engineering Data, 47 (2002) 1237-1242.

[3] B. Guo, L. Chang, K. Xie, Adsorption of carbon dioxide on activated carbon, Journal of Natural Gas Chemistry, 15 (2006) 223-229.

[4] A. Wahby, J. Silvestre-Albero, A. Sepúlveda-Escribano, F. Rodríguez-Reinoso, CO_2 adsorption on carbon molecular sieves, Microporous and Mesoporous Materials, 164 (2012) 280-287.

[5] M. Wang, A. Lawal, P. Stephenson, J. Sidders, C. Ramshaw, Post-combustion CO_2 capture with chemical absorption: A state-of-the-art review, Chemical Engineering Research and Design, 89 (2011) 1609-1624.

[6] Y. Kim, S.-R. Lim, J.M. Park, The effects of Cu(II) ion as an additive on NH_3 loss and CO_2 absorption in ammonia-based CO_2 capture processes, Chemical Engineering Journal, 211-212 (2012) 327-335.

[7] G. Xu, L. Li, Y. Yang, L. Tian, T. Liu, K. Zhang, A novel CO_2 cryogenic liquefaction and separation system, Energy, 42 (2012) 522-529.

[8] P. Chiesa, S. Campanari, G. Manzolini, CO_2 cryogenic separation from combined cycles integrated with molten carbonate fuel cells, International Journal of Hydrogen Energy, 36 (2011) 10355-10365.

[9] H. Yang, Z. Xu, M. Fan, R. Gupta, R.B. Slimane, A.E. Bland, I. Wright, Progress in carbon dioxide separation and capture: A review, Journal of Environmental Sciences, 20 (2008) 14-27.

[10] M. Bikshapathi, A. Sharma, A. Sharma, N. Verma, Preparation of carbon molecular sieves from carbon micro and nanofibers for sequestration of CO_2, Chemical Engineering Research and Design, 89 (2011) 1737-1746.

[11] S. Freguia, G.T. Rochelle, Modeling of CO_2 capture by aqueous monoethanolamine, AIChE Journal, 49 (2003) 1676-1686.

[12] A. Hart, N. Gnanendran, Cryogenic CO_2 capture in natural gas, Energy Procedia, 1 (2009) 697-706.

[13] C.-F. Song, Y. Kitamura, S.-H. Li, K. Ogasawara, Design of a cryogenic CO_2 capture system based on stirling coolers, International Journal of Greenhouse Gas Control, 7 (2012) 107-114.

[14] A.S. Holmes, J.M. Ryan, "Cryogenic distillative separation of acid gases from methane", U.S. Patent: 4 318 723, issued date March 9, 1982.

[15] Sebastiána, I. Kumakiri, R. Bredesen, M. Menéndez, Zeolite membrane for CO_2 removal: Operating at high pressure, Journal of Membrane Science, 292 (2007) 92-97.

[16] J.D. Seader, E.J. Henley, Separation process principles. 2nd ed. 2005: John Wiley & Sons, Inc.

[17] C.E. Powell, G.G. Qiao, Polymeric CO_2/N_2 gas separation membranes for the capture of carbon dioxide from power plant flue gases, Journal of Membrane Science, 279 (2006) 1-49.

[18] C. A. Scholes, S. E. Kentish, G.W. Stevens, Carbon dioxide separation through polymeric membrane systems for flue gas application, Recent Patents Chem. Eng., 1 (2008) 52-66.

[19] S.-H. Zhang, Z.-D. Tan, Prediction of glass transition temperatures of polyarylates using a support vector machine model①, Chinese Journal of Structural Chemistry, 30 (2011) 943-950.

[20] U. Buder, J.P. von Klitzing, E. Obermeier, Reactive ion etching for bulk structuring of polyimide, Sensors and Actuators A: Physical, 132 (2006) 393-399.

[21] M. Ulbricht, Advanced functional polymer membranes, Polymer, 47 (2006) 2217-2262.

[22] J.K. Adewole, A.L. Ahmad, S. Ismail, C.P. Leo, Current challenges in membrane separation of CO_2 from natural gas: A review, International Journal of Greenhouse Gas Control, 17 (2013) 46-65.

[23] Y. Zhang, J. Sunarso, S. Liu, R. Wang, Current status and development of membranes for CO_2/CH_4 separation: A review, International Journal of Greenhouse Gas Control, 12 (2013) 84-107.

[24] A. Ito, S. Duan, Y. Ikenori, A. Ohkawa, Permeation of wet CO_2/CH_4 mixed gas through a liquid membrane supported on surface of a hydrophobic microporous membrane, Separation and Purification Technology, 24 (2001) 235-242.

[25] A.H. Gorji, T. Kaghazchi, CO_2/H_2 separation by facilitated transport membranes immobilized with aqueous single and mixed amine solutions: Experimental and modeling study, Journal of Membrane Science, 325 (2008) 40-49.

[26] P. Jindaratsamee, Y. Shimoyama, A. Ito, Amine/glycol liquid membranes for CO_2 recovery from air, Journal of Membrane Science, 385-386 (2011) 171-176.

[27] P. Jindaratsamee, Y. Shimoyama, H. Morizaki, A. Ito, Effects of temperature and anion species on CO_2 permeability and CO_2/N_2 separation coefficient through ionic liquid membranes, The Journal of Chemical Thermodynamics, 43 (2011) 311-314.

[28] P. Scovazzo, D. Havard, M. McShea, S. Mixon, D. Morgan, Long-term, continuous mixed-gas dry fed CO_2/CH_4 and CO_2/N_2 separation performance and selectivities for room temperature ionic liquid membranes, Journal of Membrane Science, 327 (2009) 41-48.

[29] H.Z. Chen, P. Li, T.-S. Chung, PVDF/ionic liquid polymer blends with superior separation performance for removing CO_2 from hydrogen and flue gas, International Journal of Hydrogen Energy, 37 (2012) 11796-11804.

[30] J. Huang, J. Li, X. Zhan, C. Chen, A modified solution-diffusion model and its application in the pervaporation separation of alkane/thiophenes mixtures with PDMS membrane, Journal of Applied Polymer Science, 110 (2008) 3140-3148.

[31] J.G. Wijmans, R.W. Baker, The solution-diffusion model: a review, Journal of Membrane Science, 107 (1995) 1-21.

[32] H.B. Park, Y.M. Lee, Polymeric membrane materials and potential use in gas separation, in Advanced Membrane Technology and Applications, N.N. Li, et al., Editors. 2008, John Wiley & Sons, Inc. : Hoboken, New Jersey p. 633-669.

[33] F.F. Krull, C. Fritzmann, T. Melin, Liquid membranes for gas/vapor separations, Journal of Membrane Science, 325 (2008) 509-519.

[34] A. Ito, G. Sui, N. Yamanouchi, VOC vapor permeation through a liquid membrane using triethylene glycols, Desalination, 234 (2008) 270-277.

[35] N.N. Petra Cserjési, Katalin Bélafi-Bakó, Gas separation properties of supported liquid membranes prepared with unconventional ionic liquids, Journal of Membrane Science, 349 (2010) 6-11.

[36] T. Rhlalou, M. Ferhat, M.A. Frouji, D. Langevin, M. Métayer, J.F. Verchère, Facilitated transport of sugars by a resorcinarene through a supported liquid membrane, Journal of Membrane Science, 168 (2000) 63-73.

[37] S.-K. Jeong, C.-S. Ju, Extraction of strontium ion from sea water by contained liquid membrane permeator, Korean Journal of Chemical Engineering, 19 (2002) 93-98.

[38] I. Miesiąc, J. Szymanowski, Pertraction of Penicillin G in hollow fiber contained liquid membranes, Journal of Radioanalytical and Nuclear Chemistry, 228 (1998) 77-81.

[39] G. Muthuraman, T.T. Teng, C.P. Leh, I. Norli, Use of bulk liquid membrane for the removal of chromium (VI) from aqueous acidic solution with tri-n-butyl phosphate as a carrier, Desalination, 249 (2009) 884-890.

[40] A. Safavi, E. Shams, Selective and efficient transport of Hg(II) through bulk liquid membrane using methyl red as carrier, Journal of Membrane Science, 144 (1998) 37-43.

[41] G. León, M.A. Guzmán, Facilitated transport of cobalt through bulk liquid membranes containing diethylhexyl phosphoric acid, Desalination, 162 (2004) 211-215.

[42] S. Jafari, M.R. Yaftian, M. Parinejad, Facilitated transport of cadmium as anionic iodo-complexes through bulk liquid membrane containing hexadecyltrimethylammonium bromide, Separation and Purification Technology, 70 (2009) 118-122.

[43] A.M. Urtiaga, A. Alonso, I. Ortiz, J.A. Daoud, S.A. El-Reefy, S. Pérez de Ortiz, T. Gallego, Comparison of liquid membrane processes for the removal of cadmium from wet phosphoric acid, Journal of Membrane Science, 164 (2000) 229-240.

[44] E.A. Fouad, H.J. Bart, Emulsion liquid membrane extraction of zinc by a hollow-fiber contactor, Journal of Membrane Science, 307 (2008) 156-168.

[45] T. Enns, Facilitation by carbonic anhydrase of carbon dioxide transport, Science, 155 (1967) 44-47.

[46] N.C. Otto, J.A. Quinn, The facilitated transport of carbon dioxide through bicarbonate solutions, Chemical Engineering Science, 26 (1971) 949-961.

[47] Y. Gong, Z. Wang, S. Wang, Experiments and simulation of CO_2 removal by mixed amines in a hollow fiber membrane module, Chemical Engineering and Processing: Process Intensification, 45 (2006) 652-660.

[48] S. Paul, A.K. Ghoshal, B. Mandal, Removal of CO_2 by single and blended aqueous alkanolamine solvents in hollow-fiber membrane contactor: Modeling and simulation, Industrial & Engineering Chemistry Research, 46 (2007) 2576-2588.

[49] S. Paul, A.K. Ghoshal, B. Mandal, Theoretical studies on separation of CO_2 by single and blended aqueous alkanolamine solvents in flat sheet membrane contactor (FSMC), Chemical Engineering Journal, 144 (2008) 352-360.

[50] S. Keskin, D. Kayrak-Talay, U. Akman, Ö. Hortaçsu, A review of ionic liquids towards supercritical fluid applications, The Journal of Supercritical Fluids, 43 (2007) 150-180.

[51] J. Gorman, Faster, better, cleaner?: New liquids take aim at old-fashioned chemistry, Science News, 160 (2001) 156-158.

[52] L.A. Neves, J.G. Crespo, I.M. Coelhoso, Gas permeation studies in supported ionic liquid membranes, Journal of Membrane Science, 357 (2010) 160-170.

[53] N.V. Plechkova, K.R. Seddon, Ionic liquids: “designer” solvents for green chemistry, in Methods and Reagents for Green Chemistry, P. Tundo, A. Perosa, and F. Zecchini, Editors. 2007, John Wiley & Sons, Inc.: New Jersey. p. 105-130.

[54] O.O. Okoturo, T.J. VanderNoot, Temperature dependence of viscosity for room temperature ionic liquids, Journal of Electroanalytical Chemistry, 568 (2004) 167-181.

[55] P. Jindaratsamee, A. Ito, S. Komuro, Y. Shimoyama, Separation of CO_2 from the CO_2/N_2 mixed gas through ionic liquid membranes at the high feed concentration, Journal of Membrane Science, 423-424 (2012) 27-32.

[56] D. Han, K.H. Row, Recent applications of ionic liquids in separation technology, Molecules, 15 (2010) 2405-2426.

[57] J.E. Bara, T.K. Carlisle, C.J. Gabriel, D. Camper, A. Finotello, D.L. Gin, R.D. Noble, Guide to CO_2 separations in imidazolium-based room-temperature ionic liquids, Industrial & Engineering Chemistry Research, 48 (2009) 2739-2751.

[58] R.L. Gardas, M.G. Freire, P.J. Carvalho, I.M. Marrucho, I.M.A. Fonseca, A.G.M. Ferreira, J.A.P. Coutinho, High-pressure densities and derived thermodynamic properties of imidazolium-based ionic liquids, Journal of Chemical & Engineering Data, 52 (2006) 80-88.

[59] M.-L. Ge, R.-S. Zhao, Y.-F. Yi, Q. Zhang, L.-S. Wang, Densities and viscosities of 1-butyl-3-methylimidazolium trifluoromethanesulfonate + H_2O binary mixtures at T = (303.15 to 343.15) K, Journal of Chemical & Engineering Data, 53 (2008) 2408-2411.

[60] A. Berthod, M.J. Ruiz-Ángel, S. Carda-Broch, Ionic liquids in separation techniques, Journal of Chromatography A, 1184 (2008) 6-18.

[61] J.R.E. Lara Gala´n Sa´nchez, Ferdy Onink, G. Wytze Meindersma, and Andre´ B. de Haan, Density, viscosity, and surface tension of synthesis grade imidazolium, pyridinium, and pyrrolidinium based room temperature ionic liquids, Journal of Chemical & Engineering Data, 54 (2009) 2803-2812.

[62] L.C. Branco, J.G. Crespo, C.A.M. Afonso, Highly selective transport of organic compounds by using supported liquid membranes based on ionic liquids, Angewandte Chemie International Edition, 41 (2002) 2771-2773.

[63] P. Scovazzo, A.E. Visser, J.H. Davis Jr., R.D. Rogers, C.A. Koval, D.L. DuBois, R.D. Noble, Supported ionic liquid membranes and facilitated ionic liquid membranes, in Ionic Liquids: Industrial Applications for Green Chemistry, R.D. Rogers and K.R. Seddon, Editors. 2002, American Chemical Society: Washington, DC p. 69-87.

[64] P. Scovazzo, J. Kieft, D.A. Finan, C. Koval, D. DuBois, R. Noble, Gas separations using non-hexafluorophosphate $[PF_6]^-$ anion supported ionic liquid membranes, Journal of Membrane Science, 238 (2004) 57-63.

[65] Y. Shimoyama, A. Ito, Predictions of cation and anion effects on solubilities, selectivities and permeabilities for CO_2 in ionic liquid using COSMO based activity coefficient model, Fluid Phase Equilibria, 297 (2010) 178-182.

[66] D.H. Kim, I.H. Baek, S.U. Hong, H.K. Lee, Study on immobilized liquid membrane using ionic liquid and PVDF hollow fiber as a support for CO_2/N_2 separation, Journal of Membrane Science, 372 (2011) 346-354.

[67] S. Kasahara, E. Kamio, T. Ishigami, H. Matsuyama, Effect of water in ionic liquids on CO_2 permeability in amino acid ionic liquid-based facilitated transport membranes, Journal of Membrane Science, 415-416 (2012) 168-175.

[68] E. Norman, "Hydrophilic semi-permeable PTFE membranes and their manufacture", U.S. Patent: 5 041 225, issued date August 20, 1991.

[69] A. Ito, Dehumidification of air by a hygroscopic liquid membrane supported on surface of a hydrophobic microporous membrane, Journal of Membrane Science, 175 (2000) 35-42.

[70] J. Li, A. Ito, Dehumidification and humidification of air by surface-soaked liquid membrane module with triethylene glycol, Journal of Membrane Science, 325 (2008) 1007-1012.

[71] F.A. Chowdhury, H. Okabe, S. Shimizu, M. Onoda, Y. Fujioka, Development of novel tertiary amine absorbents for CO_2 capture, Energy Procedia, 1 (2009) 1241-1248.

[72] N. Matsumiya, S. Matsufuji, M. Nakabayashi, K. Okabe, H. Mano, M. Teramoto, Separation of CO_2 from model flue gas by facilitated transport membrane with hydrogel, membrane, 29 (2004) 66-72.

[73] M. Teramoto, Q. Huang, T. Watari, Y. Tokunaga, R. Nakatani, T. Maeda, H. Matsuyama, Facilitated transport of CO_2 through supported liquid membranes of various amine solutions - Effects of rate and equilibrium of reaction between CO_2 and amine, Journal of Chemical Engineering of Japan, 30 (1997) 328-335.

[74] Y.-Y. Jiang, Z. Zhou, Z. Jiao, L. Li, Y.-T. Wu, Z.-B. Zhang, SO_2 gas separation using supported ionic liquid membranes, The Journal of Physical Chemistry B, 111 (2007) 5058-5061.

[75] D. Morgan, L. Ferguson, P. Scovazzo, Diffusivities of gases in room-temperature ionic liquids: Data and correlations obtained using a lag-time technique, Industrial & Engineering Chemistry Research, 44 (2005) 4815-4823.

[76] S. Roland, W. Wolfgang, A new equation of state for carbon dioxide covering the fluid region from the triple-point temperature to 1100 K at pressures up to 800 MPa, Journal of Physical and Chemical Reference Data, 25 (1996) 1509-1596.

[77] J. Jacquemin, P. Husson, A.A.H. Padua, V. Majer, Density and viscosity of several pure and water-saturated ionic liquids, Green Chemistry, 8 (2006) 172-180.

[78] Y.A. Sanmamed, D. González-Salgado, J. Troncoso, L. Romani, A. Baylaucq, C. Boned, Experimental methodology for precise determination of density of RTILs as a function of temperature and pressure using vibrating tube densimeters, The Journal of Chemical Thermodynamics, 42 (2010) 553-563.

[79] Y. Jiang, Y. Wu, W. Wang, L. Li, Z. Zhou, Z. Zhang, Permeability and selectivity of sulfur dioxide and carbon dioxide in supported ionic liquid membranes, Chinese Journal of Chemical Engineering, 17 (2009) 594-601.

[80] M. Hasib-ur-Rahman, M. Siaj, F. Larachi, Ionic liquids for CO_2 capture—development and progress, Chemical Engineering and Processing: Process Intensification, 49 (2010) 313-322.

[81] R. Quinn, J.B. Appleby, G.P. Pez, New facilitated transport membranes for the separation of carbon dioxide from hydrogen and methane, Journal of Membrane Science, 104 (1995) 139-146.

[82] H. Chen, A.S. Kovvali, S. Majumdar, K.K. Sirkar, Selective CO_2 separation from CO_2-N_2 mixtures by immobilized carbonate-gycerol membranes, Industrial & Engineering Chemistry Research, 38 (1999) 3489-3498.

[83] S. Saha, A. Chakma, Separation of CO_2 from gas mixtures with liquid membranes, Energy Conversion and Management, 33 (1992) 413-420.

[84] M.G. Freire, P.J. Carvalho, A.M. Fernandes, I.M. Marrucho, A.J. Queimada, J.A.P. Coutinho, Surface tensions of imidazolium based ionic liquids: Anion, cation, temperature and water effect, Journal of Colloid and Interface Science, 314 (2007) 621-630.

[85] M. Tariq, M.G. Freire, B. Saramago, J.A.P. Coutinho, J.N.C. Lopes, L.P.N. Rebelo, Surface tension of ionic liquids and ionic liquid solutions, Chemical Society Reviews, 41 (2012) 829-868.

[86] J. Zhang, S. Zhang, K. Dong, Y. Zhang, Y. Shen, X. Lv, Supported absorption of CO_2 by tetrabutylphosphonium amino acid ionic liquids, Chemistry – A European Journal, 12 (2006) 4021-4026.

[87] S.G. Raju, S. Balasubramanian, Aqueous solution of [bmim][PF_6]: Ion and solvent effects on structure and dynamics, The Journal of Physical Chemistry B, 113 (2009) 4799-4806.

[88] R. Fortunato, M.J. González-Muñoz, M. Kubasiewicz, S. Luque, J.R. Alvarez, C.A.M. Afonso, I.M. Coelhoso, J.G. Crespo, Liquid membranes using ionic liquids: The influence of water on solute transport, Journal of Membrane Science, 249 (2005) 153-162.

[89] D. Kerlé, R. Ludwig, D. Paschek, The influence of water on the solubility of carbon dioxide in imidazolium based ionic liquids, Zeitschrift für Physikalische Chemie, 227 (2013) 167-176.

[90] W. Li, Z. Zhang, B. Han, S. Hu, Y. Xie, G. Yang, Effect of water and organic solvents on the ionic dissociation of ionic liquids, The Journal of Physical Chemistry B, 111 (2007) 6452-6456.

[91] G. Sui, J. Li, A. Ito, Separation of VOC vapor from air by a surface-soaked liquid membrane module using triethylene glycol, Separation and Purification Technology, 68 (2009) 283-287.